UNIVERSIDADE DE SÃO PAULO

Escola de Engenharia de São Carlos

A thermal management system parametric model for fuel cell powered aircraft conceptual design

Rodolfo da Silva Collares

Dissertação de Mestrado
Programa de Pós-graduação em Engenharia Mecânica
Área de concentração: Aeronáutica

EESC · USP

UNIVERSITY OF SÃO PAULO
SÃO CARLOS SCHOOL OF ENGINEERING

RODOLFO DA SILVA COLLARES

A thermal management system parametric model for fuel cell powered aircraft conceptual design

São Carlos
2024

RODOLFO DA SILVA COLLARES

A thermal management system parametric model for fuel cell powered aircraft conceptual design

Dissertation presented to the São Carlos School of Engineering of the University of São Paulo in fulfillment of the requirements for the degree of Master of Science in Mechanical Engineering

Subject area: Aeronautics

Advisor: Prof. Jorge Bidinotto.

ORIGINAL

São Carlos
2024

Index card prepared by User Service at “Prof. Dr. Sergio Rodrigues Fontes Library” at EESC/USP

C697t

Collares, Rodolfo da Silva
A thermal management system parametric model for fuel cell powered aircraft conceptual design / Rodolfo da Silva Collares; advisor Jorge Bidinotto. -- São Carlos, 2024.

Master (Dissertation) - Graduate Program in Mechanical Engineering -- São Carlos School of Engineering, at University of São Paulo, 2024.

1. Fuel cell. 2. Thermal management system. 3. Meredith effect. 4. Aircraft concept studies. 5. Hybrid-electric aircraft. 6. Sustainable aviation. I. Titulo.

Prepared by Eduardo Graziosi Silva- CRB-8/8907

FOLHA DE JULGAMENTO

Candidato: Engenheiro **RODOLFO DA SILVA COLLARES**.

Título da dissertação: "Um modelo paramétrico de sistema de gerenciamento térmico para projeto conceitual de aeronaves movidas a célula de combustível".

Data da defesa: 09/08/2024.

Comissão Julgadora	**Resultado**
Prof. Dr. Jorge Henrique Bidinotto (Orientador) (Escola de Engenharia de São Carlos/EESC-USP)	Aprovado
Prof. Dr. Helcio Francisco Villa Nova (Universidade Federal de Itajubá/UNIFEI)	Aprovado
Dr. Ricardo Gandolfi (EMBRAER S. A.)	Aprovado

Coordenador do Programa de Pós-Graduação em Engenharia Mecânica:
Prof. Associado **Adriano Almeida Gonçalves Siqueira**

Presidente da Comissão de Pós-Graduação:
Prof. Titular **Carlos De Marqui Junior**

ABSTRACT

Collares, R. S. A thermal management system parametric model for fuel cell powered aircraft conceptual design, 2024, Text for Dissertation presented to Escola de Engenharia de São Carlos da Universidade de São Paulo.

It is a widely accepted fact that the world ambient temperature is rising, and it is correlated with the CO_2 emissions produced by economic sectors such as energy, industry and transports. Aerospace segment has an important contribution to the CO_2 emissions, therefore it studies solutions to reduce or eliminate it from its products. The studies include the replacement of fossil fuel aeronautical engines per Fuel Cells, which are devices that operate with hydrogen and produce electrical energy, water, and heat. Since fuel cells release considerable amount of heat, it requires a substantial TMS (thermal management system), which impacts the airplane weight and drag. Studies of fuel cell powered aircraft have been published, and the TMS is not neglected, but a deep discussion regarding its weight and drag estimation was not found. The present work develops a TMS weight and drag parametric model for fuel cell powered aircraft conceptual design, based on fuel cell and radiators physical models, and representing an optimum compromise between weight and drag. The work reveals linear correlation between the TMS parameters and fuel cell power. Significant dependence on fuel cell temperature has also been shown, therefore, three temperature levels were tested. It has also been observed that optimum solutions tend to require too large radiators, difficult to install, so, a limitation was inserted in the optimization cycle and models for three different area limits were generated. Then, regression equations have been determined to correlate the TMS parameters with fuel cell power, for various combinations of fuel cell operating temperature and radiator area limits, accomplishing the purpose of the work. It is recommended, for future works, the conduction of studies to investigate more efficient radiators, heat enhancement devices and TMS large radiators installation solutions.

Keywords: Fuel Cell, Thermal Management System, Meredith Effect, Aircraft Concept Studies, Hybrid-electric Aircraft, Sustainable aviation**.**

RESUMO

Collares, R. S. Um modelo paramétrico de sistema de gerenciamento térmico para projeto conceitual de aeronaves movidas a célula de combustível, 2024, Texto de Dissertação apresentado à Escola de Engenharia de São Carlos da Universidade de São Paulo.

É fato reconhecido que a temperatura ambiente da Terra está aumentando e isso está associado às emissões de CO_2 provenientes de segmentos como energia, indústria e transportes. O setor aeroespacial responde por uma parcela dessas emissões, por isso pesquisa produtos para reduzi-las ou eliminá-las. Estudos incluem a viabilidade de substituir os motores a combustão por células de combustível, que consomem hidrogênio, produzindo eletricidade, água e calor. Por gerarem alta taxa de calor, esses equipamentos requerem um substancial SGT (sistema de gerenciamento térmico), que afeta o peso e arrasto da aeronave. Muitos estudos de aeronaves com célula de combustível foram publicados, e o SGT não foi ignorado, mas uma discussão dedicada a estimar seu peso e arrasto não foi encontrada. Este trabalho cria um modelo paramétrico de peso e arrasto de SGT de células de combustível para estudos conceituais de aeronaves, baseado em modelos físicos de células de combustível e radiadores, e representando o ponto ótimo entre peso e arrasto. O trabalho mostrou correlação linear entre os parâmetros do SGT e a potência da célula. Foi observada uma dependência desses parâmetros com a temperatura de operação da célula, então três temperaturas foram testadas. Observou-se que soluções ótimas requerem um SGT de grandes dimensões, de difícil instalação, então uma limitação foi inserida no ciclo de otimização e três limites de área foram testados. Regressões lineares foram, então, criadas correlacionando os parâmetros do SGT com a potência da célula, para diversas combinações de temperatura de operação e limite de área, cumprindo, assim, o propósito do trabalho. Recomenda-se, para trabalhos futuros, a condução de investigações de radiadores mais eficientes, técnicas de aumento de efetividade de troca de calor e soluções de instalação de radiadores de grandes dimensões.

Palavras-Chave: célula de combustível, gerenciamento térmico, efeito Meredith, estudos conceituais de aeronaves, aeronaves híbridas, aviação sustentável

List of Abbreviations

AFC	Acid Fuel Cell
BOP	Balance of Plant
CFD	Computational Fluid Dynamics
CRZ	Cruise
CHP	Combined Heat and Power
DMFC	Direct methanol Fuel Cell
FC	Fuel Cell
FN	Net Thrust
HHV	High Heating Value
KPI	Key Performance Indicator
LHV	Lower Heating Value
MCFC	Molten Carbonate Fuel Cell
PAFC	Phosphoric Acid Fuel Cell
PEM	Proton Exchange Membrane
Re	Reynolds Number
ROM	Rough Order of Magnitude
SAF	Sustainable Aviation Fuel
SOFC	Solid Oxid Fuel Cell
TCDS	Type Certificate Data Sheet
TMS	Thermal Management System
TO	Takeoff
VTOL	Vertical Takeoff and Landing

List of Symbols

Symbol	Unit	Description
ASR	Ω	Area specific resistance
air_{temp}	°C	Radiator air temperature
A_{c_air}	m^2	Air Side Free Flow Area
A_{c_liq}	m^2	Liquid Side Free Flow Area
A_{air}	m^2	Air Side Total Transfer Area
A_{liq}	m^2	Liquid Side Total Transfer Area
A_{FC}	m^2	Fuel Cell Area
A_{nozzle}	m^2	Nozzle Area
$A_{propeller}$	m^2	Propeller Area
cp_{air}	J/ kg / K	Air specific heat
cp_{liq}	J/ kg / K	Liquid specific heat
Cd	-	Nozzle Discharge Coefficient
Cr	-	Heat capacity ratio
$Cmin$	W/K	Minimum Heat capacity
$Cmax$	W/K	Maximum Het capacity
Cv	-	Nozzle Velocity Coefficient
D	N	Airplane Drag
$Diam$	m	Propeller Diameter
$Depth$	m	Radiator Depth
$DuctLength$	m	Duct Length
$DuctArea$	m	Duct Area
E_h	m^2	Ideal Reversible Cell Voltage
Eq_TMS_Weight	kg	Equivalent Thermal Management System Weight
E_r	V	True Reversible Cell Voltage
f	-	Friction Coefficient
F	Coulombs/mol	Faraday Constant
Fn	N	Propeller Thrust
FC_Stack_Heat	W	Fuel Cell Stack Heat
FC_Stack_Power	W	Fuel Cell Stack Power
FC_Power_norm	W/cm^2	Normalized Fuel Cell Power
$Flow\ Speed$	m/s	Coolant Flow Speed
G_{air}	$kg/s/m^2$	Radiator Air Mass Velocity
G_{liq}	$kg/s/m^2$	Radiator Liquid Mass Velocity
h_{H_2O}	J/kg	Water enthalpy
h_{H_2}	J/kg	Hydrogen enthalpy
h_{O_2}	J/kg	Oxygen enthalpy
h_{air}	J/kg	Air side convective coefficient
h_{liq}	J/kg	Liquid side convective coefficient
h_{WS}	-	Vapor Saturation Ratio
i	A	Current
i_{leak}	A	Leakage Current
j	-	Colburn Coefficient
J	-	Propeller Advance Ratio

liq_{temp}	°C	Coolant Temperature
k	W/m/K	Conduction Coefficient
L	N	Aircraft Lift
l_{fin}	m	Fin length
$L_{H_2\_vap}$	W/kg	Hydrogen vaporization latent heat
$L_{H_2O\_vap}$	W/kg	Water vaporization latent heat
$loss_{act}$	V	Activation Loss
$loss_{conc}$	V	Concentration loss
$loss_{ohmic}$	V	Ohmic loss
$Mach9$	-	Mach at Exhaust Nozzle
m_{H_2}	kg/mol	Molecular Hydrogen mass/mole
m_{O_2}	kg/mol	Molecular Oxygen mass/mole
n	1/s	Propeller rotational speed (revs/s)
N	-	Number of electrons
N_{cells}	-	Number of Cells
NTU	-	Number of Transfer Units
Nu	-	Nusselt Number
$Pamb$	Pa	Ambient Pressure
$Pt9$	Pa	Exhaust Nozzle Total Pressure
P_{H_2O}	Pa	Partial Water pressure
P_{H_2}	Pa	Partial Hydrogen
P_{O_2}	Pa	Partial Oxygen Pressure
P_{compr_out}	Pa	Compressor Outlet Pressure
$PowerPenalty$	-	Power Penalty
Pr	-	Prandtl Number
$Propeller\_Power$	W	Propeller Power
P_{turb_in}	Pa	Turbine Inlet Pressure
P_{turb_out}	Pa	Turbine Outlet Pressure
PW_{compr}	Pa	Compressor Power
PW_{motor}	W	Motor Power
P_{WS}	Pa	Saturation Pressure of Water Vapor
PW_{turb}	W	Turbine Power
R	J/kg/K	Individual Gas Constant
Re_{air}	-	Reynolds Number Air side
Re_{liq}	-	Reynolds Number Liquid side
$Reservoir\_Fluid\_Quant\_kg$	kg	Reservoir Fluid Quantity
r_{h_air}	m	Hydraulic radius Air side
r_{h_liq}	m	Hydraulic radius Liquid side
St	-	Stanton Number
Q	W	Fuel Cell Heat in kW for parametric model
$QBOP$	W	Heat in Balance of Plant
Q_{H_2}	W	Hydrogen Heat
$Q_{H_2latent}$	W/kg	Latent Heat
Q_{H_2sens}	W/kg	Sensible Heat
Q_Motor	W	Motor rejected heat
$Q_{FC\_Stack\_cooling}$	W	Fuel Cell Stack Cooling System Demand
Q_{vap}	W	Fuel Cell Water Vaporization Heat
s_{H_2O}	J/kg/K	Water entropy

s_{H_2}	J/kg/K	Hydrogen entropy
s_{O_2}	J/kg/K	Oxygen entropy
St	J/kg/K	Stanton Number
$T_{boiling\ point}$	K	Boiling point temperature
$T\_K_{compr\_out}$	K	Outlet compressor Temperature
$T\_k_{ram\_air}$	K	Ram Air Temperature for compressor inlet
$Ts9$	K	Exhaust Nozzle Static Temperature
$Tt9$	K	Exhaust Nozzle Total Temperature
T	K	Fuel Cell Reaction Temperature
$T_{FC\ op\ temp}$	K	Fuel Cell Operating Temperature
TMS_Drag	N	Thermal management System Drag
TMS_Weight	N	Thermal management System Drag Weight
$Uair$	W/K/m^2	Overall Heat Transfer Coefficient
v	V	Fuel Cell Voltage
V_a	m/s	Aircraft Speed
V_i	m/s	Air speed at diffuser inlet
V_o	m/s	Air Speed at Diffuser outlet
V_1	m/s	Air Speed at TMS Circuit inlet
V_9	m/s	Air Speed at TMS Circuit Exhaust
Volumetric Flow	m^3/s	Coolant Volumetric Flow
W_{Air}	kg/s	Fuel Cell Air mass flow
$W_{air\_main\_hx}$	kg/s	Heat exchanger air mass flow
$W_{coolant\_gpm}$	gpm	Coolant flow in gallons per minute
W_{H_2}	kg/s	Fuel Cell Hydrogen mass flow
W_{H_2O}	kg/s	Water mass flow
$W_{liq\_main\_hx}$	kg/s	Heat exchanger liquid mass flow
W_{O_2}	kg/s	Fuel Cell Oxygen mass flow
Wt_{pump_kg}	kg	Pump Weight
$Wt_{reservoir\_kg}$	kg	Reservoir Total Weight
$W_{coolant\_duct}$	kg	Coolant Weight inside duct

Greek Symbols

Symbol	Unit	Description
α	-	Arden Buck Equation Empirical Exponent
γ	-	Specific Heat Ratio
Δg	J/kg	Free Gibbs Energy Variation
Δh	J/kg	Enthalpy variation
$\triangle P$	Pa	Pressure drop
$\triangle P_{diffuser\_loss}$	Pa	Diffuser Pressure loss
$\triangle P_{exhaust\_loss}$	Pa	Exhaust Duct Pressure loss
$\triangle P_{propeller}$	Pa	Propeller variation
$\triangle P_{radiator\_loss}$	Pa	Radiator Pressure Loss
Δs	J/kg/K	Entropy variation
ϵ	-	Effectiveness
η	-	efficiency
η_{compr}	-	Compressor efficiency
η_{fin}	-	Fin efficiency
η_{motor}	-	Motor Efficiency
η_{prop}	-	Propeller Efficiency
η_{turb}	-	Turbine Efficiency
υ_i	m^3/kg	Radiator Inlet Specific Volume
υ_m	m^3/kg	Radiator Average Specific Volume
υ_o	m^3/kg	Radiator Outlet Specific Volume
η_{turb}	-	Turbine Efficiency
μ_{air}	N s /m^2	Air viscosity
μ_{liq}	N s /m^2	Liquid viscosity
ρ	kg/m^3	Density
σ_{air}	ft^2/ft^3	Compactness air side (Total Transfer Area over Radiator Volume, air side)
σ_{liq}	ft^2/ft^3	Compactness air side (Total Transfer Area over Radiator Volume, liquid side)

List of Figures

Figure 1 - CO_2 emissions, adapted from IEA (2021) 27
Figure 2 - Aircraft Powered by a Fuel Cell Propulsion System 29
Figure 3 - Fuel Cell Schematic 30
Figure 4 - Energy Density from Various Technologies, adapted from Hoogendoorn (2018) 32
Figure 5 - TMS Design Pareto Frontier, adapted from Chapman et al. (2020) 37
Figure 6 - Radiator Weight Model. Source: (Palladino et al, 2021) 38
Figure 7 - Fan Weight models. Source: (Chapman et al., 2020) 39
Figure 8 - Fuel Cell Heat and Power Flow Chart, Source: (Palladino et al, 2021) 41
Figure 9 - Thermal Management Parametric Model Notional Shape 48
Figure 10 - Thermal Management System Model Data Flow 52
Figure 11 - Fuel Cell and Thermal Management Architecture 53
Figure 12 - Voltage vs Current Density Chart, adapted from Datta (2021) 58
Figure 13 - Power vs Current Chart, adapted from: Datta (2021) 59
Figure 14 - Fuel Cell Stack Arrangement 60
Figure 15 - Power Chart vs Hydrogen Flow 61
Figure 16 - Water Vaporization Heat, Source: (Engineering Toolbox, 2010) 64
Figure 17 - Heat vs Power Chart 65
Figure 18 - Balance of Plant Schematic. 66
Figure 19 - Heat Balance Schematic 69
Figure 20 - Power vs Hydrogen flow 70
Figure 21 - Simplified Thermal Management Cycle 72
Figure 22 - TMS Design Cycle 72
Figure 23 - Heat Exchanger Types, Source: (Incropera et al, 2011) 73
Figure 24 - Heat Exchanger Performance Chart, adapted from Kays and London (1984) 75
Figure 25 - Fins efficiency Chart, adapted from Kays and London (1984) 77
Figure 26 - Air Flow Calculation Flow Chart 78
Figure 27 - Area Calculation First Iteration 79
Figure 28 - Area Calculation Second Iteration 80
Figure 29 - TMS Air circuit 81
Figure 30 - Ideal Propeller Stream Tube, Source: (Heene, 2012) 83
Figure 31 - Diffuser Pressure Loss Chart, adapted from Katzoff (1948) 84
Figure 32 - Nozzle Discharge Coefficient Chart, adapted from Walsh (2004) 86
Figure 33 - Radiator Macro and Core views, adapted from Kays and London (1984) 88

Figure 34 - Coolant Tank Size Recommendation Chart, adapted from Engineering Toolbox (2005) 89
Figure 35 - TMS Control Volume 90
Figure 36 - TMS Control Volume Downstream Propeller 91
Figure 37 - Thermal Management Routines Organization 95
Figure 38 - Optimization Routine 96
Figure 39 - TMS Weight Model Test Example (Frontal area and Depth) 97
Figure 40 - Weight sub-routine test example (Frontal area and Liquid Flow) 98
Figure 41 - Heat Exchange vs Air flow (two different depths) 99
Figure 42- Heat Exchange vs Air flow (seven different liquid Reynolds number) 100
Figure 43 - Heat Exchange vs Air flow (two different frontal areas) 100
Figure 44 - Heat Exchange versus Pressure Loss (two different areas) 101
Figure 45 - Heat Exchange versus air flow (Various operating temperatures) 101
Figure 46 - Heat Exchange versus Air flow (various ambient temperatures) 102
Figure 47 - Heat Exchange versus Air Flow (three combinations of liquid temperature and ambient temperature, same delta) 103
Figure 48 - Find Air Flow Routine Result Test (Heat Exchange versus Air Flow) 104
Figure 49 - Find Air Flow Routine Result Test (Heat Exchange versus Pressure Loss) 104
Figure 50 - Air Flow and Pressure Drop vs Area 106
Figure 51 - Pressure Nozzle Pressure vs Ambient Pressure 107
Figure 52 - Thrust versus Area 107
Figure 53 - Nozzle area versus Radiator frontal Area 108
Figure 54 - Typical Gast turbine Rated Power with Altitude 109
Figure 55 - Typical Gas Turbine Rated Power Variation with Ambient Temperature 110
Figure 56 - Population Validity Map, Re=3000 and Re = 4000 111
Figure 57 - Population Validity Map, Re=4000 and Re = 5000 112
Figure 58 - Weight versus Drag scatter (all valid population individuals) 112
Figure 59 - Weight versus Drag scatter (depth and area segregated in different lines) 113
Figure 60 - Equivalent Weight Heat Map Re=3000 and Re = 4000 114
Figure 61 - Equivalent Weight Heat Map Re=5000 and Re = 6000 114
Figure 62 - TMS Weight Heatmap 115
Figure 63 - TMS Drag Heatmap 115
Figure 64 - TMS Drag (in Power Penalty format) Heatmap 116
Figure 65 - Weight and Frontal Area (minimum area range) 118
Figure 66 - Takeoff and Cruise Power Penalty (minimum area range) 118

Figure 67 - Weight and Frontal Area (medium area range) 119
Figure 68 - Takeoff and Cruise Power Penalty (medium area range) 120
Figure 69 - Weight and Frontal Area (maximum area range) 121
Figure 70 - Takeoff and Cruise Power Penalty (maximum area range) 121
Figure 71 - Area KPI 124
Figure 72 - Weight KPI 125
Figure 73 - TO Power Penalty KPI 126
Figure 74 - CRZ Power Aid KPI 127
Figure 75 - Specific Weight Comparison (10_94 versus 10_93) 127
Figure 76 - TO Penalty Comparison (10_94 versus 10_93) 128
Figure 77 - CRZ Aid Comparison (10_94 versus 10_93) 128
Figure 78 - Inclined Radiator Installation Example, Source:(Bjorn Fehrm ,2022) 130
Figure 79 - BF109 (Inside Wing Integrated Radiator, Inlet and Cowling Installation), Source: (Piancastelli et al, 2015) 130
Figure 80 - Radiators f coefficients, adapted from Kays and London (1984) 149
Figure 81 - Radiators j coefficients, adapted from Kays and London (1984) 149

List of Tables

Table 1 - Fuel Cell Types, Source (Dicks and Rand, 2018) 30
Table 2 - Shomate equations coefficients, Source: (Chase and Jr, 1998) 56
Table 3 - Fuel Cell Types of Losses, Source: (Dicks and Rand, 2018) 57
Table 4 - Leakage Current varying with operating pressure, adapted from Data (2021) 60
Table 5 - Radiator characteristics for Air Flow sub-routine Tests 98
Table 6 - Find Air flow routine test data 103
Table 7 - Parametric Equations (minimum area range) 119
Table 8 - Parametric Equations (medium area range) 120
Table 9 - Parametric Equations (maximum area range) 122
Table 10 - Fuel Cell Polarization Curve, adapted from Datta (2021) 141
Table 11 - Fuel Cell Normalized Power Chart, adapted from Datta (2021) 141
Table 12 - Fuel Cell Stack Power Chart Data at Different Pressures 142
Table 13 - Fuel Cell Required Cooling Heat Chart Data at Different Pressures 143
Table 14 - Propeller Efficiency Results 145
Table 15 - Propeller Pressure Boost Results 146
Table 16 - Heat Dissipation 146
Table 17 - Radiators Core Geometry Information, Source (Kays and London, 1984) 150
Table 18 - Air Properties, Source: (Engineering Toolbox, 2004) 151
Table 19 - Hydrogen Properties, Source: (Engineering Toolbox, 2008) 151

Contents

1 Introduction 27
1.1 Introduction to Fuel Cells 29
1.2 Reasons to Study Fuel Cells for aircraft application 31
1.3 Sustainable Aviation Conceptual Design Efforts 32
2 Bibliography Review 35
2.1 Innovative Electrical or Hybrid Power Source Airplane Research 35
2.2 Fuel Cells Technology and Modeling 39
2.3 Thermal Management System 42
3 Problem Importance and Objective 47
3.1 Objectives 48
3.1.1 General Objective 48
3.1.2 Specific objectives 49
4 Theoretical Development for Modeling 51
4.1 Overall Idea 51
4.2 Physical Model Development 51
4.3 Fuel Cell Physical Modeling 53
4.3.1 Fuel Cell Architecture 53
4.3.2 Fuel Cell Performance Model 55
4.3.3 Fuel Cell Air Flow and Hydrogen Feeding Systems 65
4.4 Thermal Management System Physical Model 68
4.4.1 Thermal Management System Model and Design Approach 68
4.4.1.1 Magnitude of Heat Exchange Demands and Problem Simplification Rationale 68
4.4.1.2 Thermal Management System Arrangement and Design Flow 71
4.4.1.3 Candidate Heat exchanger Calculations (Air Flow Demand Determination) 73
4.4.1.4 Air Flow Compatibility 80
4.4.1.4.1 Propeller Pressure Rise Model 81
4.4.1.4.2 Diffuser and Exhaust duct Pressure Loss Models 83
4.4.1.4.3 Heat Exchanger Pressure Loss 85
4.4.1.4.4 Nozzle coefficients 85
4.4.1.4.5 Overall Air Circuit Verification 86
4.4.1.5 Thermal Management System Weight Calculation: 87

4.4.1.6 Thermal Management System Drag 90
4.4.1.7 Thermal Management System Power Penalty Parameter 91
4.4.2 Selection of Best Thermal Management Solution 92
5 Results 95
5.1 Sub-routines Tests 96
5.1.1 Weight Routine Test 96
5.1.2 Air flow Calculation Routines Tests 98
5.1.3 Air Flow Compatibility 105
5.2 Design Routine 108
5.2.1 Critical Flight Condition Definition 109
5.2.2 Overall Run 110
5.2.3 Optimizer Routine 113
5.3 Parametric Model Generation 116
5.4 Results Review 122
5.5 Modeling Use and Recommendation 123
5.6 Model Premises, Limits and Comments 129
6 Conclusion 133
7 References 135
APPENDIX A – Fuel Cell Performance Tables 141
APPENDIX B – Reference Aircraft Data 145
APPENDIX C – Radiators Data 149
APPENDIX D – Air and Hydrogen Properties Tables 151

1 Introduction

The global warming is a fact widely accepted by scientific community as Myers (2021) points out. Extensive research work has demonstrated that average earth ambient temperature is rising over the years. Moreover, Myers (2021) also quotes the strong relationship between the global warming and the CO_2 emissions.

Industry, Energy, and transports sectors still make intensive use for fossil fuels, which releases CO_2 as a product of combustion reaction. According to IEA (2021) human activities together emit 35 gigatons of CO_2 emissions per year (Figure 1)

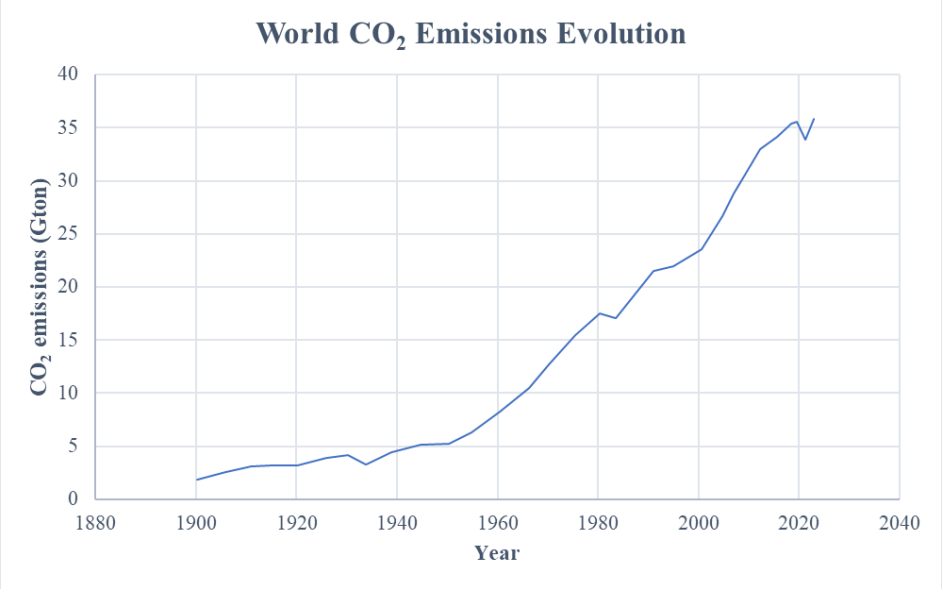

Figure 1 - CO_2 emissions, adapted from IEA (2021)

IEA (2022) demonstrates that transport sector produces 7.7 gigatons of CO_2 (per year) which corresponds to approximately 22% of world CO_2 emissions, while Airspace sector is responsible for 9% of the transports CO_2 emissions. This situation stimulates investments to develop solutions for sustainable aviation, so various alternatives of energy source are being considered.

Use of Sustainable Aviation Fuel (SAF) on the current aircraft combustion engines is one alternative under development and its adoption is being seriously considered, as U.S. Department of Energy (2022) confirms. SAF is a biofuel produced from various possible feedstocks (sugar, starch, rice straw and organic waste like cooking oil) intended to present similar properties to the currently used fuel (Jet A), to be burned on the same combustion engines that fly today. It releases CO_2 the same way as Jet A, which seems pointless as means to reduce carbon emissions, but its use stands for the concept of the Net Zero emissions. Since SAF feedstocks absorbs CO_2 from atmosphere at its growing process, the CO_2 released on the environment after combustion will be consumed by a new feedstock production cycle. SAF biggest challenges include the production in large scale, affordable costs and a free of fossil fuel use on the chain of production, in addition to bring an important concern: a possibility to raise food prices, as Frangoul (2021) alerts.

Combustion engines can also be modified to burn gaseous H_2. Since H_2 burn produces water instead of CO_2, it is considered a promising no carbon emission solution for aviation. Combustion engines burning H_2 have already been tested by research institutions as quoted by Hoogendoorn (2018) but producing H_2 in large production scale with affordable costs and real carbon emission free production chain is also a challenge.

The use of electrical motors fed by batteries as a propulsion alternative has been extensively evaluated. Such a technology is already being used in commercial products, but, since batteries present low energy density levels, the size of batteries that an airplane can afford (due to weight limitation) only allow very low range applications. Unless a technology breakthrough occurs, use of electrical motors fed by batteries only are limited to very small aircraft for general aviation.

Another line of development of carbon emission free aircraft that is gaining momentum is the adoption of Fuel Cells, which will be the object of this study. Figure 2 shows, in a very basic schematic, the fuel cell as a propulsion solution for aircraft, being fed by hydrogen tanks and electrically feeding electric motors, which power the airplane propellers.

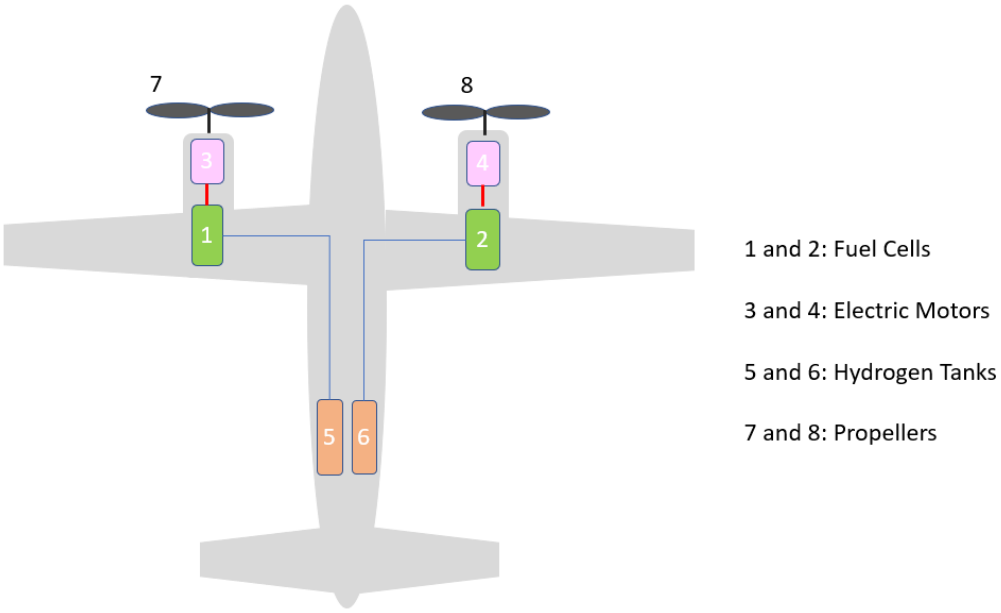

Figure 2 - Aircraft Powered by a Fuel Cell Propulsion System

1.1 Introduction to Fuel Cells

In a basic manner (details shall be presented in section 4), Fuel Cells are devices capable of performing a controlled reaction between a hydrogen supply and an oxygen supply (which can be pure or immerse in a normal air flow) producing water and electrical current. The water is expelled with the excess of air flow and the electrical current flows through a circuit, feeding electrical equipment like motors, for instance. The fuel cell presents a similar composition to the batteries comprising three elements: the anode, cathode, and the electrolyte.

Figure 3 brings a fuel cell schematic to illustrate its working principle:

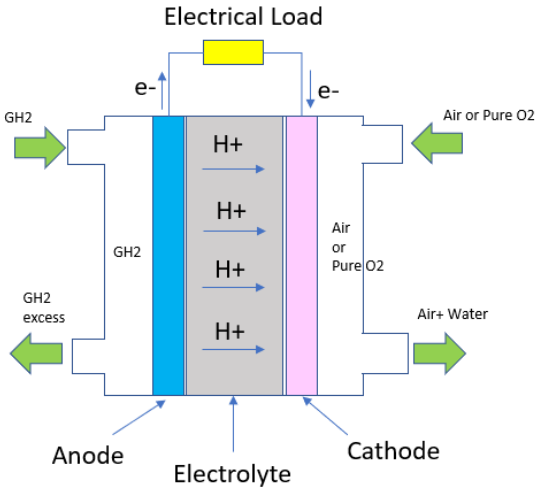

Figure 3 - Fuel Cell Schematic

The hydrogen gaseous flow feeds the anode part, while the air flow feeds the cathode. Hydrogen molecules are divided in protons, which flow though the electrolyte, and electrons, which pass through the electrical circuit. At cathode the oxygen and divided Hydrogen react producing water. Water is expelled from the fuel cell jointly to the air flow in a mixture of vapor or liquid. There are several types of fuel cells like Dicks and Rand (2018) describes:

Table 1 - Fuel Cell Types, Source (Dicks and Rand, 2018)

Fuel Cell Type	Mobile ion	Operating temperature (°C)	Fuel	Applications and notes
Alkaline (AFC)	OH^-	50 - 200	H_2	Space Vehicles
Proton Exchange Membrane	H^+	30 - 100+	H_2	Vehicles and mobile applications and for lower CHP systems
Direct Methanol	H^+	20 - 90	Methanol	Portable electronic systems of lower power running for long time
Phosphoric acid	H^+	220	H_2, (low S and low CO fuels)	Large numbers of 200 kW CHP system in use
Molten Carbonate	CO_3^{2-}	650	H_2 various hydrocarbon fuels (no S)	Medium to large scale CHP systems, up to MW capacity
Solid Oxide	O^-	500 - 1000	Impure H2, variety hydrocarbon fuels	All sizes of CHP systems, 2kW to multi MW

As exposed by Dicks and Rand (2018), the most suitable application for mobile use is the Proton-exchange membrane. Its compromise between power density, versatility and operating advantages such as short startup time (due to its low temperature operation), when compared to other fuel cells technologies, makes it more interesting for transports. For this reason, this type of fuel cell will be used in this work.

In terms of systems, the fuel cell basically requires a constant source of pressurized hydrogen flow, that is provided by a hydrogen tank, which can store the hydrogen in gaseous or liquid phase. The fuel cell also requires a constant and pressurized air flow which is typically provided by an air compressor or fan.

Another important aspect of Fuel Cells is that it dissipates a great amount of heat. Therefore, a thermal management system is another key part of a fuel cell system, and this will be the focus of this work.

1.2 Reasons to Study Fuel Cells for aircraft application

Several facts suggest that fuel cells are a promising solution for sustainable aviation.

When compared to batteries, the adoption of fuel cells is promising as Hoogendoorn (2018) demonstrates. Figure 4 presents energy density figures for fuel cells (fed by gaseous or liquid tank) and compares it to battery, showing that fuel cells, especially when fed by liquid hydrogen tanks, are many times lighter.

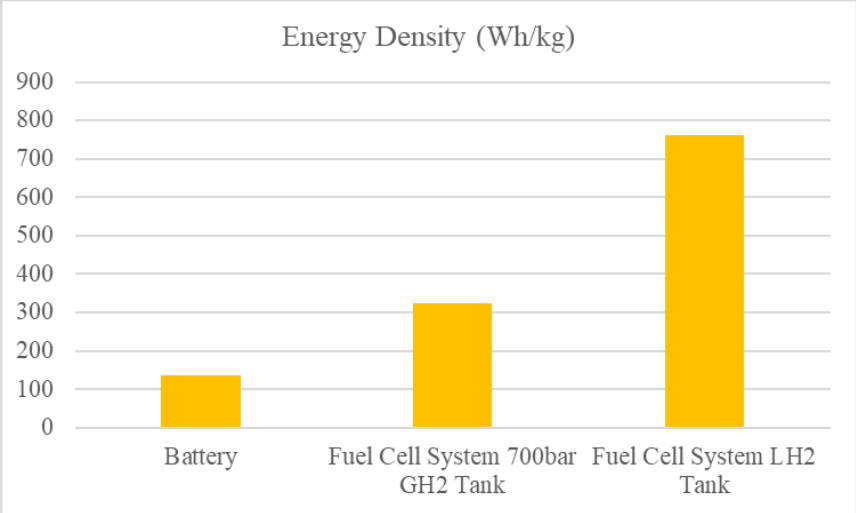

Figure 4 - Energy Density from Various Technologies, adapted from Hoogendoorn (2018)

When comparing Fuel Cells to gas turbine engines, which can also be prepared to burn hydrogen, Fuel Cells may reach efficiency levels on the order of 50% Dicks and Rand (2018), while regional turboprops gas turbine engines present efficiency levels on the order of 30%, (Ribeiro et al, 2021). It means that fuel cells consume much less Hydrogen than H_2 Gas turbines

Although some aspects suggest that the fuel cell are a promising technology, like being lighter than batteries and more efficient than gas turbine engine, Fuel Cells present a big technical challenge. Differently from combustion engines, that dissipate big portion of their heat through exhaust, fuel cells generated heat concentrates on the exchange membrane as Dicks and Rand (2018) details. The amount of heat that needs to be dissipated for a proper Fuel cell operation is huge, requiring a large and inevitably heavy cooling system. Furthermore, when considering an air-cooling system, air flow passing through heat exchanger causes drag which affects airplane performance. A heavy cooling system that presents high drag level are a concern when developing aircraft applications.

1.3 Sustainable Aviation Conceptual Design Efforts

100% SAF or H_2 combustion engines, Fuel Cell powered aircraft or battery powered aircraft are not a reality yet on the aeronautical industry. Various studies explore the potential of such power and energy solutions for specific aeronautics applications (mostly still at concept or at

demonstration stage). Moreover, many studies explore the potential to use hybrid energy solutions, that is, an aircraft that adopts more than one power source, as means to extract the main values from each technology and compensate their disadvantages in a compromise solution.

The study of suitability of aircraft solutions requires appropriate performance and weight models. The big variety of solutions, i.e., wide range of applications and diversity of hybrid arrangements results in a huge number of solution combinations. Furthermore, when a hybrid energy aircraft is included in the universe of possibilities (a Fuel Cell plus Battery for instance) it inherently generates a great number of combinations due to the possibility to explore different hybridization levels. A solution with 80% of total required power produced by the fuel cell and 20% remaining produced by a battery is an individual solution while 90% of power coming from a fuel cell and 10% from battery is another, so, one can imagine the big universe of solutions it becomes.

The aircraft conceptual design is a big analysis effort. From an aircraft mission specification (which includes range, payload, takeoff and landing field length, maximum cruise speed definition, etc) several variables like wing area, wingspan, flaps design and engine power, must be defined to generate a solution, (Raymer, 1999). By including the diversity of sustainable power source possibilities as well as eventual hybridization levels, the conceptual design becomes an even more intensive activity. In this context, fast and simple models, that are capable to provide performance, weight, and dimensions for a power solution from a given technology are crucial to enable engineers to study as many as possible combinations in the search for the best solution. In some cases, use of key performance indicators, a unique numeric ratio that defines a certain system or component feature, like efficiency (in %) or specific power (in kW/kg), for instance, are effective for modeling purposes. For some aspects or equipment, a key performance indicator is not accurate enough for conceptual design purposes. For this case, a parameterized model is the most indicated choice before a high-fidelity physical modeling is considered. Parameterized models are based on regression curves that correlate a system parameter of interest, like weight and efficiency, for instance, to a set of properly selected inputs, like maximum system power, for instance.

Specifically discussing the Fuel Cell technology, which will be the object of this work, its dependence on a large cooling system creates a natural need for effective parameterized models of

thermal management system as well. It is not a model for thermal management system detailed design, but a model for aircraft conceptual design, i.e., a model that is capable to provide weight, critical dimensions and drag.

The current study proposes the development of parametric model of a Fuel Cell Thermal Management System, suited for aircraft conceptual design. Such a model must deliver the thermal management system weight, drag and dimensions for a set of adequate inputs, i.e., inputs available at very early design stages. Although a parametric model is aimed as a result from this work, it will be developed upon physical models that represent the Fuel Cell heat rejection characteristics and the heat exchangers to address such a heat rejection. Since it is a model for aviation purpose, the thermal management system model must represent the best compromise between drag and weight. The parameterization work shall be done for a wide range of fuel cell maximum power and fuel cell limiting operating temperatures such that solution for a broad range of aeronautic applications is covered.

2 Bibliography Review

The bibliography review for the purpose of this work, which is to develop an aeronautical fuel cell thermal management system model, encompasses three research areas:

- Innovative Electrical or Hybrid power source Airplane Research
- Fuel Cell Technology
- Heat Management Systems Technology

2.1 Innovative Electrical or Hybrid Power Source Airplane Research

Many authors publish papers presenting design concept exercises of electrified or hybrid aircraft. Initiatives cover various types of applications: from very small applications, like a 1000 kg empty weight aircraft, studied by Castro et al. (2021), up to 180 passengers aircraft, studied by Kellermann et al. (2021), and include even more disruptive applications, as an electrified e-VTOL application, presented by Datta (2021). Study cases include many different architectural arrangements, testing both: single electrical power solutions or hybrid solutions, this last one covering thermal engines plus battery powered motor, fuel cell plus battery powered motor and fuel cell plus thermal engine solutions. As observed further, much use of parameterized models is found.

Palladino et al. (2021) presents a study to create a hybrid power alternative for an existing regional 70-80 pax aircraft. The proposed solution consists of a combination of a traditional gas turbine with an electric motor (powered by fuel cell), both linked to a common propeller gear box. This source performs a comprehensive conceptual design study varying the hybridization level, i.e., varying how much power for the propeller comes from the Fuel Cell and from the Gas turbine. Palladino et al. (2021) concludes, adopting current Fuel Cell technology status, that best CO_2 emissions reduction is achieved with 40% hybridization factor, i.e., 40% of the power coming from Fuel Cell and remaining coming from Gas turbine. The work does not provide deep discussion

regarding the Thermal Management design. For thermal management system, it uses a model based on a regression curve from off the shelf radiators found on industrial catalog and it does not cover the TMS drag aspect.

Kellermann et al. (2021) presents a discussion focused on the thermal management system from a hybrid electric aircraft. The most important TMS aspects for conceptual design are covered, which are weight and drag. This study is particularized for a 180 pax aircraft and investigates the TMS effects, as well as performs optimization exercises towards minimum fuel consumption, for a hybrid solution with electrical power up to 30% of the total required power. An important aspect of heat management system design is recapped by Kellermann et al. (2021) , the Meredith effect. Back in WWII, aircraft engines had to deal with high heat rejections demand, so a concept was brought up by Meredith (1935), standing for the idea that proper radiators design, equipped with adjustable area exhaust nozzles would minimize the cruise thermal management system drag and even create thrust. Such concept will be adopted in the present work.

Chapman et al. (2020) studies a thermal management system for an electric VTOL application (15 passengers). It covers the most important aspects of TMS: weight and drag and performs an optimization work. Chapman et al. (2020) proposes a method to optimize the radiator geometry. By looking at Figure 5 one can notice that a correlation between the Thermal Management System weight and the puller fan required power is established, i.e., the lighter the TMS the more power the puller fan requires. An objective function (delta fuel burn) is modeled as a function of the radiator weight and required puller fan power, and minimum value for this function selects the optimum radiator. Similar approach shall be used in the present work, but not the same cost function, since the one used by this work is proper for an e-VTOL application.

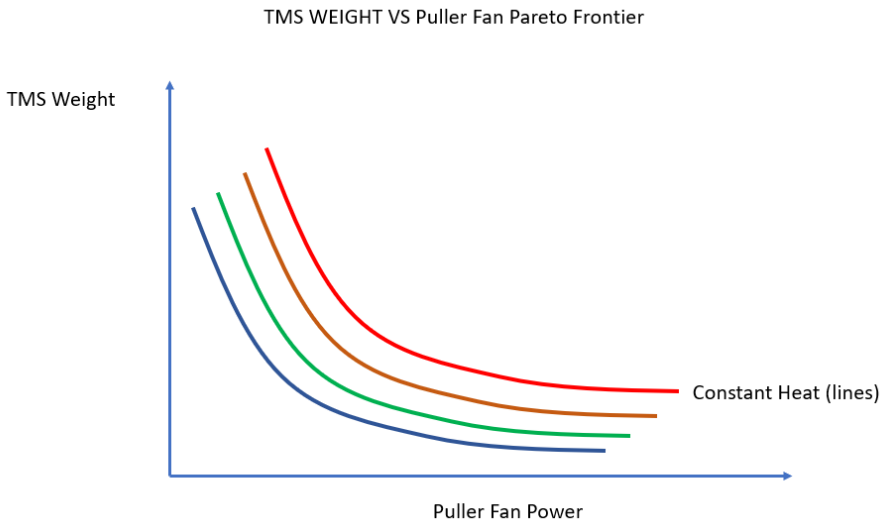

Figure 5 - TMS Design Pareto Frontier, adapted from Chapman et al. (2020)

Datta (2021) performs a complete design study of an e-VTOL application powered by electrical motors fed by Fuel Cell. The study includes a complete fuel cell design, an off-design modeling explanation. While its fuel cell modeling is based on physical principles, the Thermal Management System weight is based on parametric models, but it does not include drag. This study performs a tradeoff study in which the best solution between a minimum weight fuel cell design is compared against a higher weight but better efficiency fuel cell design. For the present work the Fuel Cell model structure proposed by Datta (2021) will be used but a more detailed Thermal Management System design technique will be adopted prior to parameterization.

Castro et al. (2021) performs a study to demonstrate fuel cell potential for a small aircraft. The exercise consists of replacing the piston engine currently installed in an existing small aircraft for a hybrid electric power solution (fuel cell plus battery). The study uses a key performance indicator for the thermal management system weight estimate, 1.14 kW/kg, based on catalog information. For the TMS drag, it does a simplification, assuming the new hybrid electric TMS drag as equal to the original airplane piston engine TMS drag, which is embedded on the original airplane drag polar.

An assessment to compare fuel cells with batteries as power source for electric motors in an e-VTOL application is presented by Ng and Datta (2019). The study includes an architecture powered by battery alone, a hybrid Fuel Cell plus battery architecture and a Fuel cell alone configuration. Ng and Datta (2019) concludes that the hybrid configuration is the best for longer than 50 miles missions, while, for shorter missions, the battery alone solution is better. This evaluation makes use of parameterized models for fuel cell stack, battery and electric motors, however, although thermal management system weight is quoted, no information is provided about the estimation technique.

All these studies make intense use of parameterized models, which are crucial for rapid conceptual design analysis. As a couple of examples, Figure 6 shows a radiator weight regression model used by Palladino et al. (2021) and Figure 7 shows a heat exchanger pulling fan weight regression model used by Chapman et al. (2020).

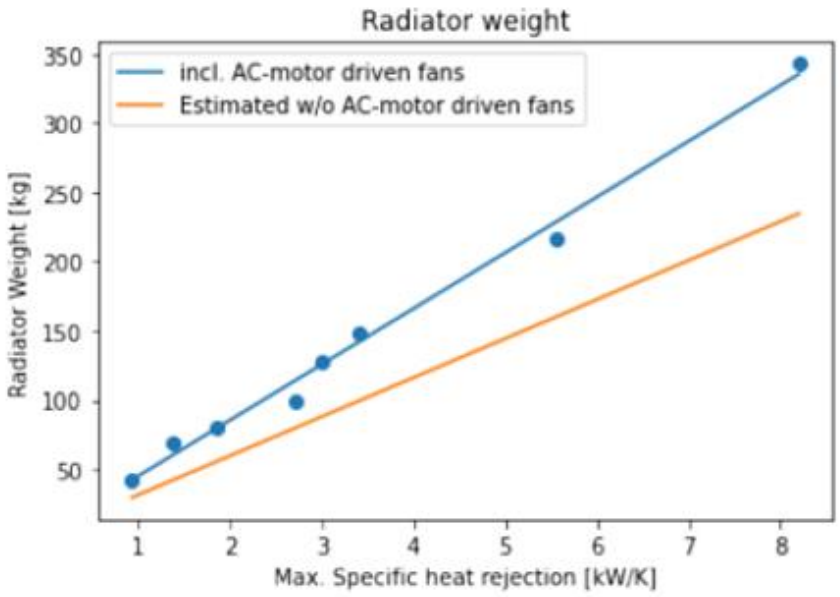

Figure 6 - Radiator Weight Model. Source: (Palladino et al, 2021)

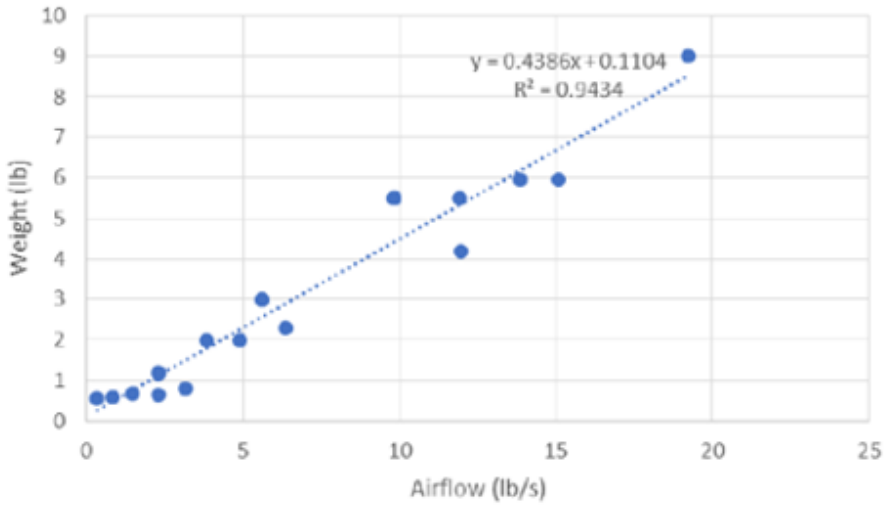

Figure 7 - Fan Weight models. Source: (Chapman et al., 2020)

While designing a dedicated solution for a certain application might be a very time-consuming activity for a conceptual design stage, trusting only individual components parameterized models or simplistic key performance indicators might be too inaccurate. Focusing on the Thermal Management System, for low heat demand applications, a regression model based on industrial radiator catalog can be enough, because errors associated do not cause a significative influence on the total aircraft weight. However, a thermal management system for a high heat dissipation system represents a big proportion of the airplane weight, so a more carefully developed model, but not necessarily a full detailed design, will provide more appropriate results. A compromise between model complexity and accuracy is the key for a productive and reliable concept design.

2.2 Fuel Cells Technology and Modeling

Dicks and Rand (2018) details the modeling approach, which includes the thermochemical equations application to the $H_2 + O_2$ reaction to obtain the Fuel cell ideal and real reversible voltages. According to Dicks and Rand (2018), Fuel Cells also present four sources of losses: activation losses, ohmic losses, leakage losses and concentration losses, which are modeled as

voltage losses. Discounting voltage losses from the reversible voltage produces the fuel cell real irreversible voltage, which can be plotted against the operating current, forming the fuel cell polarization chart.

For real data gathering, Chugh et al. (2020) and Laurencelle et al. (2001) present the results of a modeling exercise supported by experimental data, in which the polarization curve from a Ballard fuel cell is obtained.

Datta (2021) also presents results and detailed discussion for a fuel cell performance modeling. It includes data from a baseline commercial fuel cell and a Modern Fuel Cell, which equips the commercially available fuel cell powered automobile: Toyotta Mirai. It uses the classical thermo-chemical equations for the reversible voltage calculation and describes, with detail, the model for voltage losses. Datta (2021) demonstrates the Fuel Cell performance sensitivity to the reactants pressures and presents performance at different operating pressure levels. A turbo-compressor system to feed Fuel Cell is incorporated to the studies. Not only performance but also weight calculation methods are presented for all required systems.

When debating power and energy solutions for transport applications, especially aircraft, as important as modeling the performance of a Fuel Cell is to be able to calculate its weight. Datta (2021) details method to calculate the weight of the fuel cell starting from its design specification. According to Datta (2021) calculations, a modern fuel cell stack, that is, a similar model to Toyotta Mirai automobile Fuel Cell, presents a power density ranging from 2 kW/kg to 3 kW/kg.

Dicks and Rand (2018) discusses the required accessories for a Fuel Cell operation. Fuel Cell operates with continuous H_2 an O_2 flows at proper temperature and pressure. A compressor system is required to provide adequate pressures and flows from reactants. A temperature control system is also required so that Fuel Cell reactants operate at most suitable temperature condition. This reference not only introduces the need for the balance of plant (all equipment that is required so that fuel cell may operate properly) but also presents a way to calculate its influence on performance.

Modeling fuel cell includes not only the determination of its performance, that is, calculating its available power and consumed fuel flow (gaseous H_2), but also the amount of heat that must be dissipated. In very basic terms, heat can be calculated from difference between the total power provided by H_2 flow and the actual electrical delivered power, as indicated by Datta (2021) .

Palladino et al. (2021) presents a chart (Figure 8) that demonstrates the energy flow distribution along with the fuel cell processing, allowing a rough order of magnitude heat estimation. Such a picture is useful as illustration, but the present work will, however, calculate the heat dissipation based on the fuel cell working principles.

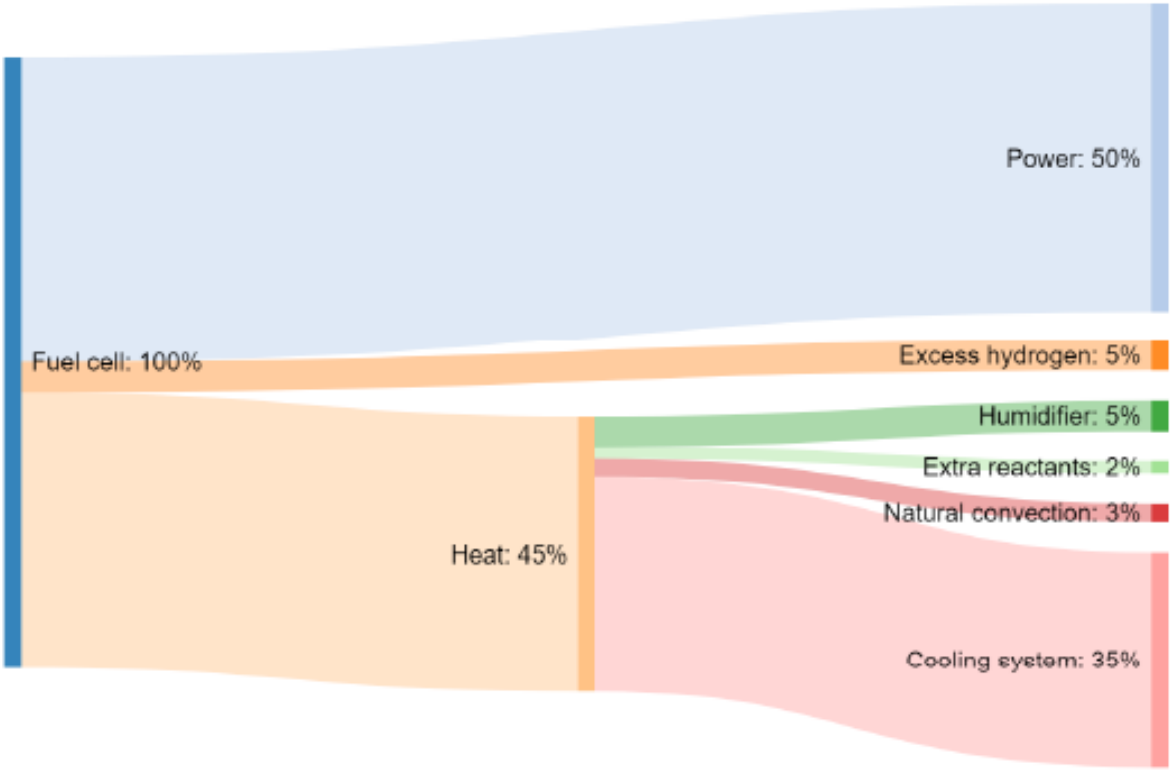

Figure 8 - Fuel Cell Heat and Power Flow Chart, Source: (Palladino et al, 2021)

All references quoted so far treat the steady state operation of fuel cells, but the transient behavior may be an important factor in some airplane operation situations. At the takeoff acceleration, for instance, the initial air dynamic pressure is too low, so airflow passing through

the TMS heat exchangers may be not satisfactory. In other hand, the takeoff run is a short phase, so, there is a possibility that the transient fuel cell heating can compensate the lack of air flow at this condition. The review of a collection of publications focused on fuel cell modeling is found on Rubio and Agila (2019) which includes transient model's research. Peng et al. (2020) present a heat transfer transient model based on CFD analysis. Huang and Li (2009) and Adzakpa et al. (2008) present dynamic fuel cell models and include experimental validation. Although the transient at takeoff may be a concern, these studies present fuel cell temperature stabilization times on the order of minutes, which is longer than a takeoff run, indicating that the fuel cell transient heating might be a compensation for the lack of air flow, thus, such investigation is recommended as subject for future works. The present work is, however, focused on steady state situations.

2.3 Thermal Management System

Despite of being counter-intuitive, fuel cell thermal management system design recovers discussions held back in 1930s when WWII aircraft, equipped with piston engines, required huge heat dissipation and a careful heat management design. Miley (1988) categorically states that the state of the art in terms of aircraft liquid cooling systems is still in WWII time and presents a series of installation concepts and design references that have been produced in pre-War period and a few years later. Katzoff (1948) presents method to calculate losses at air cooling ducts, based on experimental work, and dedicated to aircraft engines cooling systems. Although numerical design methods like CFD are broadly available nowadays, experimental methods are a powerful tool for conceptual design, mainly because these are so simple to apply, leaving a deep and sophisticated optimization CFD work for further stages of a project. Therefore, when discussing cooling ducts performance this work uses methods published by Katzoff (1948).

An important concept, the Meredith effect, is a powerful design practice and is considered in this work. Developed a few years before WWII start, it is still an up-to-date concept, as Piancastelli et al. (2015) confirms. Meredith (1935) demonstrates the Meredith effect in a study about thermal management system design for a liquid cooled aircraft piston engine. Meredith (1935) makes a theoretical development to demonstrate that performing a proper thermal management system design may not only minimize its drag but even provide thrust in cruise

conditions. A proper design should include large heat exchange frontal areas and variable exhaust area nozzles to actively control the radiators air flow. Meredith (1935) recognizes that external surface area may increase by installing big radiators in the aircraft, which increases overall wetted area, and the drag consequently, but it argues that the tradeoff is positive. A discussion about large radiator frontal area will be included in this work but is worth mentioning that volumes allocation in an aircraft is an activity very particular from each aircraft configuration and this work does not treat individual designs. While Katzoff (1948) provides means to calculate cooling system air ducts pressure losses, Gudmundsson (2014) provides theoretical approach to calculate the cooling system drag, based on the air flow and pressure losses, and this approach is used in this work.

Thulukkanam (2013) discusses all types of heat exchangers, design and modeling technique, and associated advantages from each type and associated problems. According to Thulukkanam (2013) compact heat exchanger types are the most suitable for mobile applications, which shall be the focus of this work. Thulukkanam (2013) provides performance data for a few set of radiators, but information that allows weight estimation of the radiators is not provided.

The compact heat exchangers design finds a comprehensive source of information at Kays and London (1984), which describes methods to design compact heat exchangers, calculate required air flow and air flow side pressure losses. It provides performance maps associated to the described performance calculation methods for a variety of heat exchangers, as well as it provides core geometry data like fins and tubes thickness, tubes diameters, fins spacing which can be used to calculate the radiator weight.

With heat exchangers design data and methods from Kays and London (1984), cooling ducts pressure losses models from Katzoff (1948) and drag estimate as recommended by Gudmundsson (2014), a complete design routine will be produced, which will deliver as results the radiator dimension, weight and drag.

Although no great advancements in liquid cooling systems are observed in the current aviation operating fleet, as Miley (1988) states, Academy and Industry are researching and producing solutions that can be adopted in systems that require high levels of heat exchange, like fuel cells.

Mezzotech (n.d.) describes its high-performance radiators, which incorporates microtubes technology, which is a new technology of heat exchangers that reduces air side pressure drop.

According to Mezzotech (n.d.), up to 40% reduction in the pressure drop on the air flow side can be reached and this technology is being used in racing cars. Such a technology can be a leverage for high heat exchange demanding systems.

An experimental work published by Wen-Jei and Clark (1975) demonstrates the possibility to improve the heat exchanger efficiency by applying a water spray on the surface of the heat exchanger fins. Wen-Jei and Clark (1975) show the benefits of spraying water in the heat exchanger for a range of Reynolds numbers and water atomization factors and demonstrate improvements that may reach 50% on the air side convective factor.

A patent granted by Clarke et al. (2022) reveals an integral thermal management system architecture for a Fuel Cell to power a regional aircraft. The thermal management system makes use of water spray for its heat exchange efficiency enhancement. The patent uses the water that is produced by the Fuel Cell itself, i.e., no water tank is required.

Sozer et al. (2020) performs CFD analysis to demonstrate the potential for use of outer mold line heat exchanger. The idea behind outer mold line heat exchanger is using airplane skin as means to exchange heat with atmosphere. Sozer et al. (2020) obtains significant heat flux results for airplane surfaces, such as fuselage, engine nacelles and wing: ranging from 4 kW/m^2 to 11 kW/m^2 at hot day takeoff condition and from 12 kW/m^2 to 20 kW/m^2, in cruise condition.

Yoshida and Kojima (2015) present its efforts to develop the Fuel Cell power train for the Toyotta Mirai. An important fact is demonstrated: the effect of the fuel cell operating temperature on the thermal management system. According to Dicks and Rand (2018) PEM fuel cells operate within a range of 50°C to 150°C while Yoshida and Kojima (2015) conclude that increasing the fuel cell temperature from 80°C to 120°C may reduce radiator size to 50% of its current size. Therefore, parameterized model from current work shall consider a variation in the fuel cell operating temperature.

Uniting fuel cell technology and thermal management concerns, Bargal et al. (2020) presents potential improvements under research and identifies three major areas of investigation: Fuel Cell coolant flow field, Fuel Cell coolant channel geometry and Use of Nanofluids as Fuel Cell coolant. It is worth emphasizing that these improvements are inherent to the Fuel Cell internal design. The present work is concentrated, however, in the external thermal management system, focusing on aspects of the radiator design and integration.

Although efforts to reduce impact of heat dissipation systems are being conducted, this work focus on a specific configuration of TMS, adopting conventional heat exchangers with no heat exchange enhancement system, leaving it for future research. The TMS configuration proposed in this work includes, however, Meredith effect and concepts, pursuing a suited heat exchange radiator design for aircraft application, adoption of variable area nozzle to control radiator air flow. The effects of fuel cell operating temperature is also investigated.

3 Problem Importance and Objective

As exposed, World ambient temperature is rising over the years and science has demonstrated it through extensive research. Relationship between the global warming and the human activity, mainly due to the CO_2 emissions in the atmosphere, has been established by scientific work as well.

Regulation, policy makers and monitoring agencies around the world follow the global warming issue as much as its relationship to the aspects of the human activity and create plans for recovery within their scope of activity, which includes not only time goals for CO_2 reduction, but also investments on carbon free or Net Zero emissions technologies survey.

Aviation responds for an important portion of the total CO_2 emissions. Research to reduce carbon footprint from aviation includes an intensive survey of configurations using no carbon emitting power sources. Battery powered, fuel cell powered or hybrid solutions (battery plus thermal engine, fuel cell plus thermal engine or fuel cell plus battery) integrate an enormous diversity of evaluations on the chase for viable green solutions. Evaluations consist of aeronautical concept sizing efforts which calculates airplane capabilities when adopting the new electrical technologies. In majority, studies use parameterized models and key performance indicators instead of high-fidelity physical models, which is a very effective and efficient approach for conceptual design phase, while a detailed design is a very time-consuming activity.

The use of simplistic models must, however, be judged with respect to its compatibility to expected accuracy. Systems that do not represent great portion of airplane weight may be represented by simple models with not much fidelity. On the contrary, a system that takes relevant part of the aircraft weight needs higher fidelity models.

In general, references do not treat fuel cell heat management systems with a degree of detail that such significant system seems to require. However, very complex models are not suitable for a conceptual design stage either.

A compromise between simplistic modeling approach and a more sophisticated model, such that fast analysis and fast adaptation to several scenarios is possible, but still with reasonable

accuracy, is a powerful and necessary tool to assist the current effort on the search for carbon emission free products.

3.1 Objectives

3.1.1 General Objective

The purpose of this work is to create a parameterized model for fuel cell thermal management system that delivers, as outputs, its weight, dimensions and drag as function of the fuel cell power and fuel cell operating temperature.

Ideally, it is expected that TMS weight, main dimensions and drag can be calculated as a simple function (a polynomial function for instance) of the fuel cell power and fuel cell operating temperature.

Figure 9 provides an illustration of the type of model that is being pursued:

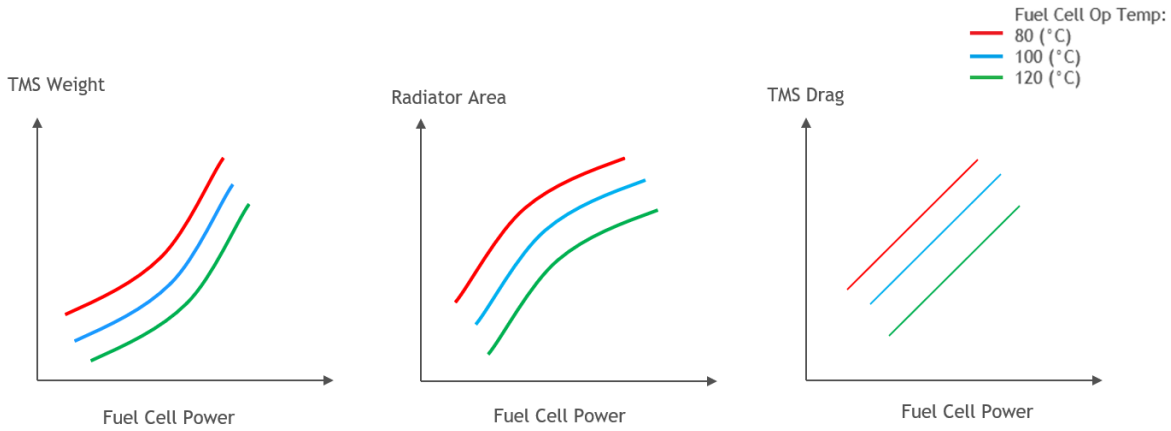

Figure 9 - Thermal Management Parametric Model Notional Shape

Note: The curves shapes are illustrative only and do not necessarily represent an expected result.

As success criteria, it is expected that the TMS parameterized models result in smooth curves, monotonically increasing and good correlation properties.

3.1.2 Specific objectives

Accomplishing final objective, which is producing a parameterized fuel cell thermal management system model, requires the following developments:

- A fuel cell performance model (described in Section 4.3), which provides the required heat dissipation of the fuel cell,
- A thermal management system model (described in Section 4.4), which includes:
    - Radiator heat exchange capability routine which calculates, for pre-specified radiator (one whose frontal area, depth and internal geometry has been chosen), the required air flow to match a certain required heat exchange, and resultant radiator air side pressure drop
    - Cooling system air side circuit flow calculation, which takes as inputs the inlet air total pressure, the radiator pressure losses, cooling duct pressure losses, exhaust nozzle characteristics and returns, as output, a solution validity status (if such air flow inlet pressure is enough to overcome the circuit pressure losses) and the resulting Drag.
    - A routine that calculates the whole thermal management system weight
    - A routine that tests a population of radiators, performs an optimization loop and selects the best weight versus drag individual
- Model parameterization exercise (described in Section 5), which is the creation of a regression model for the TMS weight and drag, by correlating it to a range of top-level inputs such as fuel cell power, operating temperature and other parameters that the sensitivity analysis may indicate as needed.

4 Theoretical Development for Modeling

4.1 Overall Idea

The development of the parametric thermal management system model for a fuel cell application requires the development of a physical model first. The physical model is based on the physical behavior of the main components of the model and appropriate numeric data for each component.

Once developed, the physical model will be run at several conditions within a range of interest (varying Fuel Cell power and operating temperature) to calculate the TMS parameters: weight, radiator required frontal area and drag for each condition. A range of fuel cell output power and operating temperatures will be defined for such excursion: from 900 kW to 2900 kW (defined with rational presented in Appendix B) and from 80°C to 120°C (which is within temperature range suggested by Dicks and Rand (2028) for proton exchange membrane fuel cell).

After running the model to all these combinations, the TMS parameters such as weight, radiator frontal area and drag will be plotted against fuel cell temperature and power level to verify if a good curve fit can be obtained.

4.2 Physical Model Development

The physical model has two main branches:

- Fuel cell, and
- Thermal management System

The fuel cell model runs to a certain required power (within its operating range) and provides as output the required heat dissipation demand.

The thermal management system model receives the heat dissipation demand and operates in two different modes: design mode and off design mode.

In design mode, the thermal management system model operates to find all thermal management specification that are required to dissipate the fuel cell generated heat: radiator geometry (frontal area and depth), coolant fluid lines, reservoir, coolant pump and air flow exhaust area. Along with the geometry, the thermal management system model, in design mode, will deliver the weight of the system and the drag at the design condition

In off design mode, given that all thermal management systems specs have been determined in design mode, the model is capable to calculate the required air flow for a desired heat dissipation, and the resulting drag, at any flight condition. It is worth mentioning that an off-design mode run can only be done after a design mode run.

Figure 10 illustrates the data flow in the two modes (design mode and off-design mode)

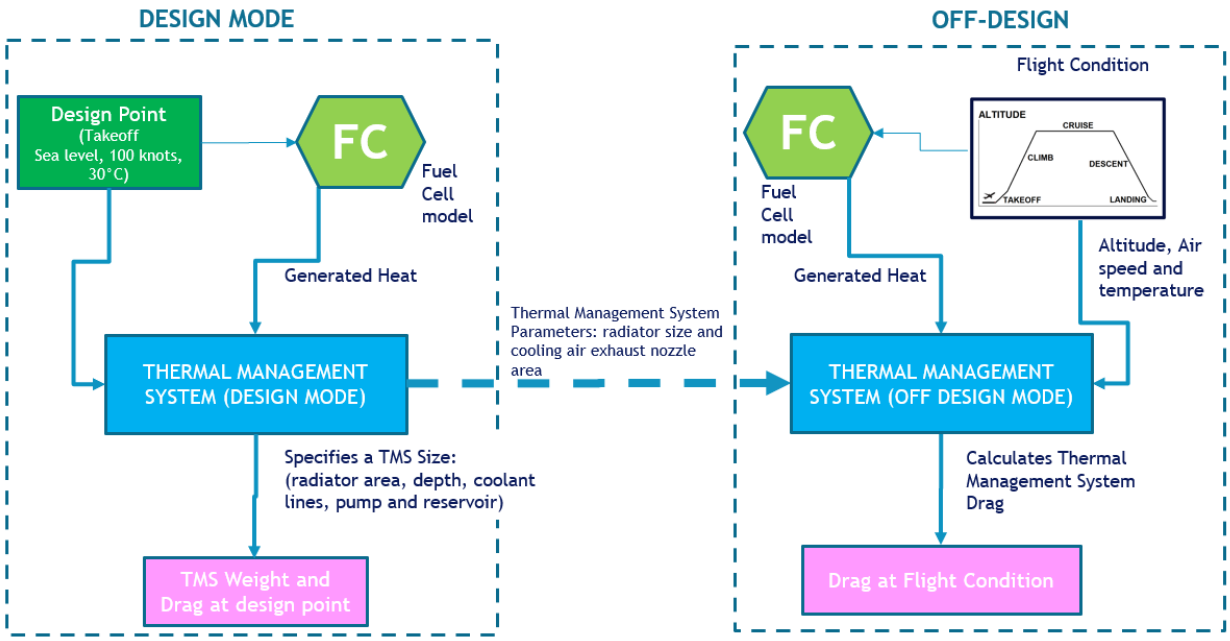

Figure 10 - Thermal Management System Model Data Flow

4.3 Fuel Cell Physical Modeling

This section is dedicated to the fuel cell heat sources calculation procedures, which shall be used for the thermal management system developments. It starts with the fuel cell system architecture followed by a physical modeling.

4.3.1 Fuel Cell Architecture

The fuel cells require a set of equipment to operate, which includes a hydrogen supply tank, a supercharger or turbo-compressor for external air flow feeding, Air and H_2 pressure and temperature control devices and a cooling circuit for the fuel cell itself. A schematic for a fuel cell and surrounding systems can be verified in Figure 11.

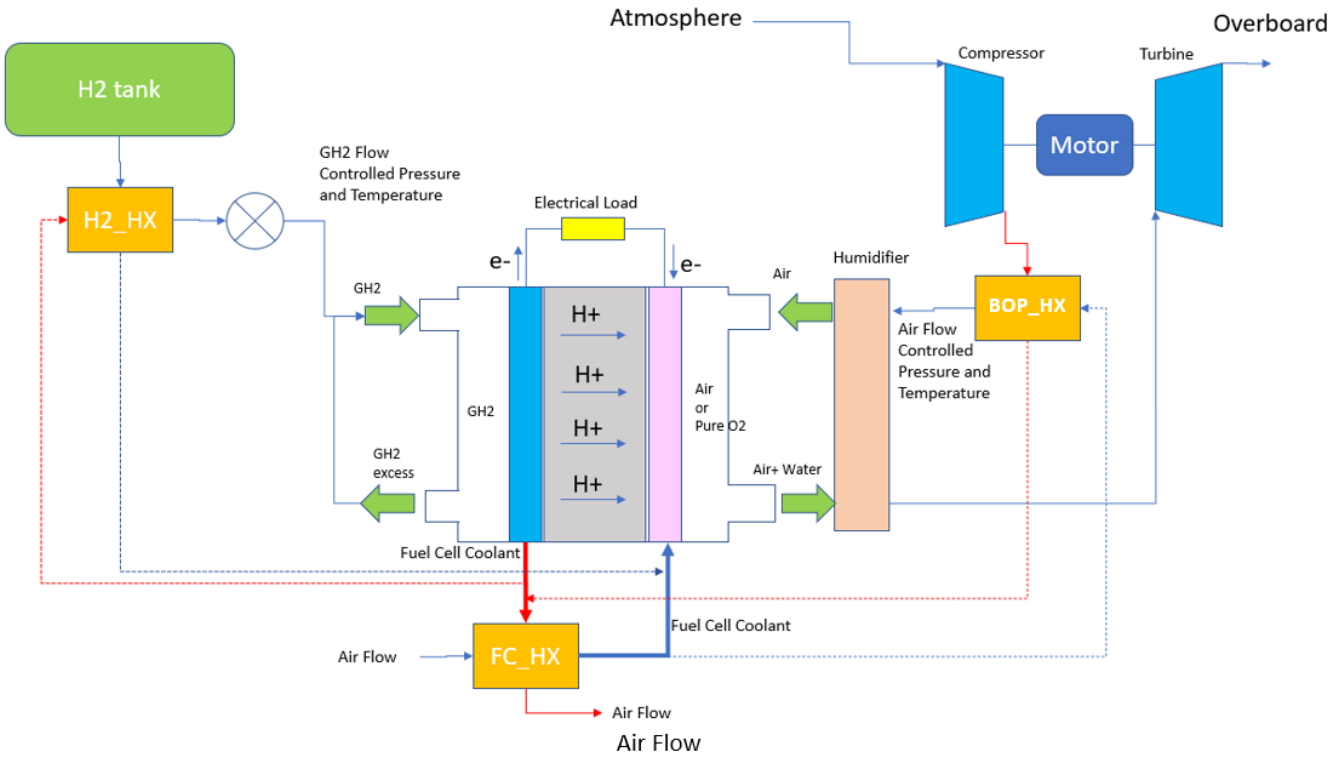

Figure 11 - Fuel Cell and Thermal Management Architecture

Figure 11 shows the hydrogen tank feeding a heat exchanger (H2_HX) installed with purpose to control the hydrogen flow temperature. Downstream this heat exchanger, a regulating valve controls the hydrogen flow pressure to suitable value for the fuel cell operation. The hydrogen flow enters the anode where it is separated in protons and electrons, the first flowing through the electrolyte and the second flowing through the circuit. The fuel cell operating air flow comes from the atmosphere and passes through an air compressor, to get suitable pressure for the fuel cell operation. The air compressor does not only compress the air flow but warms it as well, which is a normal flow machine behavior. Downstream the compressor outlet, an air heat exchanger (BOP_HX) is installed to control the air flow temperature to an adequate value for the fuel cell operation. This fuel cell air feeding device is known as balance of plant (BOP). After exiting the air heat exchanger, the air flow passes through a humidifier, capturing some water content from the Fuel Cell exhaust air/water mixture to humidify itself, which is critical for the fuel cell performance, as Dicks and Rand (2018) points out.

The air and water mixture that exits from the fuel cell expands in a turbine that extracts its energy to assist the air compressor work. The power consumed by the compressor is higher than the powered recovered by the turbine, so a motor to complement the required power is installed in the same shaft.

The fuel cell presents losses that are modeled as voltage losses and current leakages. The losses become heat, which needs to be removed from the fuel cell electrolyte, cathode, and anode, so that its temperature remains within their operating limits.

A cooling system, represented by a fuel cell coolant line and heat exchanger (FC_HX), performs, respectively, the absorption of the fuel cell generated heat and dissipation into the atmosphere air flow.

In summary, the Fuel cell system TMS includes three heat exchangers, indicated in Figure 11, each with a specific temperature control purpose. The Fuel Cell heat exchanger (FC_HX) uses external atmosphere air flow for the fuel cell coolant cooling. It is important to notice that both the fuel cell air flow temperature control heat exchanger (BOP_HX) and the hydrogen flow temperature control heat exchanger (H2_HX) use a derivation from the fuel cell coolant, the first to cool down the compressed air flow and the second to warm up the hydrogen flow.

It is important to remark that this work concentrates efforts to specify a system based on heat dissipation to the atmosphere air (typically called ram air thermal management). Use of forced cooling techniques like a vapor cycle machine is not under the scope of this work.

4.3.2 Fuel Cell Performance Model

As stated, the fuel cell is an apparatus that operates with the water formation reaction and absorbing its released energy as illustrated in Eq 4.1

$$H_2 + \frac{1}{2}O_2 \rightarrow H_2O(liq) + \frac{energy}{mole} \qquad \text{Eq 4.1}$$

The fuel cell performance model is based on the formulation and further development of the Free Gibbs energy equation (Eq 4.2):

$$\Delta g = \Delta h - T\Delta s \qquad \text{Eq 4.2}$$

Where:

$$\Delta h = h_{H_2O} - h_{H_2} - h_{O_2} \qquad \text{Eq 4.3}$$

And:

$$\Delta s = s_{H_2O} - s_{H_2} - s_{O_2} \qquad \text{Eq 4.4}$$

Equations 4.3 and 4.4 are valid for a standard reference pressure at which products and reactants enthalpy and entropy are tabulated.

At a non-standard pressure environment, the Gibbs free energy receives a correction based on the reactants and products pressures ratios (actual pressure divided per standard reference pressure):

$$\Delta g = \Delta h + \Delta s + R\ T\ ln\left(\frac{P_{H_2O}}{P_{H_2}\ P_{O_2}^{\frac{1}{2}}}\right) \qquad \text{Eq 4.5}$$

Enthalpy and entropy from products and reactants at standard reference pressure (101325 Pa) can be calculated as a function of reaction temperature, through Shomate (1954) equations:

$$h = A\,t + \frac{B}{2}\,t^2 + \frac{C}{3}\,t^3 + \frac{D}{4}\,t^4 - \frac{E}{t} + F - H \qquad \text{Eq 4.6}$$

$$s = A\,ln\,(t) + B\,t + \frac{C}{2}\,t^2 + \frac{D}{3}\,t^3 - \frac{E}{2t^2} + G \qquad \text{Eq 4.7}$$

Where t is equal to the fuel cell temperature (T) divided by 1000.

Coefficients for calculations of equations 4.6 and 4.7 can be found at Table 2

Table 2 - Shomate equations coefficients, Source: (Chase and Jr, 1998)

	H_2O	H_2	O_2
A	-203.606	33.066178	31.32234
B	1523.29	-11.363417	-20.23531
C	-3196.413	11.432816	57.86644
D	2474.455	-2.772874	-36.50624
E	3.855326	-0.158558	-0.007374
F	-256.5478	-9.980797	-8.903471
G	-488.7163	172.707974	246.7945
H	-285.8304	0	0

From the enthalpy variations and free Gibbs energy variation, obtained from the fuel cell reaction, two fuel cell voltage definitions are formulated: the ideal reversible voltage (Eq 4.8) and the true reversible voltage (Eq 4.9), both calculated with Nernst equation.

$$E_h = -\frac{\Delta h}{N\,F} \qquad \text{Eq 4.8}$$

$$E_r = -\frac{\Delta g}{N\,F} \qquad \text{Eq 4.9}$$

Where N is the number of electrons per Hydrogen molecule (2) and F is the Faraday constant (Coulomb/mole)

For notion of values, at 1 atm and 80°C, E_h = 1.45 V and E_r = 1.17 V.

Neither Eh or Er can be assumed as the actual fuel cell delivered voltage. Fuel cells present electrical losses. Dicks and Rand (2018) identify four mechanisms of losses as escribed in table 3.

Table 3 - Fuel Cell Types of Losses, Source: (Dicks and Rand, 2018)

Loss	Description
Activation	Voltage drop to activate reaction
Ohmic Losses	Resistance to the electrons flow through electrodes
Concentration or Mass Transport	Loss due to concentration variation in the electrodes
Internal Currents and fuel cross over	Current and fuel passing through the membrane

A fuel cell performance model requires that such losses are modeled. Datta (2021) presents an equation to calculate the fuel cell real voltage (Eq 4.10)

$$v = E_r - loss_{act} - loss_{ohmic} - loss_{conc} \qquad \text{Eq 4.10}$$

Note: the internal currents and fuel cross over are not included in this equation but it will be treated as current leakage in further developments.

O'Hayre et al. (2016) proposes the formulation for each loss according to equations 4.11 and 4.13.

$$loss_{act} = a_A + b_A\ ln(i + i_{leak}) + a_C + b_C\ ln(i + i_{leak}) \qquad \text{Eq 4.11}$$

$$loss_{ohmic} = i\ ASR \qquad \text{Eq 4.12}$$

$$loss_{conc} = C \ \ln \frac{i_L}{i_L - (i - i_{leak})} \qquad \text{Eq 4.13}$$

From equations 4.11 to 4.13, Losses Equations are dependent on the fuel cell operating current and a set of constants (a_A, b_A, a_C, b_C, ASR, i_{leak} and i_L) which are particular from each fuel cell and experimentally demonstrated. Datta (2021) presents a fuel cell polarization curve (Figure 12), which is the real fuel cell voltage (v), calculated with equation 4.10, plotted against the operating current density (current per area unit). This data will be used as base for the fuel cell performance and heat calculations as explained in the sequence of this section.

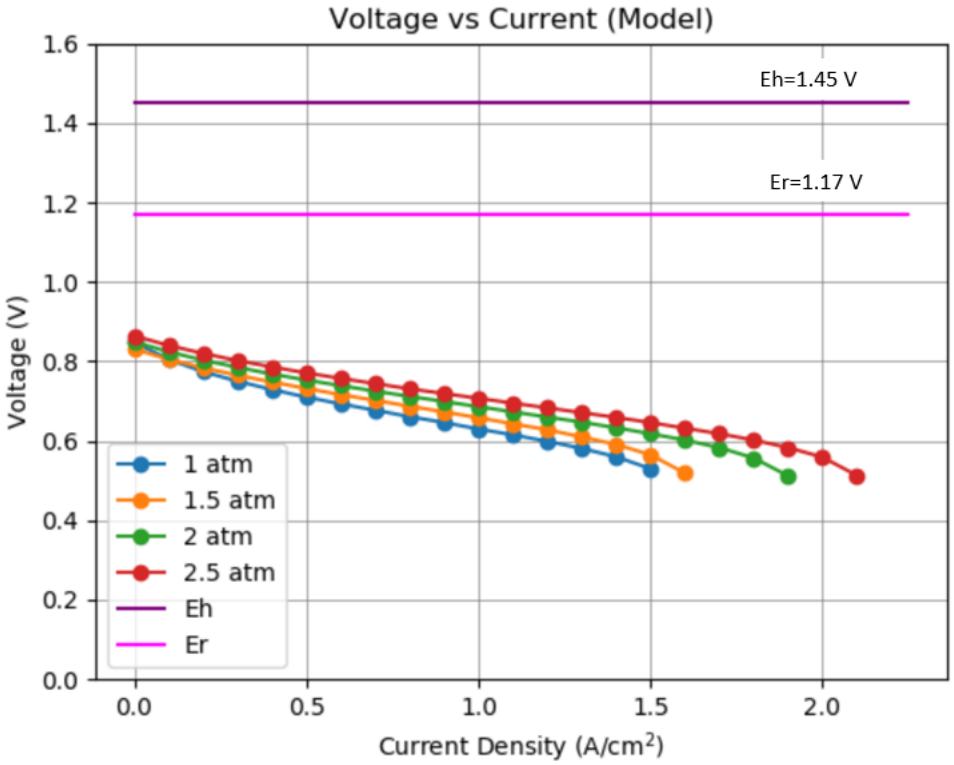

Figure 12 - Voltage vs Current Density Chart, adapted from Datta (2021)

Note: Appendix A Table 10 presents the values in Figure 12.

From voltage versus current density chart, it is possible to obtain the power density versus current density chart, calculated with equation 4.14. The result is demonstrated in Figure 13.

$$FC\_Power\_Norm = i\ v \qquad \text{Eq 4.14}$$

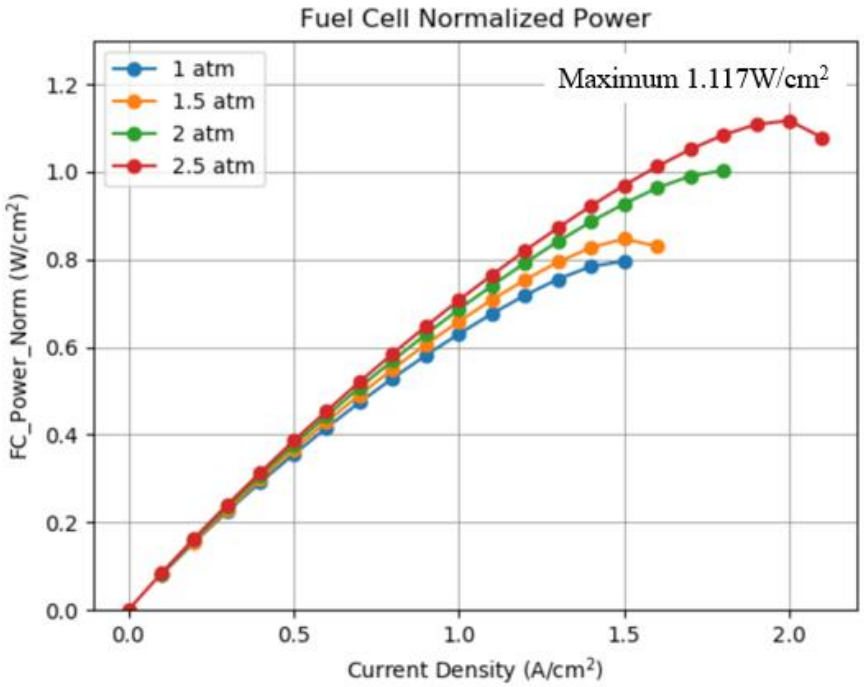

Figure 13 - Power vs Current Chart, adapted from: Datta (2021)

Note: Appendix A Table 11 presents the values in Figure 13

Charts from Figure 12 and Figure 13 show performance from a single fuel cell, normalized per area unit. A fuel cell stack system includes an assembly that comprises a cell area (Afc) and a series of cells (Ncells). Figure 14 shows a very simple schematic of a fuel cell stack which define the two variables for a fuel cell stack power calculation (Number of cells, which multiplies the voltage from a single cell, and the area which multiplies the current area density). 1.117W/cm^2

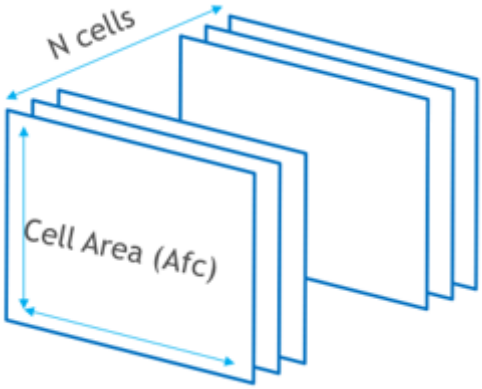

Figure 14 - Fuel Cell Stack Arrangement

Equation 4.15 shall be used to calculate the total Fuel Cell Stack power.

$$FC\_Stack\_Power = v\ i\ N_{cells}\ A_{FC} \qquad \text{Eq 4.15}$$

As important as calculating the Fuel Cell Stack power is to calculate the demanded Hydrogen Flow. That can be done with the conversion of fuel cell current to moles of hydrogen per second, through the Faraday constant (F) and number of electrons per hydrogen molecule (N), then from moles of hydrogen per second to hydrogen mass flow, through the hydrogen molar mass flow (m_{H_2}), and all multiplied by the stack product ($A_{FC}\ N_{cells}$). Equation Eq 4.16 expresses this conversion, as proposed by Datta (2021)

$$W_{H_2} = m_{H_2} \frac{(i+\ i_{leak})}{N\ F} A_{FC}\ N_{cells} \qquad \text{Eq 4.16}$$

Note: the current term of the equation 4.16 includes i_{leak} (leakage current density), which represents the Internal Currents and fuel cross over losses.

Datta (2021) shows values for the leakage current density, for various fuel cell operating pressures (Table 4)

Table 4 - Leakage Current varying with operating pressure, adapted from Data (2021)

Pressure (atm)	1.0	1.25	1.5	2.0	2.5
Leakage Current (A/cm^2)	0.15	0.15	0.20	0.25	0.30

From FC_Stack_Power (Eq 4.15) and Hydrogen Mass flow equation (Eq 4.16) it is possible to generate a performance chart as illustrated in Figure 15. Notice that a stack arrangement has been created to provide a maximum power of 1000 kW, which was obtained by a number of cells and fuel cell area product ($A_{FC}\ N_{cells}$) of 900000.

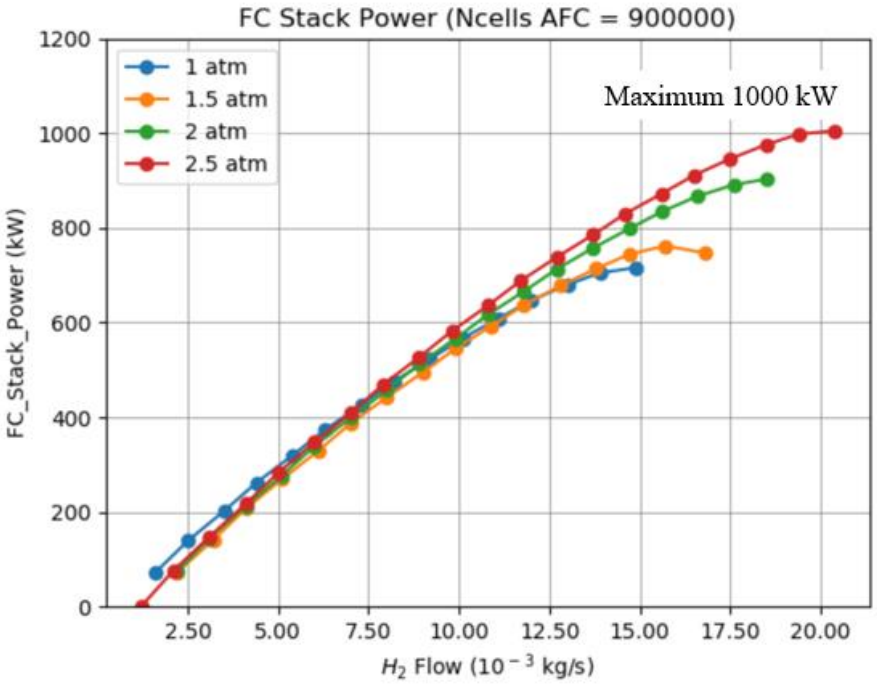

Figure 15 - Power Chart vs Hydrogen Flow

Note: Appendix A Table 12 presents the values in Figure 15.

For the heat calculation, Datta (2021) proposes an efficiency term (equation 4.17), based on the fuel cell voltages (real irreversible and ideal reversible) and fuel cell currents (operating and leakage currents)

$$\eta = \frac{v\ i}{E_h(\ i + \ i_{leak})} = \frac{FC\_Stack\_Power}{FC\_Stack\_Heat + FC\_Stack\_Power} \qquad \text{Eq 4.17}$$

With the efficiency term, the dissipated heat can be calculated, as demonstrated in equation 4.18

$$FC\_Stack\_Heat = \frac{FC\_Stack\_Power}{\eta} - FC\_Stack\_Power \quad \text{Eq 4.18}$$

Regarding the heat generated, an important discussion needs to be made, part of the heat is consumed by water vaporization. Since a cooling system parametric model is the purpose of this work, defining the amount of heat that is consumed by water vaporization is important to identify how much remaining heat is really removed by the cooling system.

Water and air flow masses can be calculated through stoichiometric relationships (equations 4.19 to 4.21):

$$W_{O_2} = 0.5 \frac{m_{O_2}}{m_{H_2}} W_{H_2} \quad \text{Eq 4.19}$$

$$W_{H_2O} = W_{O_2} + W_{H_2} \quad \text{Eq 4.20}$$

$$W_{Air} = \frac{W_{O_2}}{0.21} = 38.1 W_{H_2} \quad \text{Eq 4.21}$$

According to Datta (2021), excess of air flow is required for the proper working the fuel cell and a factor to 2 to 2.5 is recommended. So, if assuming 2 as the excess factor, fuel cell air flow is given by equation 4.22:

$$W_{Air} = 76.2\, W_{H_2} \quad \text{Eq 4.22}$$

Datta (2021) presents a path to calculate the heat consumed by the water vaporization. First, it is necessary to calculate the amount of water that can be absorbed by air in vapor format. Buck (1981) proposes an empirical set of equations to calculate it (equations 4.23 to 4.31):

$$\alpha = (18.678 - \frac{Temp_{degC}}{234.5})(\frac{Temp_{degC}}{257.14 + Temp_{degC}}) \quad \text{Eq 4.23}$$

$$P_{WS} = 611.21\, e^{\alpha} \quad \text{Eq 4.24}$$

Where Pws is the water saturation pressure. The vapor saturation ratio can be determined by equation 4.25

$$h_{WS} = 0.622 \frac{P_{WS}}{P - P_{WS}} \quad \text{Eq 4.25}$$

Equations 4.26 to 4.31 allow to finally determine the amount of water in liquid and vapor conditions:

$$If\ h_{WS}\, W_{Air} \geq W_{H_2O} \quad \text{Eq 4.26}$$

$$W_{H_2O\_vap} = W_{H_2O} \quad \text{Eq 4.27}$$

$$W_{H_2O\_liq} = 0 \quad \text{Eq 4.28}$$

$$\text{If } h_{WS}\, W_{Air} < W_{H_2O}: \quad \text{Eq 4.29}$$

$$W_{H_2O\_vap} = h_{WS}\, W_{Air} \quad \text{Eq 4.30}$$

$$W_{H_2O\_liq} = W_{H_2O} - W_{H_2O\_vap} \quad \text{Eq 4.31}$$

Once the water vapor formation portion is calculated, it is possible to calculate the heat that is consumed by the vaporization by application of the latent water vaporization heat described in Eq 4.32.

$$Q_{vap} = L_{H_2O\_vap}\, W_{H_2O\_vap} \quad \text{Eq 4.32}$$

Water vaporization latent heat can be obtained from Figure 16.

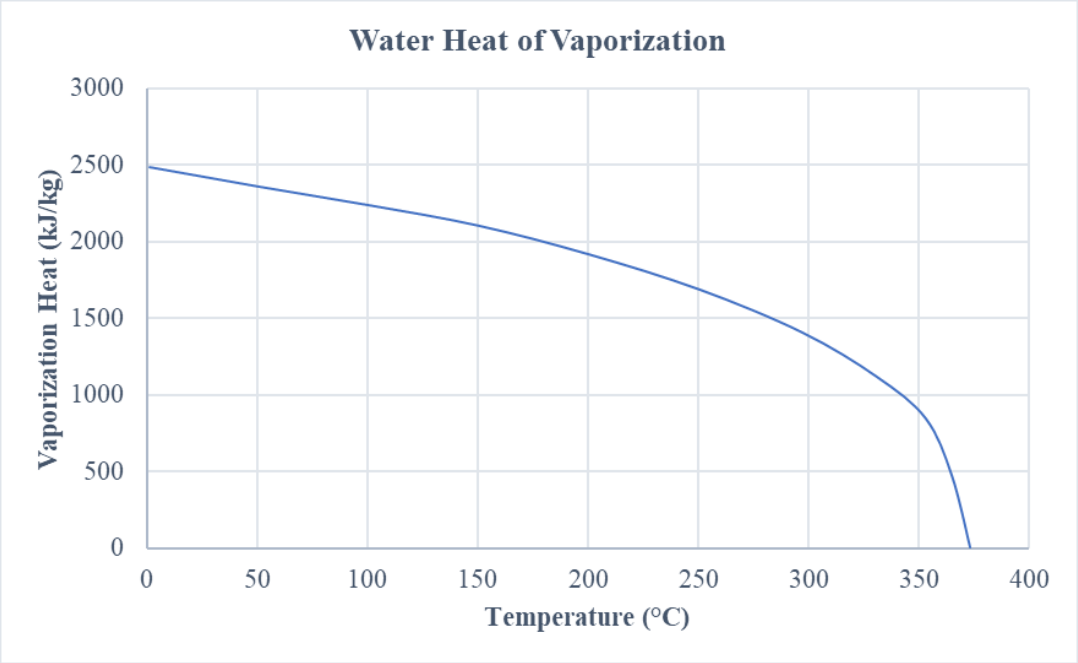

Figure 16 - Water Vaporization Heat, Source: (Engineering Toolbox, 2010)

The cooling that needs to be effectively removed by the cooling system can be obtained from equation 4.33.

$$Q_{FC\_Stack\_cooling} = FC\_Stack\_Heat - Q_{vap} \quad \text{Eq 4.33}$$

From equations described in this section it is possible to calculate the heat dissipation as a function of the fuel cell power level, which is depicted in Figure 17, that represents a 1000 kW fuel cell.

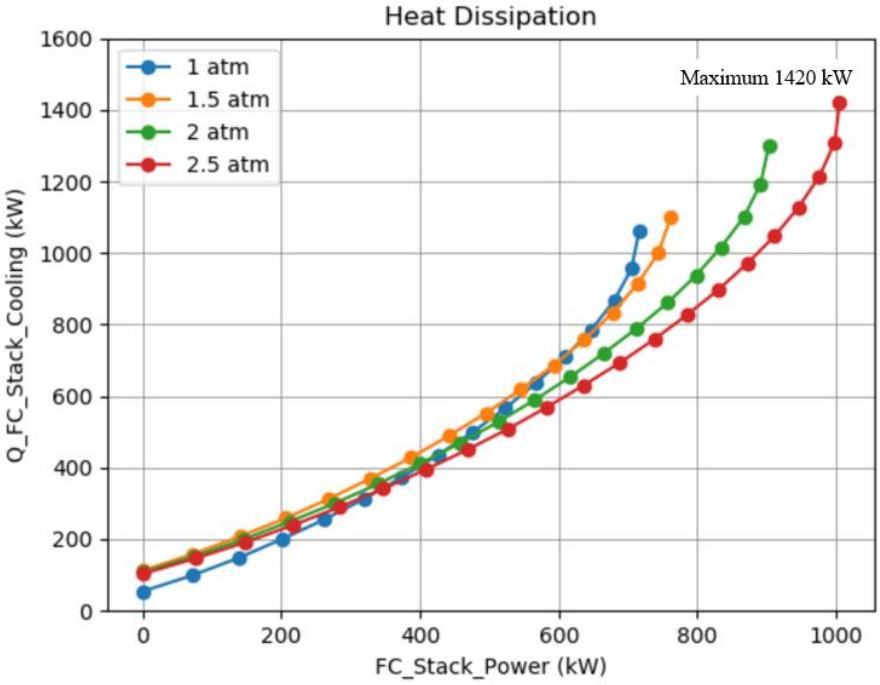

Figure 17 - Heat vs Power Chart

Note: Appendix A Table 13 presents the values in Figure 17

So, one can notice that the 1000 kW, of maximum power, Fuel Cell dissipates 1420 kW as maximum heat. Besides that, this analysis allows the adoption of a practical way to calculate the heat demand for different maximum power fuel cell stacks with the same losses' characteristics. Since the stack product ($A_{FC}\ N_{cells}$) is inherently present in all equations as a scaling factor to produce a desired maximum fuel cell power, the ratio between the dissipated heat (1420 kW) and the fuel cell stack power (1000 kW) is valid for fuel cells of different maximum power levels as well. So, for this work, a heat over stack power ratio of 1.42 (equation 4.34) will be used to estimate heat for fuel cells of the same characteristic.

$$Q_{FC\_Stack\_cooling} = 1.42\ FC\_Stack\_Power \qquad \text{Eq 4.34}$$

4.3.3 Fuel Cell Air Flow and Hydrogen Feeding Systems

As Figure 15 shows, the fuel cell operating pressure has an important influence on the maximum fuel cell available power, therefore the Turbo-compressor becomes one of the main fuel cell system accessories.

Figure 18 shows the fuel cell system air circuit which includes the moto-turbo-compressor receiving air flow from atmosphere, compressing it to the required fuel cell pressure, the compressed air flow passing through a heat exchanger, which controls the air flow temperature as per fuel cell requirement. That part of the system is usually known as balance of plant. After leaving the fuel cell, a mixture of air and water expands in the turbine, recovering some energy to the moto-turbo-compressor assembly and exhausting in the overboard nozzle.

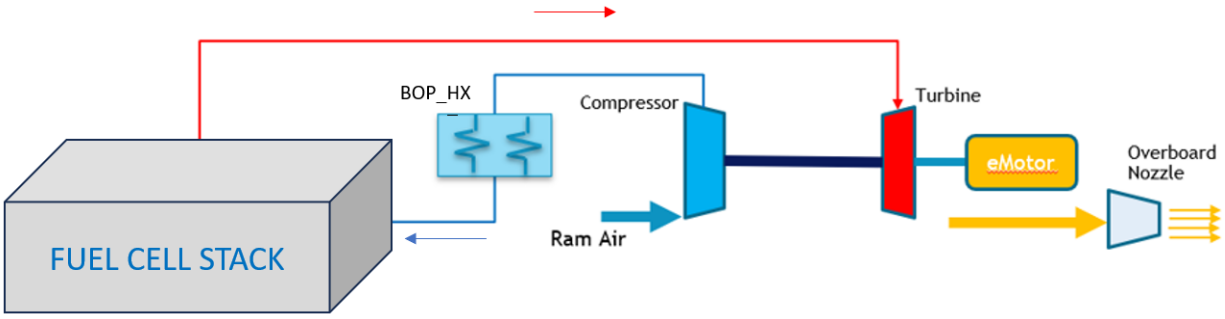

Figure 18 - Balance of Plant Schematic.

From flow machines and compressible fluid mechanics theories, the power consumed by the compressor is described in equation 4.35:

$$PW_{compr} = \frac{cp_{air}\, W_{air}\, T\_k_{ram\_air}}{\eta_{compr}} \left[\left(\frac{P_{compr\_out}}{P_{ram\_air}} \right)^{\frac{\gamma-1}{\gamma}} - 1 \right] \qquad \text{Eq 4.35}$$

Notice that Dicks and Rand (2018) recommends for compressor efficiency the value of 75%.

Equation 4.36 demonstrates the Air temperature after the compression:

$$T\_K_{compr\_out} = \frac{T\_k_{ram\_air}}{\eta_{compr}} \left[\left(\frac{P_{compr\_out}}{P_{ram\_air}} \right)^{\frac{\gamma-1}{\gamma}} - 1 \right] + T\_k_{ram\_air} \qquad \text{Eq 4.36}$$

The required heat exchange in the BOP_HX, to make air flow cool down to the fuel cell operating temperature is given by Equation 4.37:

$$QBOP = cp_{air} W_{air} (T\_K_{compr\_out} - T_{FC\ op\ temp}) \quad \text{Eq 4.37}$$

Note: Air specific heat (cp) and specific heat ratio (γ) can be obtained from Appendix D (Table 18)

Equation 4.38 shows the turbine recovered power:

$$PW_{turb} = \frac{cp_{air} W_{air} T\_k_{fc\_outlet}}{\eta_{turb}} \left[\left(\frac{P_{turb_{in}}}{P_{turb_{out}}} \right)^{\frac{\gamma-1}{\gamma}} - 1 \right] \quad \text{Eq 4.38}$$

By calculating the turbine power, it is possible to calculate the remaining required electric motor power:

$$PW_{motor} = PW_{comp} - PW_{turb} \quad \text{Eq 4.39}$$

And the motor heat can be calculated through equation 4.40:

$$Q\_Motor = PW_{motor} (1 - \eta_{motor}) \quad \text{Eq 4.40}$$

Chapman et al (2020) recommends using 95% as the motor efficiency.

Notice that the proposed heat management system includes a heat exchange with the hydrogen flow from the tank (at H2_HX). As proposed by this study, hydrogen is stored in liquid phase, since it results in the lighter tank configuration. So, Liquid Hydrogen needs to be converted to gas and heated to the fuel cell operating temperature. Equations 4.41 show required heat exchange to gasify the hydrogen and heat it to proper temperature:

$$Q_{H_2} = Q_{H_2 latent} + Q_{H_2 sens} \quad \text{Eq 4.41}$$

Where:

$$Q_{H_2 latent} = L_{H_2} W_{H_2} \quad \text{Eq 4.42}$$

$$Q_{H_2 sens} = cp_{H_2} W_{H_2} (T_{boiling\ point} - T_{FC\ op\ temp}) \quad \text{Eq 4.43}$$

Note: Appendix D, Table 19 describes the Hydrogen thermophysical properties, including latent heat of vaporization (L_{H_2}) and specific heat (cp_{H_2})

4.4 Thermal Management System Physical Model

4.4.1 Thermal Management System Model and Design Approach

The thermal management system model operates in two modes: design, when all geometric parameters are defined for a critical design condition and off design mode, when a TMS system has been specified (in design mode) and characteristics such as drag in any flight condition is calculated.

Before developing design and modeling technique it is important to delimit the arrangement context within the thermal management system will be designed.

4.4.1.1 Magnitude of Heat Exchange Demands and Problem Simplification Rationale

As illustrated in Figure 11, there are basically three heat exchangers involved in the heat management system: one for the hydrogen flow temperature control, one for the fuel cell balance of plant air flow and the last one for the Fuel Cell coolant. This section is intended to present the magnitudes involved in this heat exchanges and present a rationale to simplify the problem to design the fuel cell thermal management system.

The schematic in Figure 11 shows a specific architecture in which the Fuel Cell is cooled down by a coolant fluid which dissipates the Fuel Cell heat in the main air/liquid radiator (FC_HX). It is worth noting that, in this arrangement, this is the only heat exchanger that exchanges heat with external air flow, i.e., this is the only heat exchanger that can creates ram air drag. Before entering in the FC_HX, the Fuel Cell main coolant stream diverges a portion of its flow to provide heat for the hydrogen heating (in H2_HX). That hydrogen heating stream returns and remixes to the main coolant stream before it returns to the fuel cell. In the other side, a portion

of the main coolant stream, when returning to the fuel cell, diverges to cool down the fuel cell balance of plant air flow (in BOP_HX) and returns from it to remix with the main coolant stream. With that architecture, the fuel cell, the hydrogen and the balance of plant air flows heat exchange systems share the same heat exchange transport means (coolant line). Moreover, while the fuel cell and the balance of plant need to dissipate heat, the hydrogen requires to receive heat, which represents a synergy potential.

Figure 19 shows the heat balance of the whole fuel cell system.

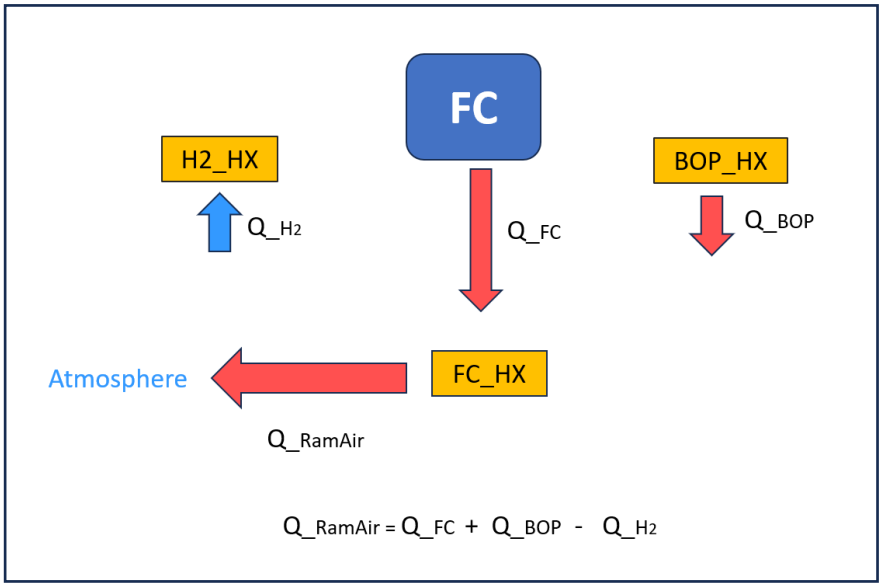

Figure 19 - Heat Balance Schematic

To evaluate the magnitude of the heat partials involved in this system a fuel cell with 1000 kW of maximum power will be used as example (power chart in figure 15). Two representative conditions (to be further explained in section 5.2.1 and 5.3) will be used: a takeoff condition (1000 kW, sea level and 30°C of ambient temperature) and a cruise condition (500 kW, 7620 m of altitude and -34.6°C of ambient temperature). At 1000 kW (takeoff condition), the fuel cell dissipated heat is 1420 kW and at 500 kW (cruise condition) the dissipated heat is 470 kW (both data collected from figure 17).

From the 1000 kW fuel cell Power versus Hydrogen flow chart (figure 15) the required hydrogen mass flow at these two conditions can be picked to evaluate the required H2_HX heat. Figure 20 illustrates this procedure.

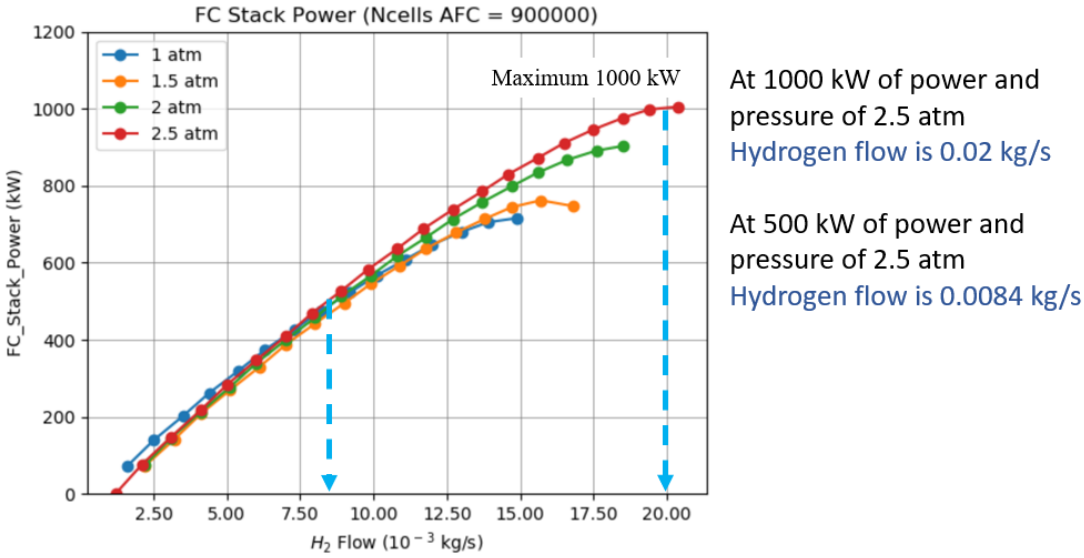

Figure 20 - Power vs Hydrogen flow

Figure 20 shows that, at the highest power condition, the required hydrogen flow is 0.02 kg/s. As discussed in the section 4.3.3, the hydrogen will be stored in its liquid form, i.e., at -253°C (20 K), APPENDIX D, Table 19. Assuming a Fuel cell operating with gaseous hydrogen at 100 °C (373 K), which is within the range suggested by Dicks and Rand (2018), the heat required to raise the hydrogen flow to this condition can be calculated with equation 4.44.

$$Q_{H_2} = L_{H_2} W_{H_2} + cp_{H_2} W_{H_2} \left(T_{FC\ op\ temp} - T_{boiling\ point}\right) = 110kW \qquad \text{Eq 4.44}$$

The balance of plant air flow is compressed to feed the fuel cell, which is a process that also warms the air. With equations 4.22 and 4.45 the required balance of plant air flow can be calculated as a function of the desired hydrogen flow:

$$W_{Air} = 76.2\, W_{H_2} = 1.52\ kg/s \qquad \text{Eq 4.45}$$

Assuming an aircraft takeoff condition at sea level, an ambient temperature of 30°C and a compression ratio of 2.5, the Balance of Plant heat can be obtained from equation 4.46.

$$QBOP = cp_{air} W_{air} \left(T\_K_{compr\_out} - T_{FC\ op\ temp} \right) = 82.6\ kW \quad \text{Eq 4.46}$$

Where $T\_K_{compr\_out}$ is calculated with equation 4.36

From the calculation above, the heat required to vaporize and raise the Hydrogen temperature exceeds the value required to cool the balance of plant air down by 27.4 kW, which represents 2% of the fuel cell heat dissipation (1420 kW, figure 17). That means a net alleviation of 2% that could be transported to the fuel cell heat exchanger (FC_HX), through the coolant circuit, i.e., atmosphere air receives 1393 kW instead of 1420 kW.

Similar calculation can be repeated to the cruise condition. At cruise, the fuel cell requires a Hydrogen flow of 0.0084 kg/s. A compression ratio of 5.9 is assumed so that the balance of plant air flow reaches the maximum fuel cell operating pressure of 2.5 atm, at altitude of 7620 m. Replicating calculations done for the takeoff case, in the cruise condition, a total of 45 kW is required to heat the Hydrogen flow while 44 kW is required to cool the balance of plant air flow down. That represents 0.2% of net heat exchange difference (relative to the fuel cell total heat dissipation at this condition), that can be transported to the fuel heat exchanger (FC_HX) through the coolant line.

Since the heat magnitudes involved in the hydrogen heating process and balance of plant air flow cooling are similar, are in opposite directions, and its difference results in a very small and benign net difference, this work concentrates efforts on the parameterization of the fuel cell ram air heat exchanger (FC_HX) system only, assuming the fuel cell stack dissipated heat as the reference for the design.

4.4.1.2 Thermal Management System Arrangement and Design Flow

Figure 21 shows the arrangement in which the heat exchanger will be assembled. Downstream propeller an air circuit which includes an intake, diffuser, heat exchanger and exit

duct is defined. The exit duct incorporates a variable area nozzle, which is a key element to reduce TMS drag, according to Meredith (1935)

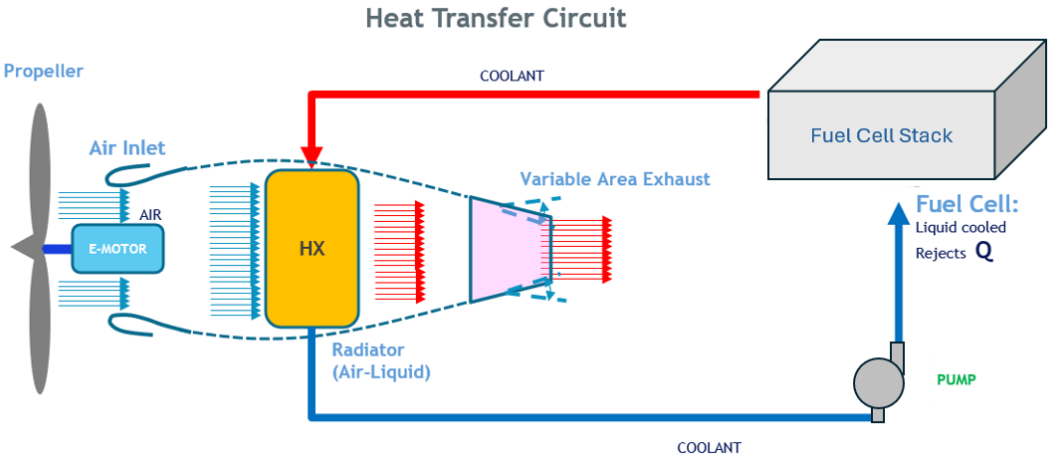

Figure 21 - Simplified Thermal Management Cycle

The thermal management model for this work will be divided in two modes: design mode and off design mode. The design mode calculates the required heat exchanger to address a certain heat exchange demand, which must be done at the most critical operating condition. The off-design mode calculates the heat exchange at any condition within its operating envelope.

The diagram in Figure 22 shows the flowchart of the heat exchanger design:

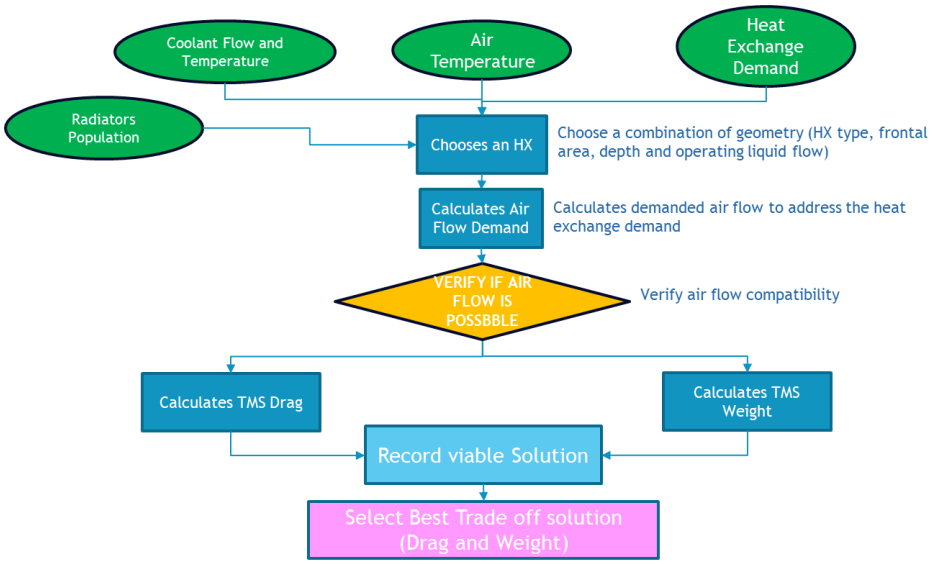

Figure 22 - TMS Design Cycle

The design mode will work with three inputs: the Fluids conditions (Air Temperature and Liquid coolant Temperature and flow) and heat exchange demand. A candidate heat exchanger (combination of heat exchanger type, frontal area and depth) is chosen from a radiator's population. With the air temperature, liquid flow and temperature, and a candidate heat exchanger, the routine looks for the demanded air flow to match the required heat dissipation, based on the heat exchanger effectiveness (obtained from its features as exposed further, in section 4.4.1.3). With such demanded air flow calculated, the candidate heat exchanger pressure loss is also determined. With knowledge of the candidate heat exchanger pressure loss and all remaining air circuit pressure drop characteristics, a second routine determines if that demanded air flow is allowed by that air circuit, i.e., if the inlet air has enough total pressure to flow through this circuit. In positive case the candidate heat exchanger is approved as a valid solution and its drag and weight are recorded to go through a selection process, in which the best (for aeronautical performance) among the valid population will be chosen, to be explained latter.

4.4.1.3 Candidate Heat exchanger Calculations (Air Flow Demand Determination)

Thulukkanam (2013) brings a broad discussion of heat exchangers covering performance calculation approach, various types of heat exchanger and indicating most suited type for each application. From Thulukkanam (2013), it can be concluded that most adequate heat exchangers for aircraft engines application, in which volume allocation is an important matter, are the compact tube and thin radiators. Figure 23 shows a schematic of three variations of tube and fin radiators, both arranged so that air flows through the fins and liquid flows through the tubes, which can be circular or flat.

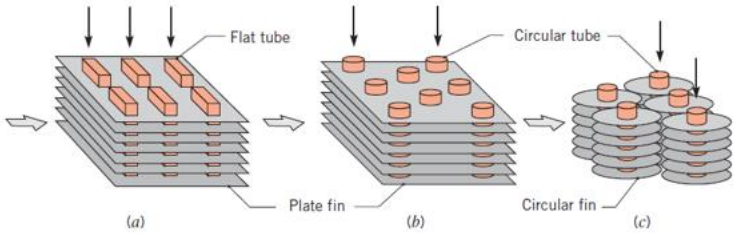

Figure 23 - Heat Exchanger Types, Source: (Incropera et al, 2011)

According to Thulukkanam (2013), compactness is defined as the ratio between the total heat exchange surface area and the heat exchanger volume. Compact heat exchangers present compactness value equal or above 700 m^2 / m^3.

Kays and London (1984) brings a complete description of means to design the compact heat exchangers, that is, defining the heat exchanger type and geometry features as the frontal area and depth. Such a reference documents not only the means to design the heat exchanger but also includes several real heat exchanger performance maps and all core geometry features.

As mentioned in previous session, for a given candidate heat exchanger and heat exchange demand, along with air and liquid temperatures, first step is to calculate the demanded air flow to reach the required heat exchange.

The formulation described in Kays and London (1984) allows the calculation of the heat exchange as output to a given air flow, heat exchange core geometry and performance chart. Required Air flow is, then, obtained iteratively by guessing a first value and iterating until heat demand reaches desired level.

Formulation starts calculating the convective heat exchange coefficients from each side (air side and liquid)

Air side:

From a guessed air flow, first step is to calculate the free flow mass velocity, with equation 4.47.

$$G_{air} = \frac{W_{air\_main\_hx}}{A_{c\_air}} \qquad \text{Eq 4.47}$$

Where $W_{air\_main\_hx}$ is the atmosphere main radiator air flow and A_{c_air} is the free flow frontal area. From such a calculation and radiator type hydraulic radius, the Reynolds number can be determined:

Eq 4.48

$$Re_{air} = \frac{4r_{h\_air}\, G_{air}}{\mu}$$

A particular heat exchanger performance map comprises the Colburn factor and the friction coefficient, both as function of Reynolds number. Figure 24 illustrates a typical heat exchanger performance map:

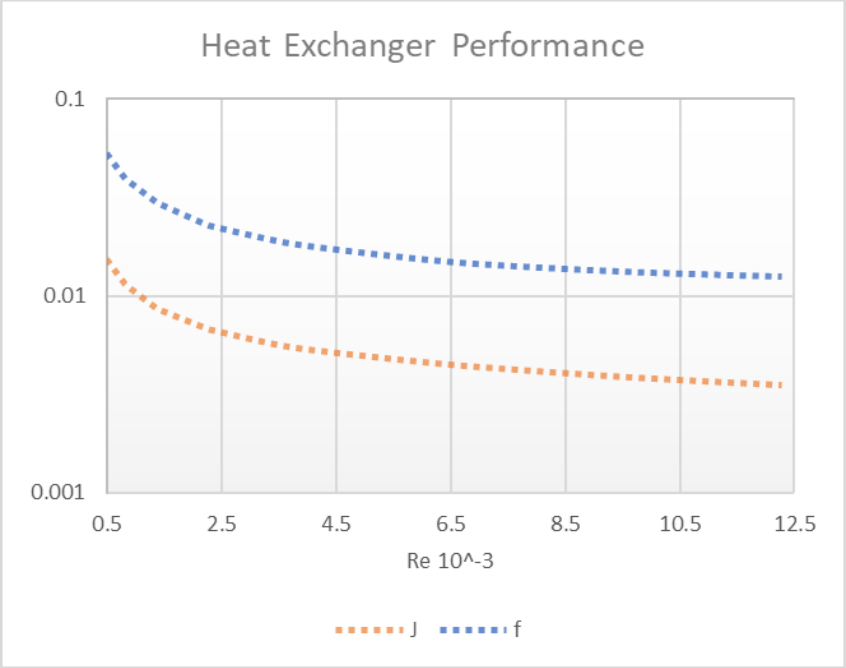

Figure 24 - Heat Exchanger Performance Chart, adapted from Kays and London (1984)

So, from Reynolds number (obtained from given mass flow and heat exchanger geometry) the Colburn number is obtained.

From Colburn factor value and Prandtl number, which is a function of air flow pressure and temperature, Stanton number can be determined, equation 4.49. In sequence the convective heat coefficient can be determined as function of the Stanton number, mass velocity and air specific heat.

$$St = \frac{j}{Pr^{0.67}} \qquad \text{Eq 4.49}$$

$$h_{air} = St\ G_{air}\ cp_{air} \quad \text{Eq 4.50}$$

Liquid Side:

Heat Transfer coefficient from liquid side can be calculated with equation 4.51:

$$h_{liq} = \frac{Nu\ k}{4r_h} \quad \text{Eq 4.51}$$

Where Nusselt number can be obtained with the empirical equation 4.52, presented by Holman (2009)

$$Nu = 0.023\ {Re_{liq}}^{0.8} {Pr_{liq}}^{0.23} \quad \text{Eq 4.52}$$

Note: this empirical equation is valid for turbulent flows with minimum Reynolds number of 3000:

Where:

$$Re_{liq} = \frac{4r_{h\_liq}\ G_{liq}}{\mu_{liq}} \quad \text{Eq 4.53}$$

Being G_{liq}, the liquid mass velocity, which is calculated from the liquid mass flow and liquid side free flow area, equation 4.54.

$$G_{liq} = \frac{W_{liq\_main\_hx}}{A_{c\_liq}} \quad \text{Eq 4.54}$$

Then, overall Heat transfer coefficient from the heat exchanger (relative to air side area) is calculated from the combination of air and liquid side coefficients (equation 4.55),

$$U_{air} = \frac{1}{\frac{1}{\eta\_fin\ h_{air}} + \frac{1}{\left(\frac{A_{liq}}{A_{air}}\right) h_{liq}}} \quad \text{Eq 4.55}$$

Notice that A_{liq} and A_{air} are the total transfer area in each side (particular from the chosen heat exchanger), which can be determined from σ_{air} and σ_{liq} compactness factors (Table 17) and the radiator volume. η_{fin} is obtained from Figure 25

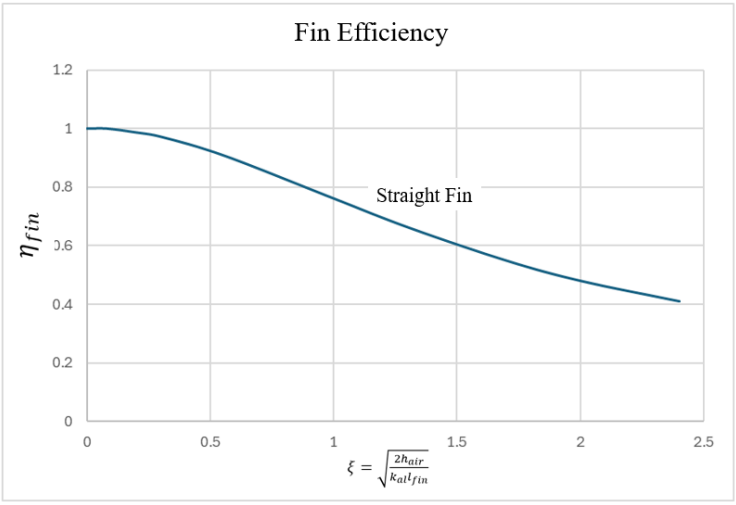

Figure 25 - Fins efficiency Chart, adapted from Kays and London (1984)

The NTU (Number of transfer units), which is a non-dimensional heat transfer parameter, can be calculated with equation 4.56:

$$NTU = \frac{U_{air} A_{air}}{Cmin} \qquad \text{Eq 4.56}$$

Where $Cmin$ is the smaller of both sides heat capacities as indicated in equation 4.57

$$Cmin = min\,(W_{air\_main\_hx} cp_{air}, W_{liq\_main\_hx} cp_{liq}) \qquad \text{Eq 4.57}$$

Incropera et al (2011) presents a method, described in equation 4.58, that correlates the radiator effectiveness to NTU and Cr, being Cr determined by equations 4.59 and 4.60.

$$\epsilon = 1 - e^{\frac{1}{Cr} NTU^{0.22} e^{(-Cr\, NTU^{0.78} - 1)}} \qquad \text{Eq 4.58}$$

Eq 4.59

$$Cr = \frac{Cmin}{Cmax}$$

$$Cmax = max\ (W_{air\_main\_hx} cp_{air}, W_{liq\_main\_hx} cp_{liq}) \qquad \text{Eq 4.60}$$

It is important to note that the equation 4.58 is valid for single pass cross flow type of radiators, that will be the object of interest in this work.

Finally, the heat exchange can be calculated from the equation 4.61:

$$Q = \epsilon\ Cmin\ (liq_{temp} - air_{temp}) \qquad \text{Eq 4.61}$$

From now on, the routine that encapsules the set of equations from 4.47 to 4.61 that outputs the heat (Q) will be referred as HX Heat model.

As explained before, such a heat calculation is used in an iterative computational process to find the required air flow for a desired heat exchange, as depicted in flow chart on Figure 26

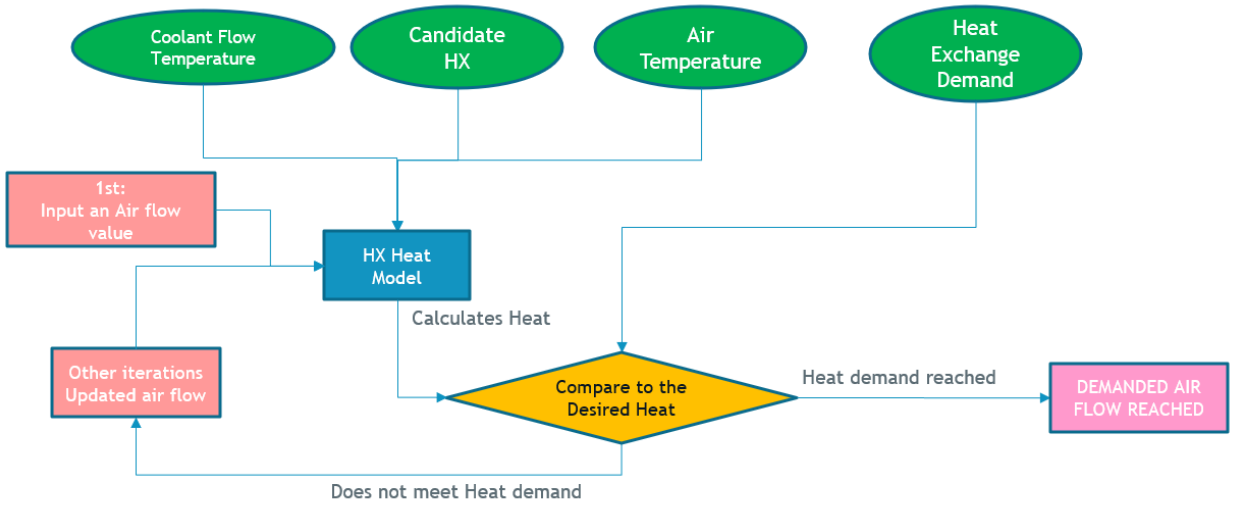

Figure 26 - Air Flow Calculation Flow Chart

An iteration method was implemented so that air flow convergence is fast. Since heat exchanger maps operates within a Reynolds number range, as depicted in Figure 27, at first

iteration, Maximum and minimum allowed air flows from the candidate heat exchanger (referent to maximum and minimum map Reynolds number) are calculated. Such air flow values allow the calculation of their respective heat exchange capabilities (from HX heat model). A linear interpolation is performed with the maximum and minimum heat exchange capabilities and the required heat exchange to calculate the required air flow, as if it was a linear function, as shown in Figure 27. With this value the HX heat model is used to calculate the heat at this condition and compare it to the required heat, generating an error as shown in Figure 27.

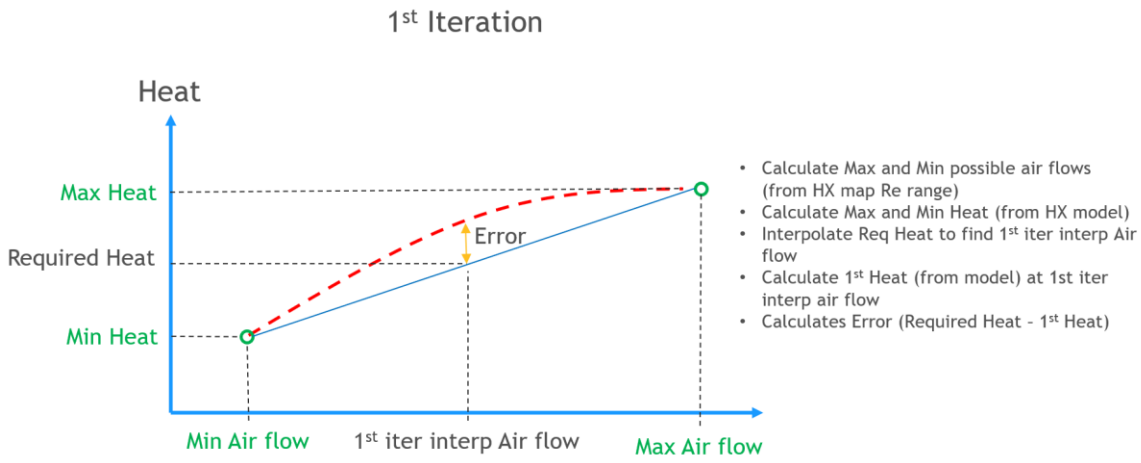

Figure 27 - Area Calculation First Iteration

If error is not acceptable, an additional iteration is performed updating the maximum and minimum air flows to the average between their first values and the first step interpolated air flow. New heat values at these new bounds are calculated and a 2nd iteration interpolated air flow value is calculated (Figure 28). From this value a new heat is calculated using the HX heat model and a new error is also calculated. Process is naturally repeated until error is acceptable.

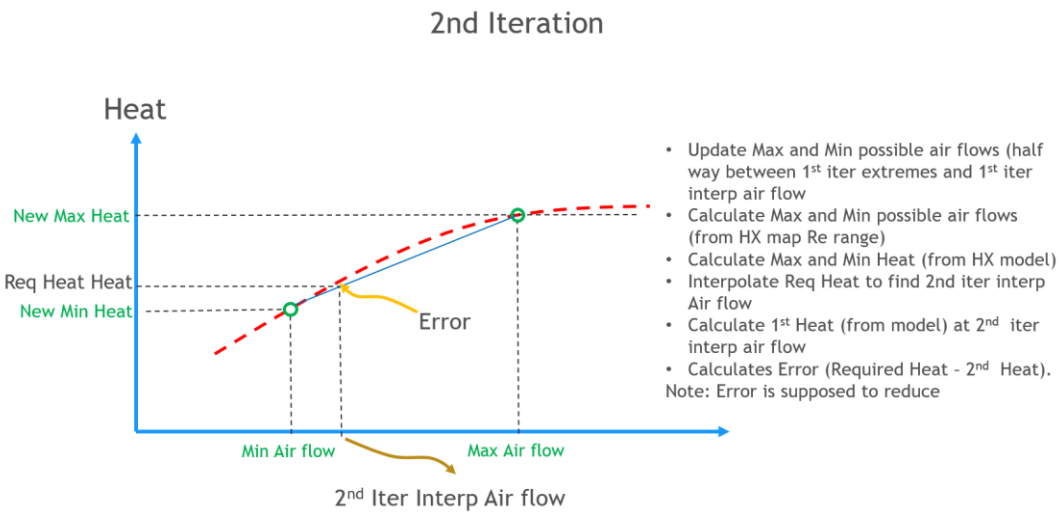

Figure 28 - Area Calculation Second Iteration

With that accomplished a pair of demanded heat dissipation, resulted from the fuel cell model, and air flow resulted from chosen radiator model are known. Next step is to verify the compatibility of this air flow to pass through the proposed air circuit.

4.4.1.4 Air Flow Compatibility

Once the air flow demand to dissipate the heat has been determined, it is necessary to verify if such air flow is feasible at the proposed thermal management air circuit (Figure 29), which means checking if the available pressure at exit station (Pt9) is higher than the ambient pressure.

Figure 29 air circuit shows five basic elements: propeller, diffuser, radiator, exhaust duct and variable nozzle area.

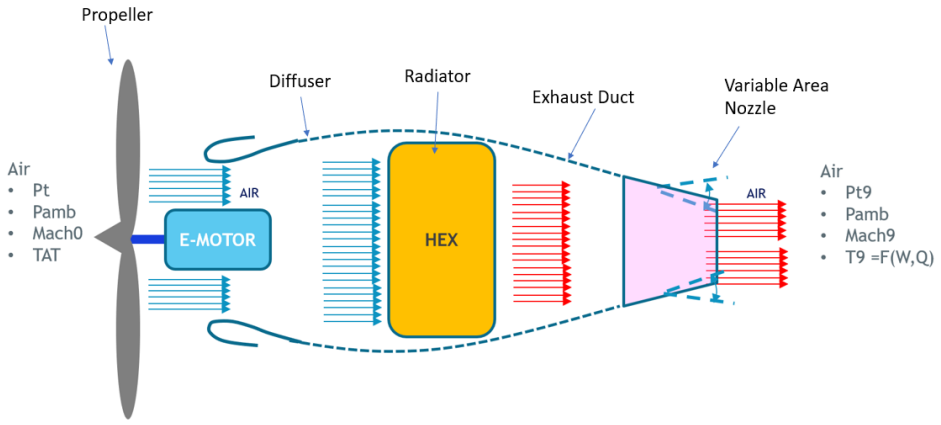

Figure 29 - TMS Air circuit

Determination of the air flow compatibility requires to know the air conditions at exit, that is, determine Pt9 and Tt9. Pt9 must be calculated by applying the propeller pressure rise, and the pressure losses throughout the diffuser, radiator, and exhaust duct. Variable Area nozzle loss is concentrated on the nozzle coefficients as explained further in this section. Tt9 is calculated by a simple energy balance within the heat exchange.

4.4.1.4.1 Propeller Pressure Rise Model

The ideal way to calculate the propeller pressure rise is applying a propeller performance model based on blade element method, which can calculate not only the basic performance parameters, such as thrust and torque, but also the pressure throughout the blade line.

Since this work is intended for conceptual design studies, when a propeller is not defined yet, a method based on conceptual techniques is used.

According to Howe (2000), efficiency of propeller can be estimated using the empirical equations (4.62 to 4.65):

$$For\ 0.4 <= J < 1.0 \qquad \eta_{prop} = 0.72\, J^{0.4} \qquad \text{Eq 4.62}$$

$$For\ J >= 1.0 \qquad \eta_{prop} = 0.82\ \frac{J^{0.16}}{10^{x}} \qquad \text{Eq 4.63}$$

Where:

$$x = 0.3\ (log\ J)^{2.4} \qquad \text{Eq 4.64}$$

And J is the advance ratio, given by the equation 4.65:

$$J = \frac{V_a}{n\ Diam} \qquad \text{Eq 4.65}$$

Being Va the free stream air velocity in m/s, n is the propeller rotational speed in revolutions per second and Diam is the propeller diameter in m.

The propeller thrust can be derived from the efficiency, air speed and input power, which is given by equation 4.66:

$$Fn = \eta_{prop}\ \frac{Propeller_{power}}{V_a} \qquad \text{Eq 4.66}$$

Where $Propeller_{power}$ is the propeller shaft power ideally equal to the Fuel Cell Stack Power (if losses are neglected for the sake of simplicity), and V_a is the airplane air speed.

Heene, 2021 provides fluid mechanics equation development over the propeller stream tube (Figure 30), to obtain a straightforward $\triangle P$ calculation method.

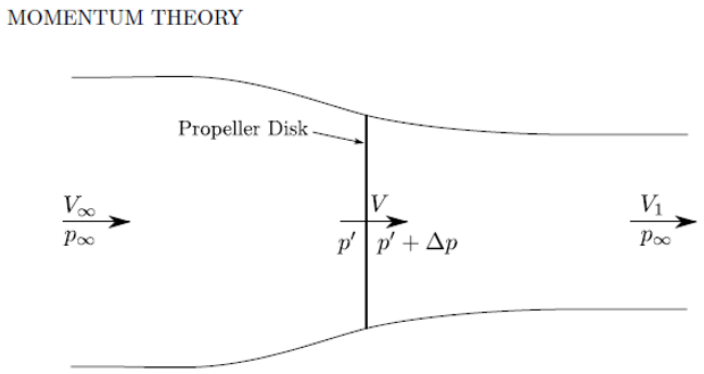

Figure 30 - Ideal Propeller Stream Tube, Source: (Heene, 2012)

$$\triangle P_{propeller} = \frac{Fn}{A_{propeller}} \qquad \text{Eq 4.67}$$

Therefore, with a specification of the propeller shaft power, the knowledge of the propeller efficiency and the momentum theory equation, it is possible to estimate the delta pressure provided by the propeller.

4.4.1.4.2 Diffuser and Exhaust duct Pressure Loss Models

The diffuser pressure loss calculation can be done according to recommendations from Katzoff (1948), which is a reference dedicated to aircraft piston engine cooling systems. Diffuser pressure losses are mainly caused by flow separations throughout the expansion process. A simple pressure loss model is proposed in Figure 31:

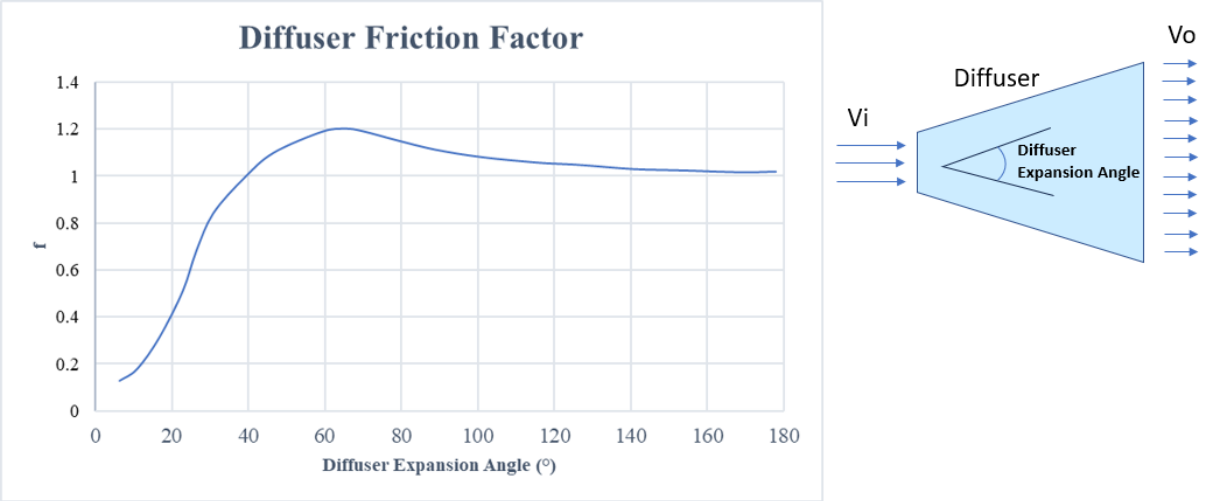

Figure 31 - Diffuser Pressure Loss Chart, adapted from Katzoff (1948)

Thus, pressure loss can be derived from equation 4.68:

$$\triangle P = f\frac{\rho}{2}(V_i - V_0)^2 \qquad \text{Eq 4.68}$$

Where V_i and V_o are, respectively, the inlet and outlet diffuser speeds, and f is the friction coefficient given by the chart model.

Still according to Katzoff (1948), since a converging straight pipe does not present relevant flow separation, the pressure loss from the exhaust duct might be considered as negligible

It can be noticed that such a proposed idealized installation is not necessarily adequate for a specific aircraft, which may impose restrictions to it. As a project evolves the real installation, which will be integrated to the real airplane, will be defined, possibly, more complex than this one. Then, pressure losses throughout the ducts are better calculated via computational fluid dynamics techniques, however, this work is dedicated to conceptual design studies, when a geometry is far from being detailed. Assuming simple models as the ones proposed by Katzoff (1948) is the ideal technique to adopt in a development effort in which detailed geometric definitions are not available. Uncertainties associated to it are to be interpreted as inherent limitations of the

conceptual design stage, therefore, this work will define a baseline geometry for the thermal management ducts to estimate the pressure losses, while an optimized one and limited to a certain aircraft geometry restriction is out of the scope.

4.4.1.4.3 Heat Exchanger Pressure Loss

Heat exchanger pressure loss can be calculated as defined by Kays and London (1984), which brings an empirical equation that calculates the pressure loss ratio ($\frac{\Delta p}{p}$).

$$\frac{\Delta p}{p} = \frac{{G_{air}}^2}{2} v_i \left[(1 + \sigma^2) \left(\frac{v_o}{v_i} - 1 \right) + f \frac{L}{r_h} \frac{v_m}{v_i} \right] \quad \text{Eq 4.70}$$

Where: G_{air} is the mass velocity, v_i, v_o, and v_m are the inlet outlet and average specific volumes, σ is the ratio between free flow area and total frontal area, L is the radiator length and f is the friction coefficient obtained from radiators performance map like in Figure 24.

4.4.1.4.4 Nozzle coefficients

The nozzle also present losses. According, to fluid mechanics principles (further expose din sections 4.4.1.4.5), the air flow and air speed flowing through a nozzle can be theoretically determined with air flow total pressure (Pt9), total temperature (Tt9), nozzle area and the ambient pressure (Pamb), all indicated in Figure 29. However, these calculations represent ideal values, and the correction to real values is done with the definition of two coefficients (discharge and velocity). Walsh (2004) illustrates how nozzle coefficients vary throughout the nozzle pressure ratio, as indicated in Figure 32. These coefficients will be used further to correct the theoretical calculations.

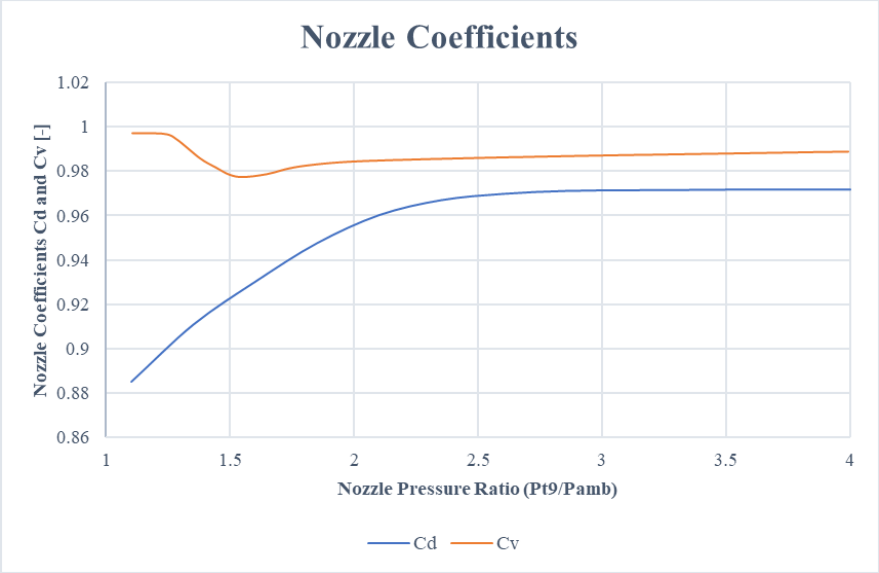

Figure 32 - Nozzle Discharge Coefficient Chart, adapted from Walsh (2004)

4.4.1.4.5 Overall Air Circuit Verification

As stated before, calculating the required nozzle area starts by calculation the Temperatures and Pressure at nozzle station (designated as Pt9 and Tt9). Pt9 is calculated by applying a boost provided by the propeller and debiting all pressure losses within the air circuit, as shown in equation 4.71.

$$Pt9 = Pt + \triangle P_{propeller} - \triangle P_{radiator_{loss}} - \triangle P_{diffuser\_loss} \quad \text{Eq 4.71}$$

Tt9 is calculated with the increment resulting from the heat exchange in the main radiator:

$$T9 = \frac{Q_{FC\_Stack\_cooling}}{W_{air\_main\_hx}\, cp_{air}} + TAT \quad \text{Eq 4.72}$$

Speed can be calculated via compressible flow fluid mechanics equations:

$$Mach9 = \sqrt{5\left[\left(\frac{Pt9}{Pamb}\right)^{0.286} - 1\right]} \quad \text{Eq 4.73}$$

It can be noticed that equation 4.73 imposes the air flow feasibility check:

If the Pt9 and Pamb ratio is lower than 1.0 the equation does not result in a real value.

Nozzle Area can be finally determined with equations 4.74 to 4.77. It must be noticed that a discharge coefficient (Cd) is adopted in the equation for a real nozzle behavior characterization

$$Ts9 = \frac{T9}{(1+0.2\ Mach9^2)} \quad \text{Eq 4.74}$$

$$\rho 9 = \frac{Pamb}{R*Ts9} \quad \text{Eq 4.75}$$

$$V9 = Mach9 * \sqrt{\gamma\ R\ Ts9} \quad \text{Eq 4.76}$$

$$A_{nozzle} = \frac{W_{air}}{Cd\ V9\ \rho 9} \quad \text{Eq 4.77}$$

4.4.1.5 Thermal Management System Weight Calculation:

Weight calculation from thermal management system can be divided in the radiator, and fluid systems weight: storage, filter, ducts and pumping.

The Radiator weight is calculated based on the core geometry definition and the macro dimensions (frontal area and length).

Core geometry definitions for each radiator type are provided by Kays and London (1984) These include the fins and tubes thickness, number of fins per length unity and number of tubes per area unity. Figure 33 helps to understand the dimensions provided by Kays and London (1984). The frontal height (H) and fins spacing allow to calculate the number of fins while width (W) and depth (D) allow to calculate their area. With thickness number of fins and their area their volume

can be determined and consequently their weight, once material is chosen. Tubes weight can be determined in similar manner, since their occupied transversal area (referent liquid flow direction) and the space between it, along with macro dimensions Width and Depth, allow calculation of the number of tubes while thickness and height allow calculate their shell and internal volumes. Internal volumes will be filled with the liquid, whose specific gravity allows calculating its weight.

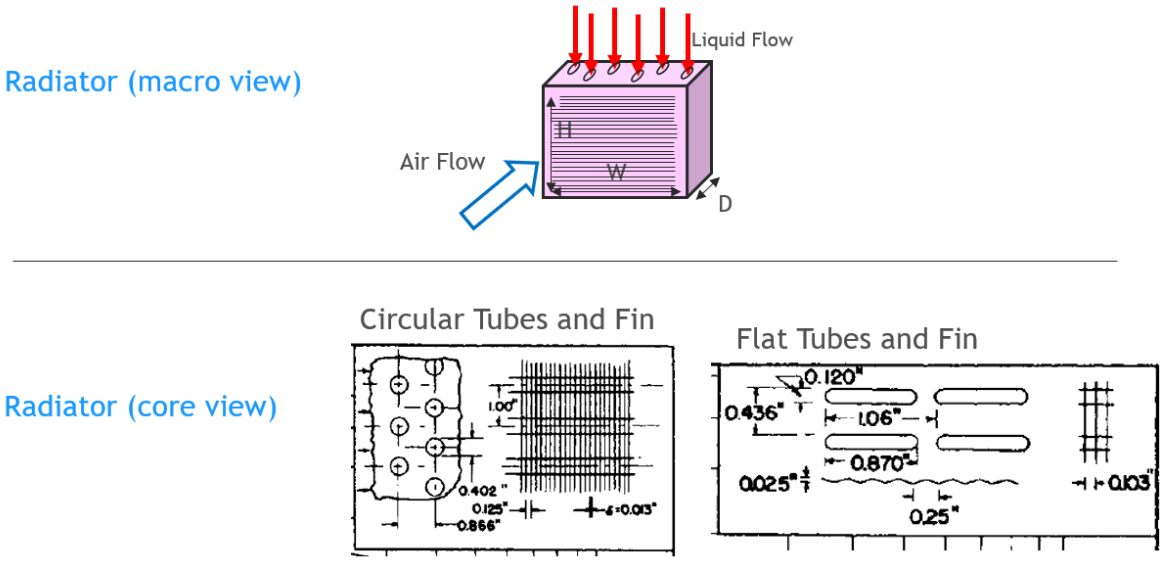

Figure 33 - Radiator Macro and Core views, adapted from Kays and London (1984)

Note: Information about the radiators core geometry used in this work are provided in APPENDIX D, Table 17.

Relevant part of the thermal management system weight is composed by the coolant, which occupies the ducts, reservoir and radiator and fuel cell galleries.

For ducts fluid weight:

$$W_{coolant\_duct} = \rho_{coolant}\ DuctLenght\ DuctArea \qquad \text{Eq 4.78}$$

$$DuctArea = \frac{VolumetricFlow}{FlowSpeed} \qquad \text{Eq 4.79}$$

The coolant duct length is an inherent feature from the position where systems like the fuel cell radiator and reservoir are to be installed in the aircraft. As already mentioned, an aircraft layout is not defined in such an early stage of studies, so a baseline length is defined. Duct area is a function of the coolant required volumetric flow and design fluid flow speed. Engineering Toolbox (2014) recommends operating with no more than 2.4 m/s, due to noise and erosion issues, so this is the value that is used in this work.

Another important component of the weight is the reservoir. Engineering Toolbox (2005) recommends that the reservoir quantity is calculated as a function of the maximum fluid operating temperature as the Figure 34 shows. Same reference recommends a safety factor of 2.

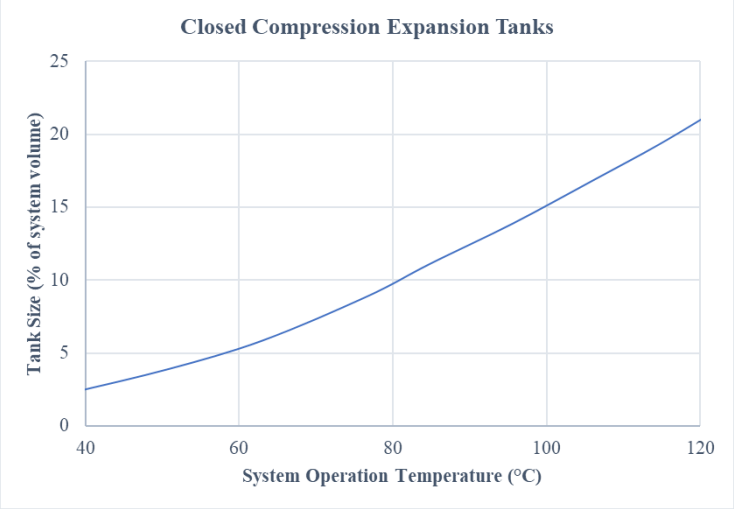

Figure 34 - Coolant Tank Size Recommendation Chart, adapted from Engineering Toolbox (2005)

The total weight of the reservoir (equipment plus fluid) can be calculated through equation (4.80), derived from industrial catalogue, (American Water Heaters Expansion Tanks, n.d.):

$$Wt_{dryreservoir\_kg} = 1.21\ Reservoir\_Fluid\_Quan\_kg + 0.90 \qquad \text{Eq 4.80}$$

The coolant pump weight can be calculated with equation 4.81, derived from an industrial catalogue (Gemmecotti Pumps, n.d.):

$$Wt_{pump\_kg} = 0.1\ W_{coolant\_gpm} + 2.2 \qquad \text{Eq 4.81}$$

Ducts and Filter weights represent a small portion of the total system weight and may be calculated by adding total of 2% on the sum of the weights calculated so far as suggested by Datta (2021)

4.4.1.6 Thermal Management System Drag

The drag can be calculated via momentum conservation theory, which is the approach recommended by Gudmundsson (2014), when discussing method for aircraft TMS drag estimation.

First, by looking at the thermal management system isolated from the propeller (Figure 35), it can be modeled as a control volume delimited by far field frontiers.

Figure 35 - TMS Control Volume

Drag can be expressed by the air flow momentum variation (equation 4.82).

$$Drag = W\ V_\infty - W\ V_0 \qquad \text{Eq 4.82}$$

Where V_a is the aircraft air speed (far from the TMS inlet, at atmosphere pressure) and $V_\infty$is the exit speed after fully expansion back atmosphere pressure. For this type of air flow device, which experiences low nozzle pressure ratios, it is expected that the pressure stablished at the nozzle exhaust is equal to the ambient pressure, so, no expansion is expected, therefore V_∞ is equal V_9 (the speed at the nozzle exhaust and calculated with equation 4.67)

In the arrangement in which thermal management system is downstream propeller (Figure 36) a correction is needed. Since the TMS air circuit is not exposed directly to aircraft speed, a

downstream propeller air speed, that represents the air flow fully expanded momentum at this condition (boosted by the propeller), needs to be calculated

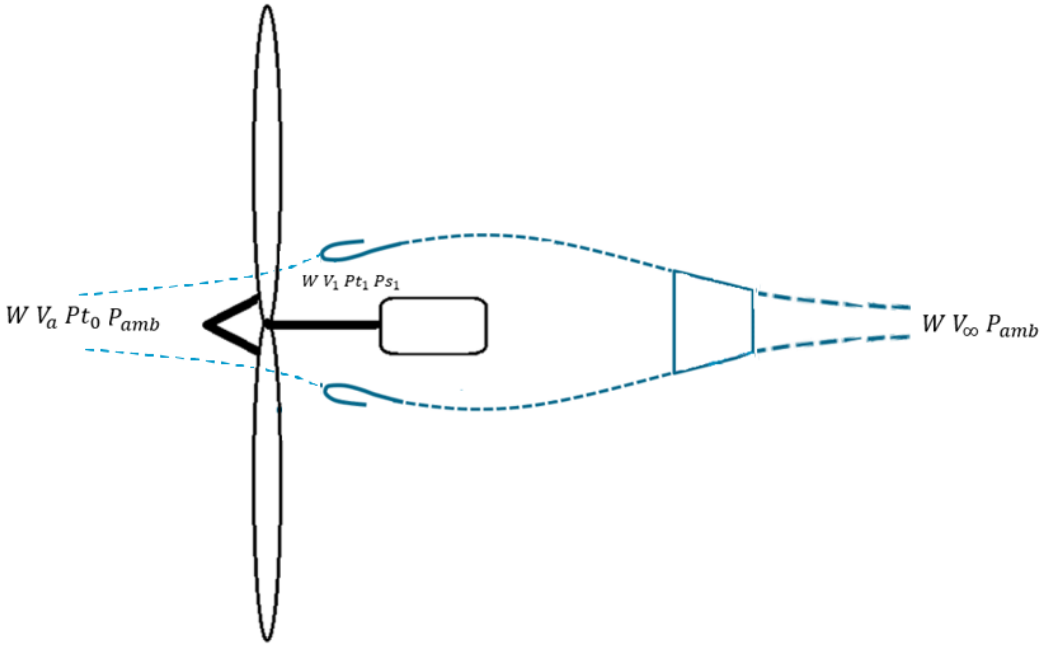

Figure 36 - TMS Control Volume Downstream Propeller

Equation 4.83 expresses the speed to be used for the TMS air circuit inlet momentum calculation.

$$V_1 = \sqrt{2\frac{(Pt_1 - P_{amb})}{\rho}} \qquad \text{Eq 4.83}$$

Where $Pt_1 = Pt_0 + \triangle P_{propeller}$

and $\triangle P_{propeller}$ can be calculated through equation 4.67.

Thus, the TMS drag can be calculated with equation 4.84, which includes the velocity nozzle coefficient (discussed in section 4.4.1.4.4).

$$TMS\_Drag = cv\ W\ V_9 - W\ V_1 \qquad \text{Eq 4.84}$$

4.4.1.7 Thermal Management System Power Penalty Parameter

A more practical way to consider the thermal management drag is to convert it into a propeller power penalty, which is given by equation 4.85.

$$PowerPenalty = \frac{Drag\ V_a}{\eta_{prop}} \quad \text{Eq 4.85}$$

That approach creates a more useful parameter since it can be compared directly to the engine delivered power.

4.4.2 Selection of Best Thermal Management Solution

As described in section (4.4.1.3), when running in design mode, for every fuel cell power to be tested, several solutions (different radiator geometries) is tested, and all the solutions that are capable of dissipating the required Fuel Cell generated heat is recorded as feasible individuals. Every one of these solutions will deliver, as output, a set of thermal management characteristics which are: radiator frontal area, depth, weight, and drag.

Here, an important compromise that is intrinsic to the radiators sizing practice can be anticipated: weight versus drag. A very compact radiator is lighter than a large one, however, a compact radiator operates with higher air flow velocity which causes more pressure loss and, consequently, it presents more drag than a large one.

Since this work proposes the development of a parametric model that correlates the thermal management system size to the fuel cell power for aircraft application, it imposes the need for a consistent criterion to select one among all the solutions that are created for any fuel cell power.

To accomplish that purpose, a figure of merit is proposed and named as Equivalent Thermal Management System Weight (Eq 4.86). It fuses the TMS drag and TMS weight, which affect the airplane performance in different manners, in a single equation. According to aircraft flight principles, the drag directly affects the required propulsive thrust, while the weight affects the required aerodynamic lift, which produces drag itself, in a proportion given by the aircraft drag polar, (Roskam, 1997). Thus, still considering airplane performance fundamentals, an imaginary weight that is equivalent to the TMS drag in terms of drag generation, can be determined, and the

airplane Lift over Drag characteristic (L/D, obtained from the aircraft drag polar) can be used to estimate such imaginary weight. This imaginary weight replaces the TMS drag, due to its equivalence in the airplane performance effect, and it can be added directly to the TMS actual weight. Equation 4.86 expresses the equivalent weight.

$$Eq\_TMS\_Weight = TMS\_Weight + \frac{L}{D} TMS\_Drag \quad \text{Eq 4.86}$$

By calculating this figure of merit for each feasible thermal management solution and selecting the one the presents the minimum equivalent TMS weight, it is expected to obtain a consistent selection method for the range of fuel cell power so that a parametric model can be created from this exercise.

5 Results

The results will be obtained with the development and use of a set of Python sub-routines that implement the Thermal Management System Design and Optimization framework, described in Section 4. Figure 37 shows the overall run manager flowchart, which submits a population of radiators to a data processing job that calculates the weight, the required air flow and the air flow compatibility. It returns, as output, the weight, the power penalty, and compatibility status from each valid radiator.

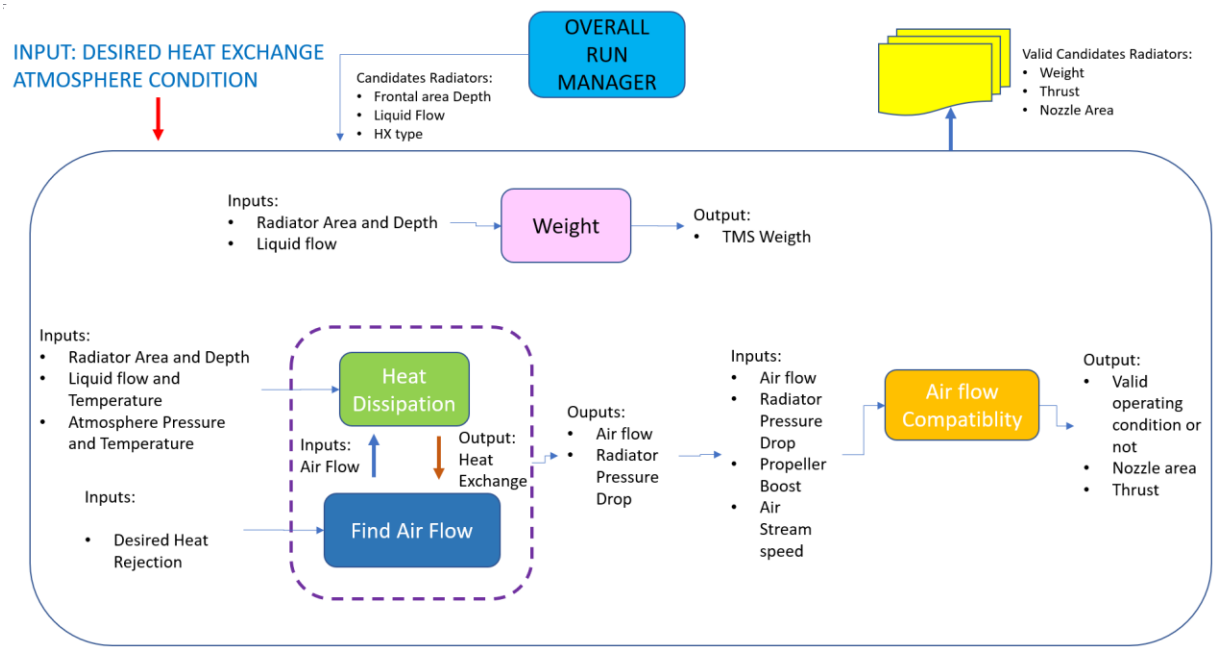

Figure 37 - Thermal Management Routines Organization

Following the radiators population results processing, an optimizer routine (Figure 38) will choose the most suitable radiator according to the procedure proposed in section 4.4.2.

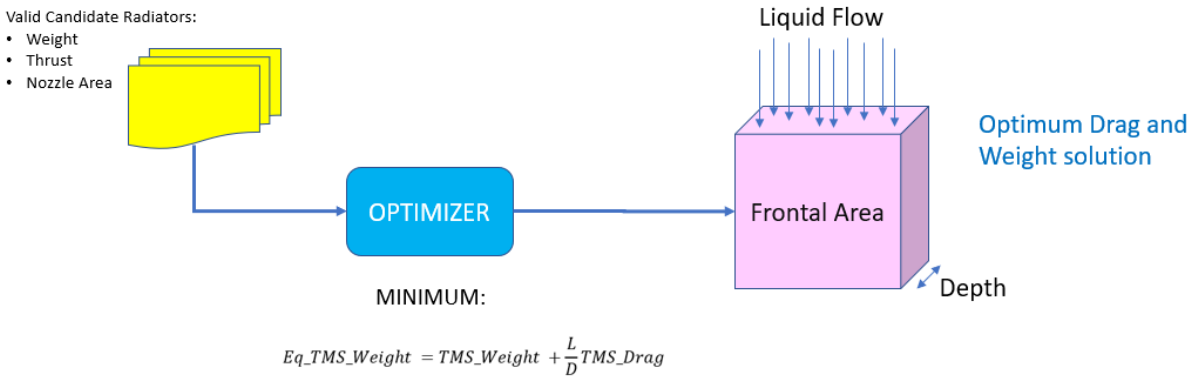

Figure 38 - Optimization Routine

5.1 Sub-routines Tests

Before applying this process, the subroutines behavior will be reviewed to verify if its results are reasonable and to understand the behavior of the thermal management aspects as modeled.

Note: For all tests and parametric model creation the radiator data documented in APPENDIX C will be used.

5.1.1 Weight Routine Test

The weight routine calculates the weight of the Thermal Management System based on procedures declared on section 4.4.1.5. It receives, as inputs, the radiator area, and depth, and radiator core features to calculate the radiator weight. It also receives, as input, an intended coolant liquid flow (expressed in Reynolds Number format) to calculate the liquid circuit weight, which includes the ducts, reservoir, and liquid pump.

The routine results can be reviewed in an exercise to calculate the weight of various combinations of radiators frontal area and depth (at a constant liquid flow Reynolds Number of 4000). Figure 39 shows the results of such exercise.

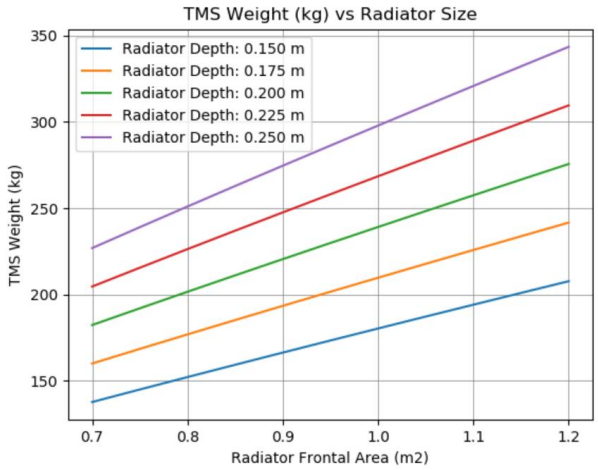

Figure 39 - TMS Weight Model Test Example (Frontal area and Depth)

Results from weight model show monotonically increasing and linear behavior with radiator dimensions as expected.

A second plot (Figure 40) can be used to verify the influence of the liquid coolant flow. As explained in section 4.4.1.5, there is a recommended maximum liquid speed inside the ducts to avoid erosion. A higher liquid coolant flow, operating at a constant reference recommended speed (section 4.4.1.5), requires thicker flow lines and, consequently, more fluid accumulated in the lines and the reservoir.

Figure 40 demonstrates that the model calculates the weight for different liquid coolant flow values consistently to expectation.

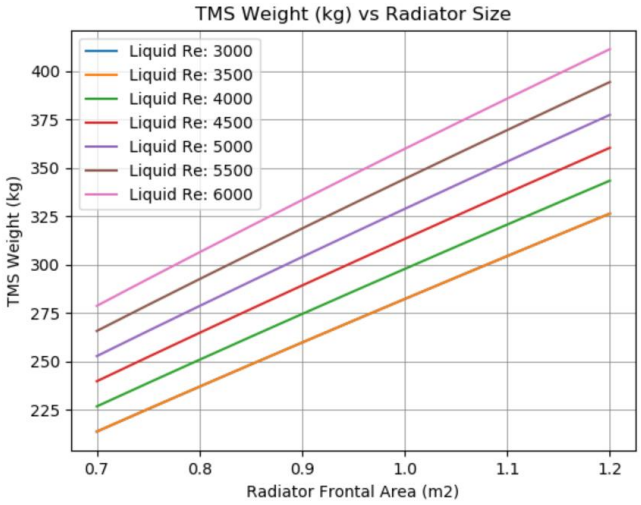

Figure 40 - Weight sub-routine test example (Frontal area and Liquid Flow)

5.1.2 Air flow Calculation Routines Tests

This procedure is accomplished by the in-combination use of two routines developed in Python 3.0:

- Heat Dissipation
- Find Air Flow

The heat dissipation routine is capable to calculate an arbitrarily defined radiator exchanged heat for a given set of inputs: radiator type, radiator frontal area, radiator depth, cooling air flow temperature, liquid flow temperature, air flow and liquid flow.

As an exercise, the routine will be run for two different radiators (both with 1 m^2 of frontal area but the first with 0.15 m of depth and the second with 0.25 m of depth) and to a range of air flow (expressed in Reynolds number format, within the radiators heat performance map boundaries). Table 5 show all the inputs for the routine test.

Table 5 - Radiator characteristics for Air Flow sub-routine Tests

Parameter	Value
Radiator Frontal Area (m^2)	1
Radiator Depth (m)	0.15 and 0.25
Air flow (in Reynolds number)	Radiator Map Range (Figure 24)

Liquid flow (in Reynolds number)	4000
Ambient Pressure (Pa)	101325
Ambient Air Temperature (°C)	30
Liquid Temperature (°C)	100

The routine outputs the exchanged heat as function of air flow for both radiators, as it can be reviewed in Figure 41.

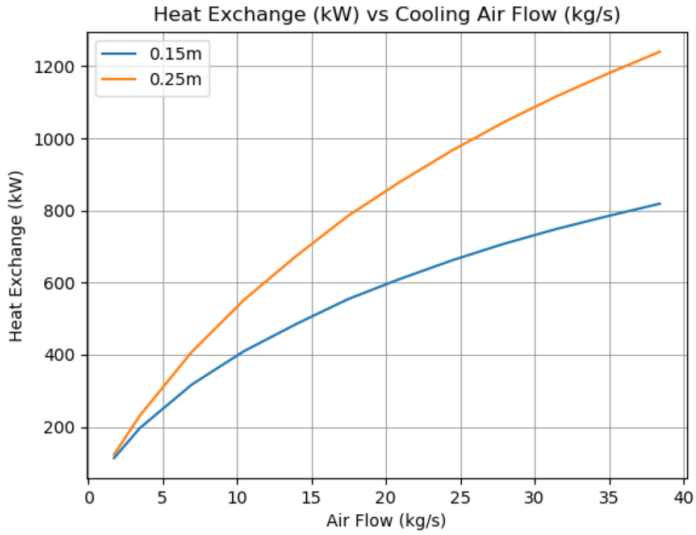

Figure 41 - Heat Exchange vs Air flow (two different depths)

One can notice the monotonically increasing nature of the heat exchange behavior with air flow. It can also be observed that the heat exchange increases with the radiator depth increase. Both radiators operate at same range of air flow because both have the same frontal area. It is important to notice the smoothness of the curve as well, which is important so that the ending result of this work is a smooth and well-behaved model.

By exercising various liquid flows, it can be noticed that the higher is the liquid coolant flow, the higher is the exchanged heat, as depicted in Figure 42.

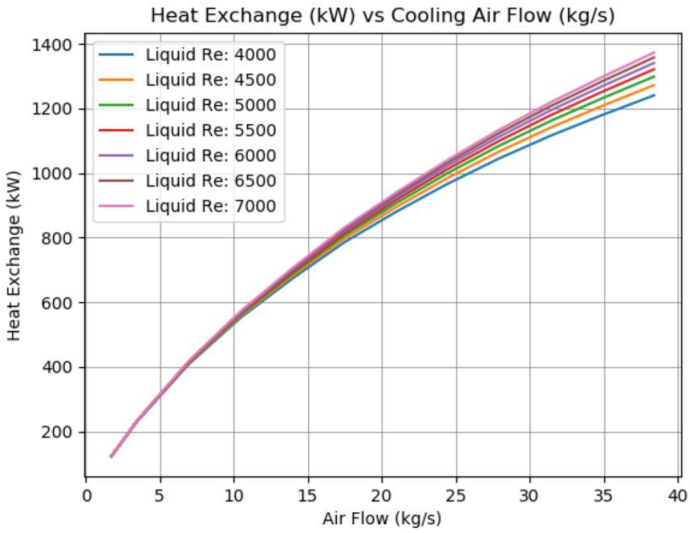

Figure 42- Heat Exchange vs Air flow (seven different liquid Reynolds number)

Another exercise can be made keeping the radiators depth at 0.25 m and varying the frontal area (having the first radiator 0.7 m^2 and the second 1 m^2), and maintaining all other inputs constant.

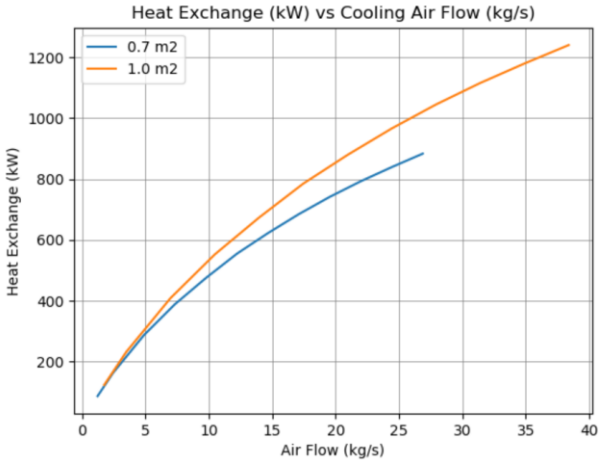

Figure 43 - Heat Exchange vs Air flow (two different frontal areas)

From Figure 43, it can be noticed, at this example as well, how well behaved the curves are: continuous, monotonically increasing and without inflection points. It is worth mentioning that the radiators were tested at same Reynolds number range but, since different areas, air flow ranges are different

Another important parameter to be calculated by this routine is the pressure drop. The Heat dissipation routine also outputs it, and the results can be reviewed in Figure 44:

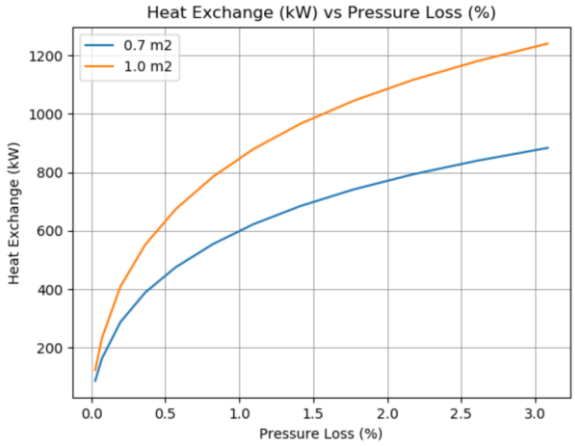

Figure 44 - Heat Exchange versus Pressure Loss (two different areas)

As pointed by Yoshida and Kojima (2015), the operating temperature of the fuel cell has an important effect on the thermal management system design. Running the routine "Heat Exchange" to different liquid temperatures (but the same cooling air temperature) demonstrates that the routine is sensitive to this effect, which can be reviewed in Figure 45.

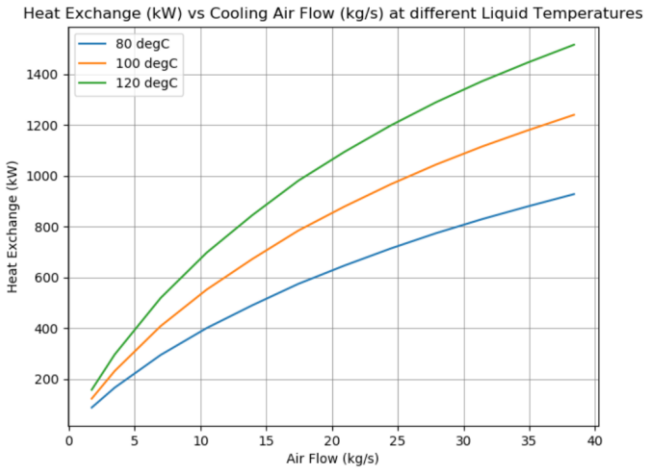

Figure 45 - Heat Exchange versus air flow (Various operating temperatures)

The result demonstrates the capability of the routine of calculating the heat dissipation at different liquid temperatures and the effect of operating at different liquid temperatures, that is, the higher is the liquid temperature the higher is the exchanged heat.

Another important conclusion can be made if the routine is run to the same liquid temperature but different ambient temperatures. Figure 46 shows the sensitivity of the exchanged heat to the air flow for various ambient temperature, all at the same coolant operating temperatures, showing that the less is the ambient temperature the higher is the exchanged heat.

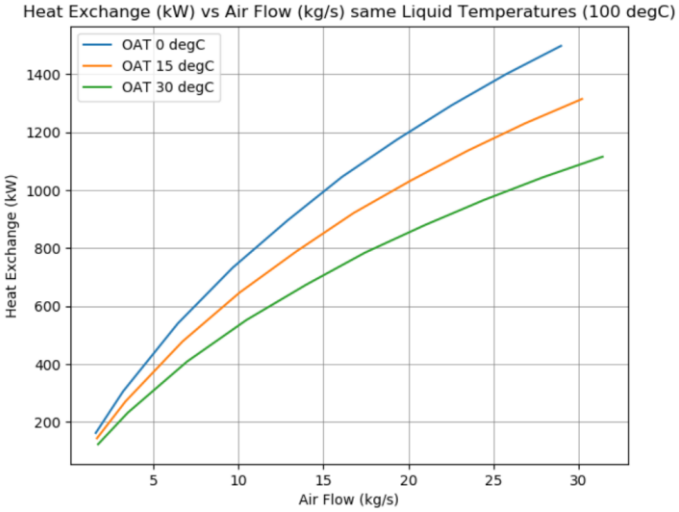

Figure 46 - Heat Exchange versus Air flow (various ambient temperatures)

As predicted by heat transfer theory, the exchanged heat is in fact a function of the temperature difference between hot source (the fuel cell coolant) and the cold source (ambient temperature). Figure 47 shows how the heat rejection curves get close when three different coolant temperatures are tested, but with ambient temperature adjusted so that all are at the same difference. The curves do not collapse in a single one because, although theory predicts the heat exchange is dependent on the delta temperature it is also dependent on the radiator, air flow and liquid properties, which change. But the plot shows the coherence of the model capturing the

proper trends and presenting always continuous, monotonically increasing and no inflations behavior.

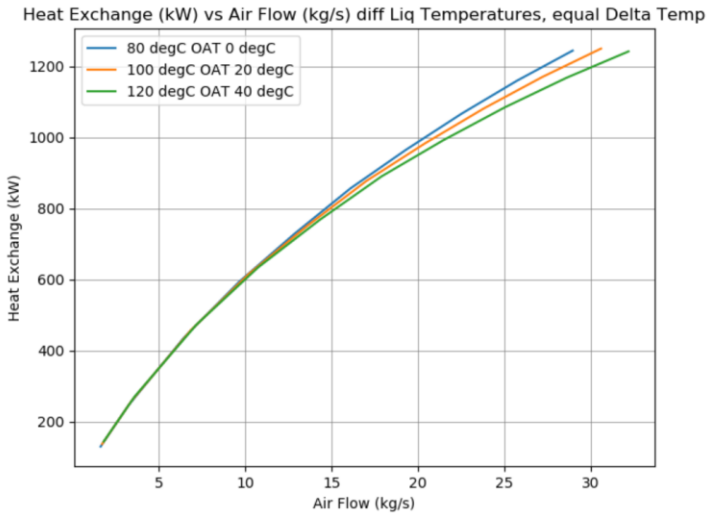

Figure 47 - Heat Exchange versus Air Flow (three combinations of liquid temperature and ambient temperature, same delta)

The second routine to be reviewed is the Find Air Flow routine, which calculates the air flow and the pressure loss required by a given radiator to exchange a certain desired heat dissipation. As explained in section 4.4.1.3 it runs a solver strategy over the Heat Dissipation routine following. Table 6 shows the results of an exercise made with this routine in which the Air Flow and Pressure Drop are calculated for a combination of two radiator sizes and three different desired heat exchange values.

Table 6 - Find Air flow routine test data

GIVEN DATA					OUTPUTS	
Radiator	Frontal Area (m^2)	Depth (m)	Weight (kg)	Heat Dissipation Target (kW)	Air Flow (kg/s)	Pressure Drop (%)
Radiator 1	0.7	0.25	211	400	7.64	0.387
				600	13.81	0.996

				800	22.37	2.37
Radiator 2	1.0	0.25	281	400	6.79	0.188
				600	11.84	0.437
				800	17.97	0.86

An inspection on the plots on Figure 48 and Figure 49 demonstrate that the find air flow routine is operating properly encountering the air flow and pressure drop relative to the desired heat exchange indicated in Table 6.

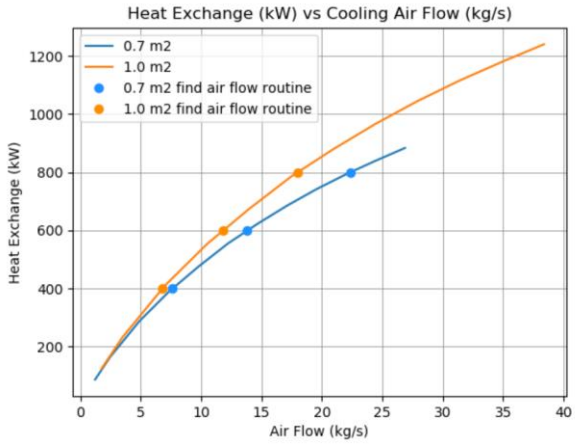

Figure 48 - Find Air Flow Routine Result Test (Heat Exchange versus Air Flow)

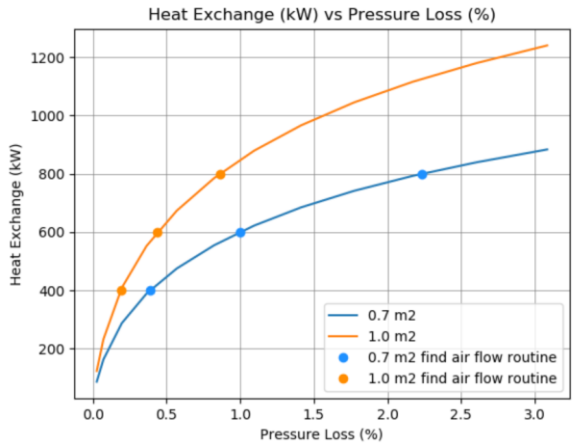

Figure 49 - Find Air Flow Routine Result Test (Heat Exchange versus Pressure Loss)

5.1.3 Air Flow Compatibility

The next step is the review of the air flow compatibility routine, which verifies if the air flow required is an operating condition, i.e. if the air flow has enough pressure to overcome the pressure loss of the thermal management system and returns the Drag of the air circuit.

Accomplishing it requires to join all thermal management system air circuit pressure losses. The radiator pressure loss is obtained directly from the heat dissipation and find air flow routines, as demonstrated in previous section. For the diffuser duct pressure loss calculation, a reference geometry will be adopted (described as follows):

- Throat Area vs Discharge Areas ratio = 1/3
- Expansion ratio angle = 30°

With these two nondimensional geometric features the diffuser pressure loss can be calculated according to equation and pressure loss chart from section 4.4.1.4.2. Equation 5.1 shows the result of the diffuser pressure loss for such geometric definition.

$$\triangle P = 1.6\, \rho\, V_o{}^2 \qquad \text{Eq 5.1}$$

The Air Flow Compatibility implements the procedures described in section 4.4.1.4.5. It receives as input, the desired air flow, static ambient pressure, intake total pressure and temperature. It takes the total air stream pressure, adds the propeller boost pressure and subtracts the calculated pressure loss inside the circuit (from ducts and radiator), resulting in the exhaust nozzle total pressure. If the total exhaust nozzle pressure is less than the ambient pressure, the condition is considered as a non-operating condition and that radiator is considered discarded.

It is worth making an exercise to test this routine to review its behavior. A set of radiators with frontal area varying from 1.75 m^2 to 3.00 m^2 (in steps of 0.25 m^2), all with 0.25 m of depth, and a desired heat dissipation condition of 2000 kW will be used for this test. Conditions are defined as follows:

Flight condition:

- Altitude: Sea Level, Ambient Pressure (101325 Pa)
- Ambient Temperature: 30 °C
- True Flight Speed: Mach 0.18

Heat Management Data:

- Liquid Temperature: 100 °C
- Radiators Frontal Area: 1.75 m^2 to 3.00 m^2 (in steps of 0.25 m^2)
- Heat Dissipation: 2000 kW.

Since the proposed air circuit counts on a propeller to provide a pressure boost, real aircraft data will be used to estimate the pressure rise provided by it. Appendix B shows the rationale to calculate the pressure boost provided by the propeller, applying the procedures described at 4.4.1.4.1. An average pressure boost of 1.6% of the Sea Level Ambient Pressure is obtained.

Thus, Figure 50 shows the required air flow and the resulting pressure drop to meet 2000 kW as function of the radiators frontal area (obtained by Running the Find Air Flow Routine).

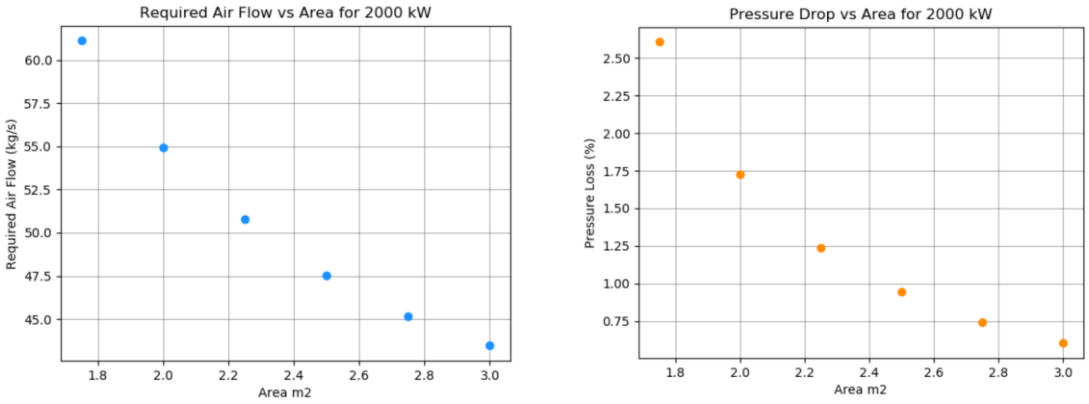

Figure 50 - Air Flow and Pressure Drop vs Area

With these conditions, the air flow compatibility routine can calculate the exhaust nozzle pressure for each radiator. Figure 51 shows the nozzle exhaust total pressure and compares it to the ambient pressure.

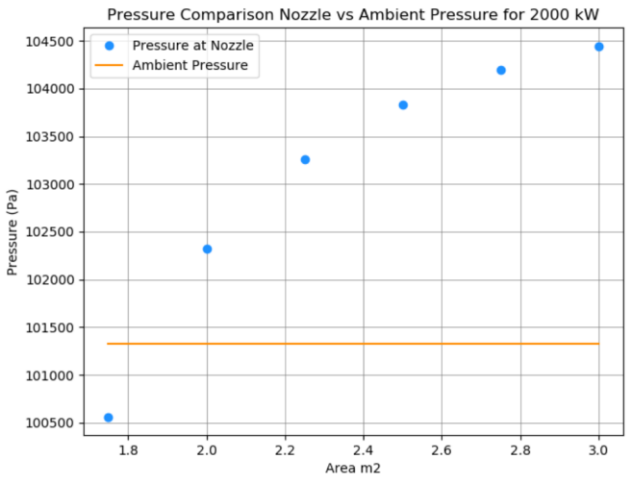

Figure 51 - Pressure Nozzle Pressure vs Ambient Pressure

One can notice that the total exhaust pressure for the lower area radiator (1.75 m^2) is lower than the ambient pressure. That is a non-operating condition, because the required air flow cannot be met at this condition.

The routine also calculates the thrust and exhaust nozzle area which can be verified in the Figure 52 and Figure 53

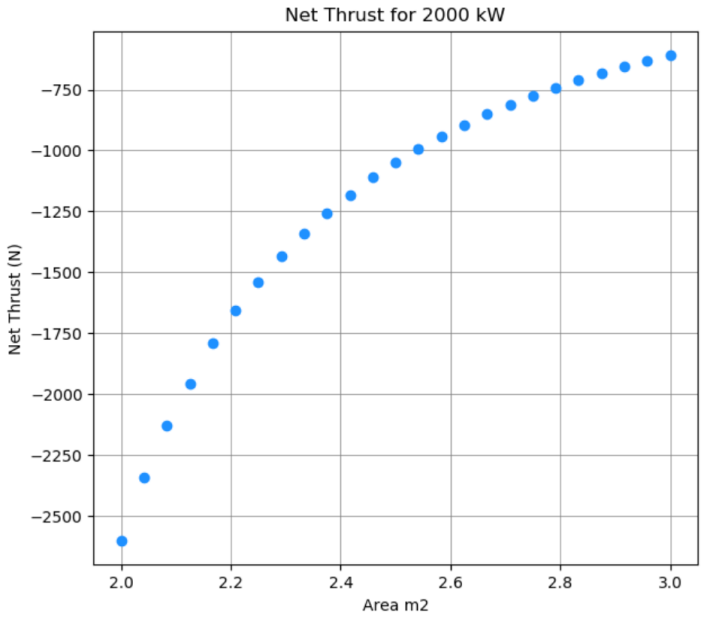

Figure 52 - Thrust versus Area

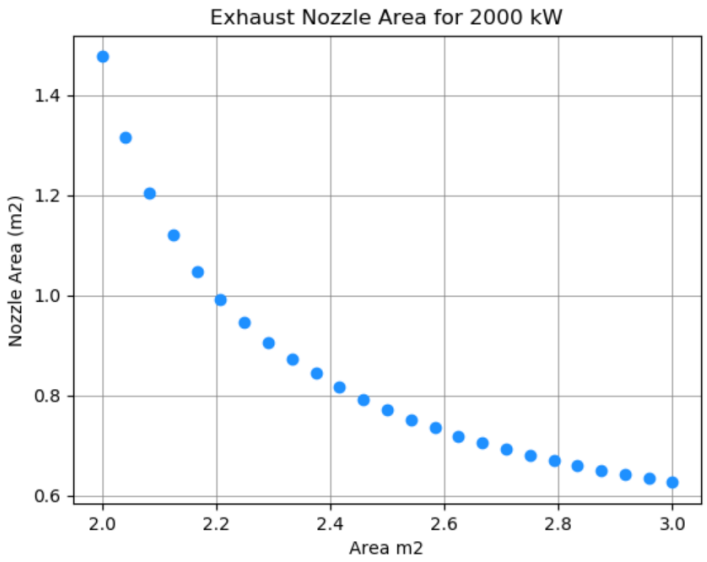

Figure 53 - Nozzle area versus Radiator frontal Area

By reviewing the curves, it can be observed that the thrust curve is smooth and monotonically increasing, matching the expectation that larger radiators require less air flow and results in less drag. The nozzle area is also a smooth curve and the reduction of nozzle area with the radiator frontal area agrees with expectation as well, since larger radiators require less air flow.

5.2 Design Routine

After verifying the sub-routines behavior, it is the proper moment to test the design routine, which will run these previously tested sub-routines searching for an optimized thermal management system solution. It is worth to remind that, for the parametric model creation, the radiator data documented in Appendix C will be used. All analysis will be done to the radiator designated as 10_94 (in Appendix C) because, from friction charts, it is one of the most promising radiators, due to its low friction values (which means less drag perspective). A comparison to 10_93, which presents similar levels of friction coefficients, will be presented to confirm the perspective.

5.2.1 Critical Flight Condition Definition

Before executing the design routine, it is necessary to define a design condition.

From Figure 45 and Figure 46 it is possible to state that the heat dissipation capability is positively correlated to the air flow and negatively correlated to the coolant/ambient temperature difference. Therefore, the most critical condition for design is expected to be at combination of the highest required heat dissipation and the least coolant/temperature difference.

Considering that this is an aircraft application, this work assumes that the fuel cell must deliver the power in a similar manner as the turboprop gas turbine engines. Walsh (2004) presents how aeronautical gas turbines rated power behave with altitude and temperature. In terms of altitude, the power decreases directly driven by the altitude pressure decrease, that is, the power at a certain altitude can be calculated by the power at Sea Level multiplied by the ratio between the Local pressure and Sea Level ambient Pressure, which can be observed in Figure 54

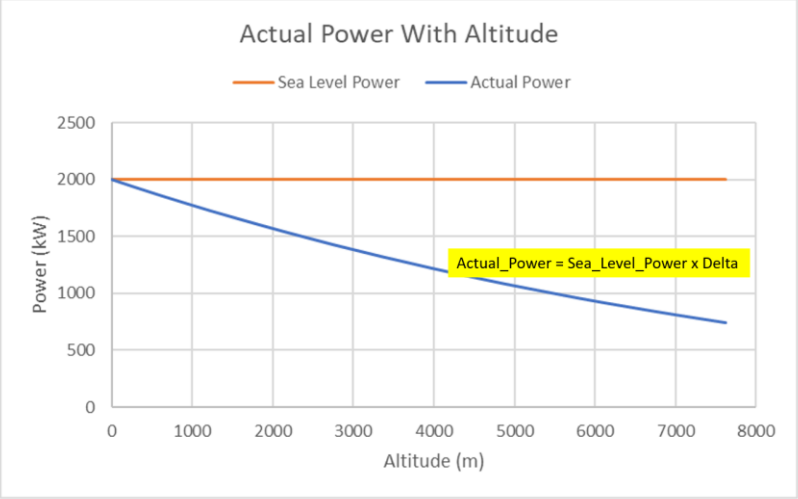

Figure 54 - Typical Gast turbine Rated Power with Altitude, adapted from Walsh (2004)

Figure 55 shows how gas turbine power behaves with temperatures. According to Walsh (2004), power is maintained constant with ambient temperature increase, while the Turbine Exhaust Gas Temperature increases, up to a point where the Exhaust Gas Temperature reaches a

limit. From this point (known as corner point) the power starts to decrease to maintain the turbine EGT constant.

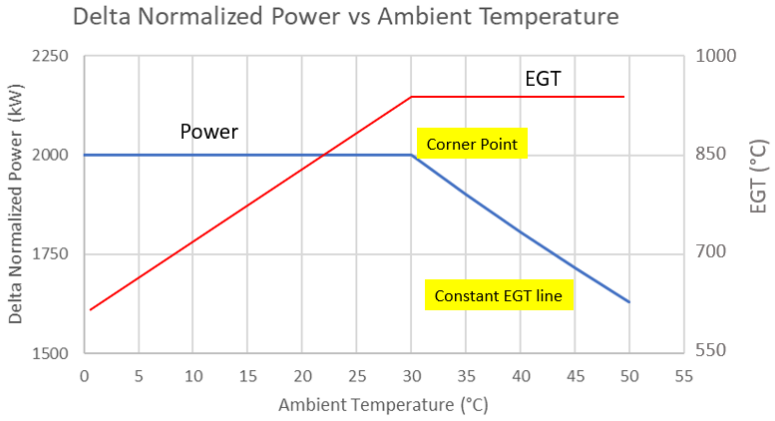

Figure 55 - Typical Gas Turbine Rated Power Variation with Ambient Temperature

This work takes credit from the same principle. Appendix B presents a rational to define a proper corner point for this exercise: 30°C. So, the highest fuel cell power will occur at Sea Level and at a 30 °C A. Since the demanded heat dissipation is directly related to the Fuel Cell Delivered Power, that will be the thermal management system design point.

5.2.2 Overall Run

Once all subroutines have been reviewed and the critical design point has been defined, it is necessary to perform the overall run. A population of radiators will be created, and each individual will pass through to the air flow compatibility routine, which will classify every radiator individual as a valid solution or not, and, for each valid solutions, record its weight and drag for a further optimum individual selection.

For this exercise, the flight condition and heat management will be defined as follows.

Flight condition (representative from takeoff situation):

- Altitude: Sea Level, Ambient Pressure (101325 Pa)

- Ambient Temperature: 30 °C
- True Flight Speed: Mach 0.18

Heat Management Data:

- Liquid Temperature: 100 °C
- Heat Dissipation: 2000 kW

Radiator Population:

- Radiators Frontal Area: 1.75 m^2 to 4.00 m^2 (in steps of 0.25 m^2)
- Radiators Depth: 0.15 m to 0.4 m (in steps of 0.015 m)
- Liquid Flow: Reynolds Number from 3000 to 6000 (in steps of 500)

Notice that proposed variation for radiators parameters (area, depth, and operating liquid flow) creates a population of 420 individuals.

After the overall run, in which the air flow compatibility routine has been run to all the radiators population, the individuals have been separated in valid and non-valid solutions and Figure 56 and Figure 57 show a map of the candidates' situation with respect to the combination of operating Liquid flow, frontal area and depth.

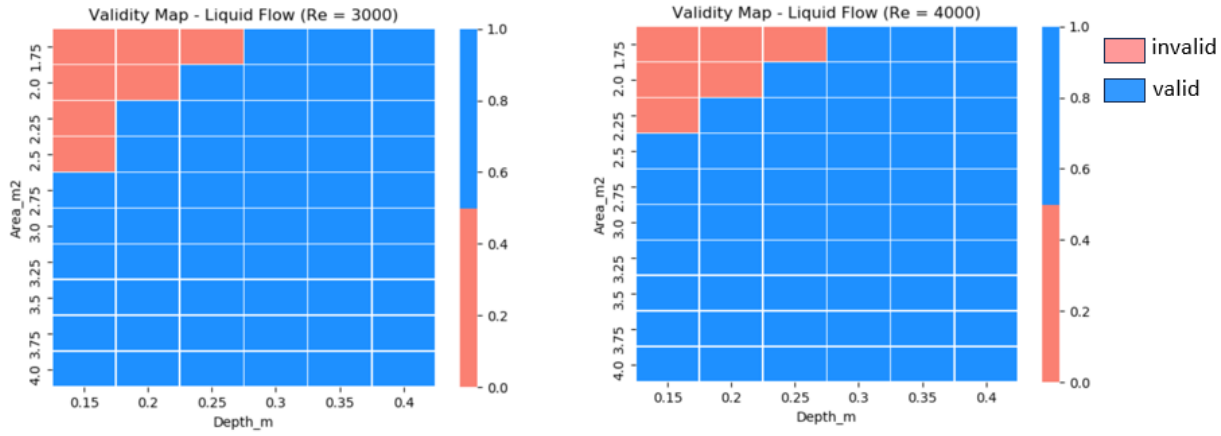

Figure 56 - Population Validity Map, Re=3000 and Re = 4000

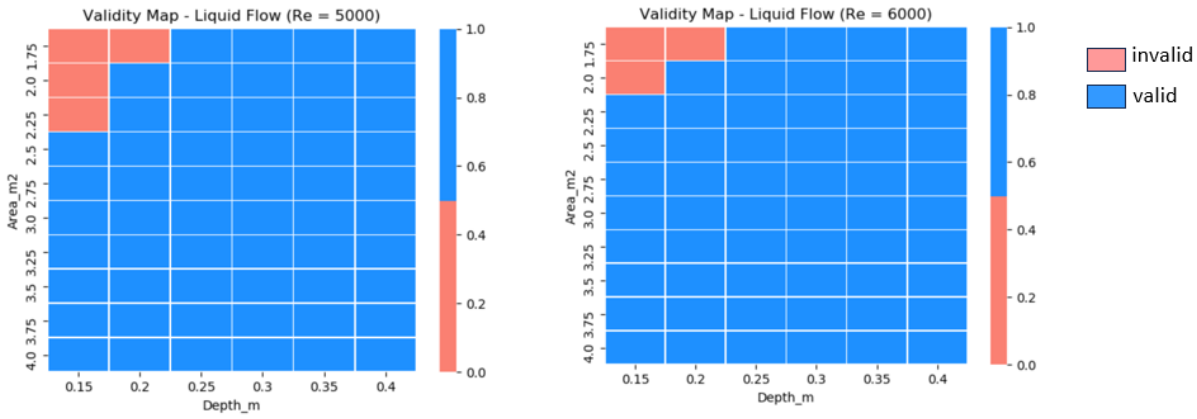

Figure 57 - Population Validity Map, Re=4000 and Re = 5000

Figure 56 and Figure 57 show a portion of the population that do not represent valid candidates. As explained before, these are conditions in which the air flow compatibility function results in a total air flow pressure at exhaust nozzle less than the ambient pressure. It can be noticed that the smaller frontal area radiators are the ones excluded, as expected, due to the higher air flow demand and higher resulting pressure loss. It can also be observed that the higher the liquid flow, the lower the number of invalid solutions. This is explained by the fact that, with higher liquid flow, the heat exchange requires less airflow (Figure 42), which creates less pressure drop.

With the data from this run, it is worth drawing a scatter plot to review the TMS weight and drag from this population of radiators:

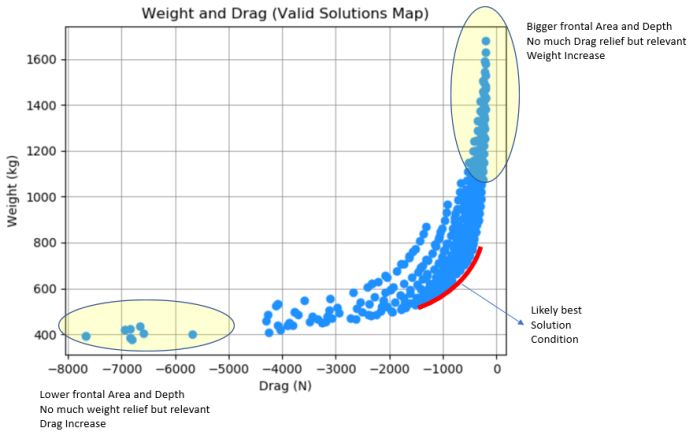

Figure 58 - Weight versus Drag scatter (all valid population individuals)

A review of the plot shown in Figure 58 confirms an expected trend that heavier thermal management systems present less drag and vice versa. The trend has a clear limit since, as shown in lower-left quarter of plot, the drag increases with no relevant weight decrease. On the upper-right quarter the opposite is observed, larger and heavier thermal management systems do not present much drag improvement. Identified as likely best solution, a red line drawn in the plot indicates the region which combines the smaller weight and drag levels.

The Figure 59 helps to understand how the radiators characteristics are positioned inside this weight versus drag map. When observing the scatter plots separated by depth (Figure 59, left chart) and separated by frontal area (Figure 59, right chart), it becomes clear that best solutions are on combinations of larger areas and smaller depths.

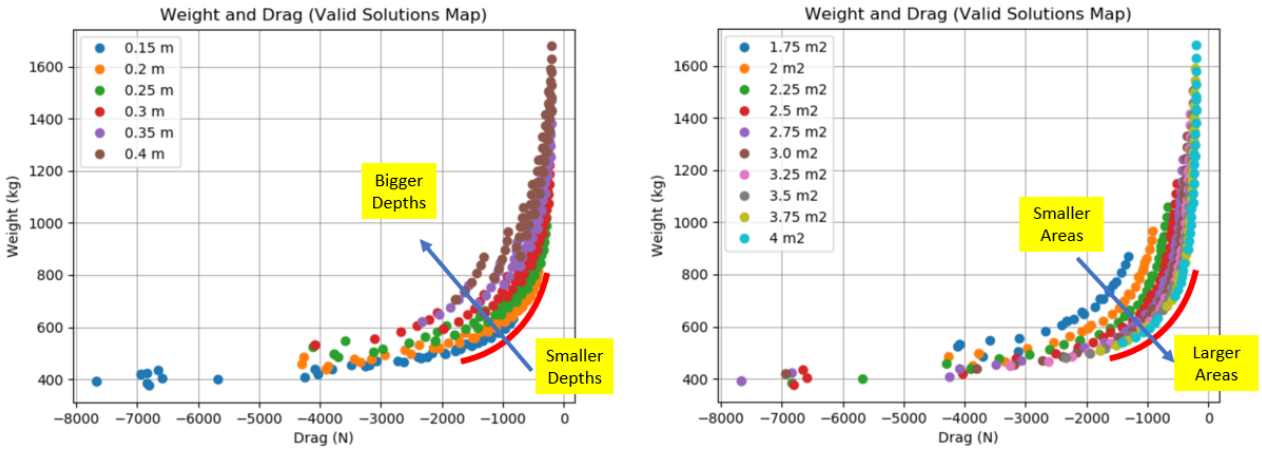

Figure 59 - Weight versus Drag scatter (depth and area segregated in different lines)

5.2.3 Optimizer Routine

The last step is to select the best solution for aircraft performance purposes. Section 4.4.2 proposes a method to select the best solution, by calculating an equivalent weight figure of merit for each of the population samples and the optimizer routine will select the least equivalent weight.

A set of heatmap plots (Figure 60 and Figure 61) can be used to show the equivalent weight figure of merit of all valid individuals proposed in this test. Each heat map is tied to a specific liquid coolant flow and will show the equivalent weight for all combinations of frontal area and depth.

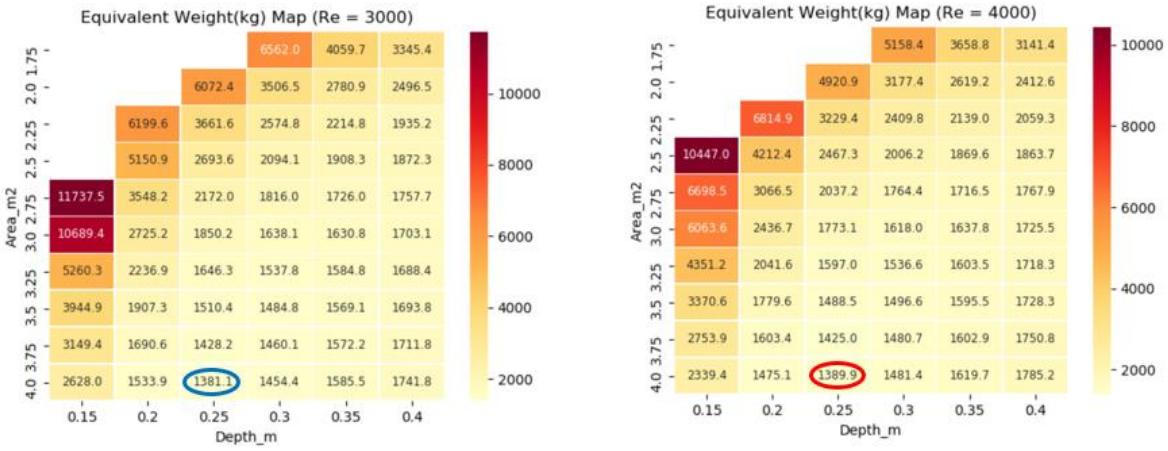

Figure 60 - Equivalent Weight Heat Map Re=3000 and Re = 4000

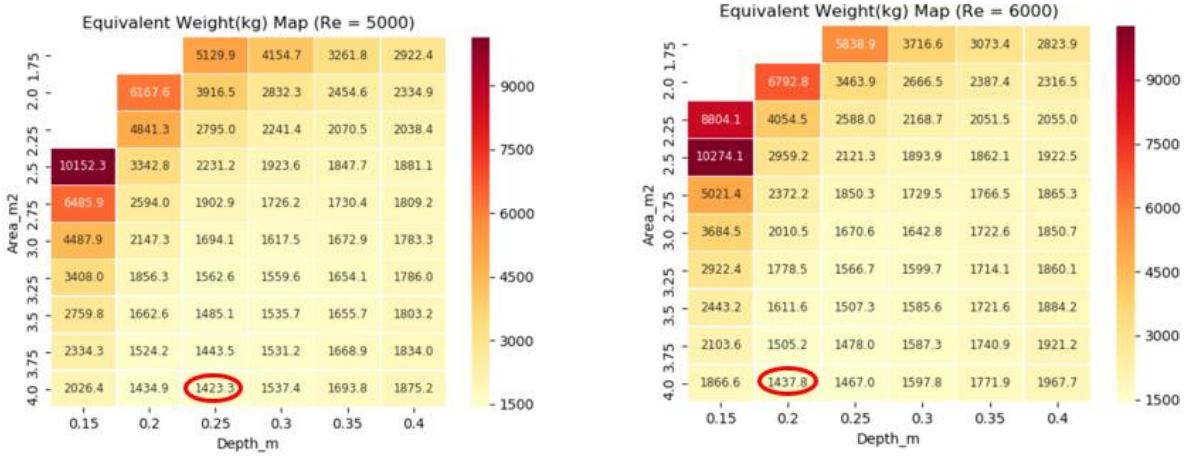

Figure 61 - Equivalent Weight Heat Map Re=5000 and Re = 6000

Ellipses in each heatmap (Figure 60 and Figure 61) indicate the least equivalent weight. It shows that the best solution is the Radiator with 4.0 m^2 of frontal area, 0.25 m of depth and operating with liquid flow at Reynolds Number of 3000, equivalently weighting 1381 kgf.

Weight and drag from the TMS solutions can also be plotted, as it can be verified in Figure 62, Figure 63 and Figure 64. Best solution weight is 897 kg and drag is 328 N or 31 kW (in power penalty format). It is interesting to observe that these values do not represent neither the least weight nor the least drag condition, but the compromise indicated in Figure 60 and Figure 61.

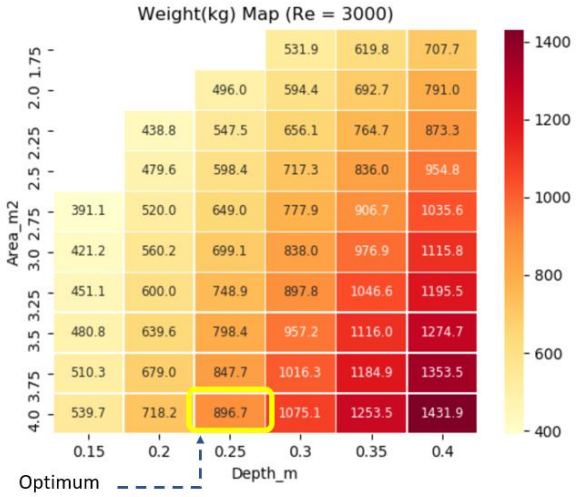

Figure 62 - TMS Weight Heatmap

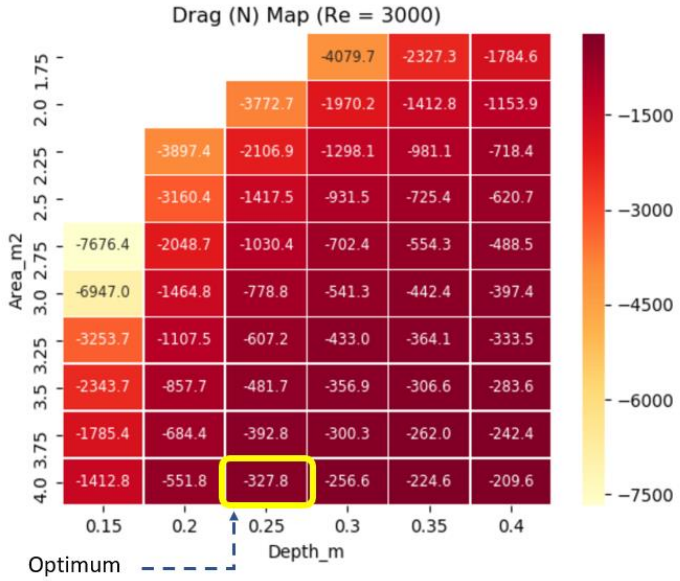

Figure 63 - TMS Drag Heatmap

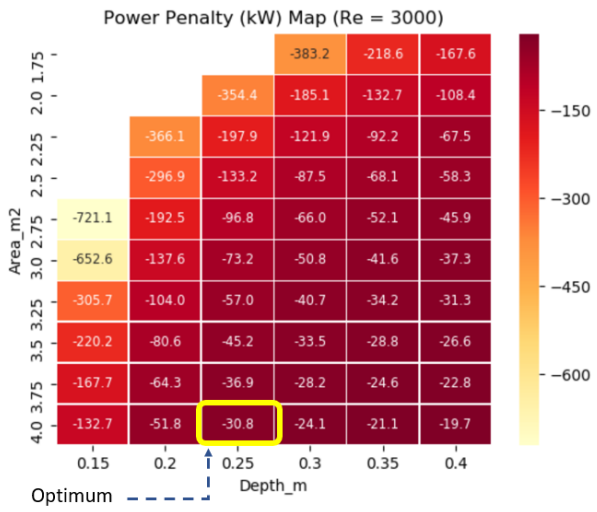

Figure 64 - TMS Drag (in Power Penalty format) Heatmap

5.3 Parametric Model Generation

At previous step, the optimizer routine was run to a specific dissipation heat (2000 kW) as an example to verify the routine behavior and consistency. However, the intent of this work is to create a parametric model that can calculate the thermal management system parameters for a range of heat dissipation. Assuming the range of engine power typically adopted in the segment of concern (Appendix B) and fuel cell heat rejection factor (Equation 4.63), the range of heat dissipation for is from 900 kW to 2900 kW.

Therefore, the routine will be run within 900 kW to 2900 kW range as the heat exchange target and for three options of liquid operating temperatures, 80°C, 100 °C and 120°C. The design condition will remain the same (Sea Level, 30°C of ambient temperatures).

For every power condition, in addition to calculate the optimum thermal management system weight, radiator area, and the design condition drag, the parametric routine will calculate an off-design parameter: the drag in cruise condition, which is very important to assist the conceptual design of aircraft. For cruise, the routine will assume the following flight conditions as follows: Altitude (7620 m), Mach (0.45) and Ambient temperature (-34.6°C), which is a typical cruise condition for turboprop airplanes and the power will be a fraction of the design condition power, obtained from Figure 54.

Since the thermal management system parametric model is intended for aeronautical application, the size is a very important and geometric restrictions should be considered by a designer. As already exposed, the overall run routine takes as input a population of radiators with ranges of frontal area, length, and operating coolant flow for test selection of the best condition. For this reason, the overall run will be executed with 3 different population frontal area ranges:

- Minimum Frontal Area: 0.9 m^2 to 3.6 m^2
- Medium Frontal Area: 1.2 m^2 to 4.8 m^2
- Maximum Frontal Area: 1.5 m^2 to 6 m^2

Note: these previously described frontal area ranges represent the ranges alternatives adopted to the highest heat dissipation tested (2900 kW). For the heat dissipation values excursion, which will go from 2900 kW down to 900 kW, the area ranges will vary assuming a proportional value. In other words, the minimum area, which ranges from 0.9 m^2 to 3.6 m^2 for 2900 kW, will range from 0.45 m^2 to 1.8 m^2 for 1450 kW for example.

The results from the model can be reviewed in Figure 65 which shows the weight and radiator frontal area as function of heat dissipation and Figure 66 which shows the TO and CRZ drag (in power penalty format) also as function of the heat dissipation:

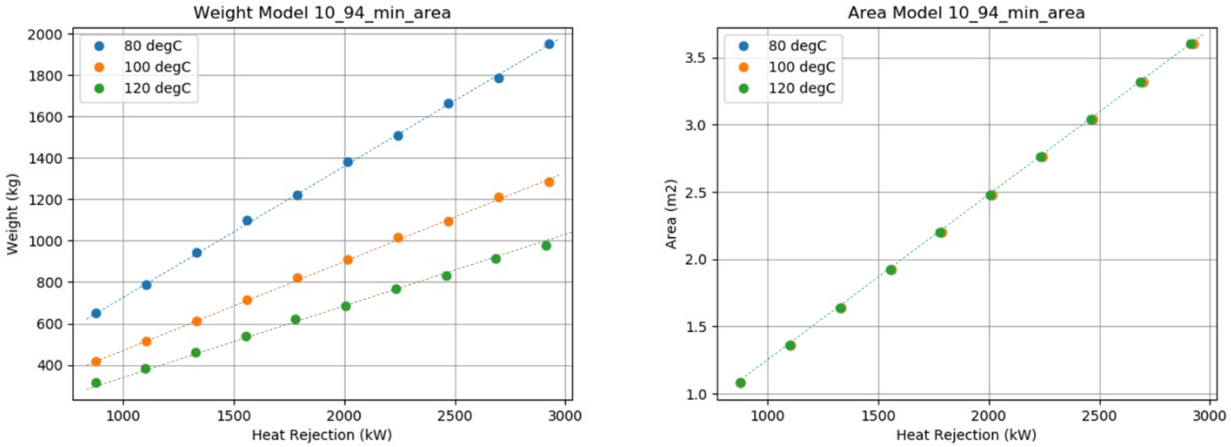

Figure 65 - Weight and Frontal Area (minimum area range)

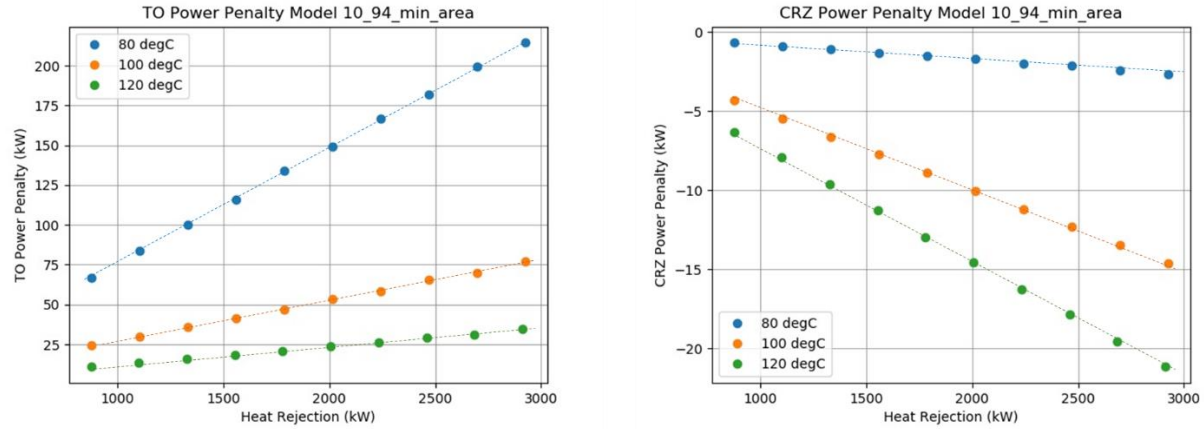

Figure 66 - Takeoff and Cruise Power Penalty (minimum area range)

The result from the overall run shows a linear relationship between the thermal management parameters (Weight, radiator frontal area, TO power penalty and CRZ power penalty) and the heat dissipation. It can also be observed that different relationships are established for each coolant temperature.

Note: it is worth mentioning that the frontal areas found in this exercise are very large. A discussion about it will be done in section 5.6.

Table 7 shows a linear regression exercise that creates an analytical way for the calculation of the thermal management parameters:

Table 7 - Parametric Equations (minimum area range)

TMS / Liquid Temp	Weight (kg)	Area (m^2)	TO power penalty (kW)	CRZ power penalty (kW)
80 °C	0.63 Q + 101	0.00123 Q - 0.00034	0.072 Q + 3.553	-0.00095 Q + 0.14337
100 °C	0.43 Q + 44	0.00123 Q - 0.00034	0.025 Q + 1.738	-0.00501 Q + 0.06087
120 °C	0.33 Q + 28	0.00124 Q - 0.0014	0.011 Q + 0.93	-0.0073 Q + 0.07855

Note: Q is fuel cell heat dissipation in kW

Figure 67 and Figure 68 shows the results for the frontal area range designated as medium (1.2 m^2 to 4.8 m^2 for 2900 kW and proportional values for the lower power conditions).

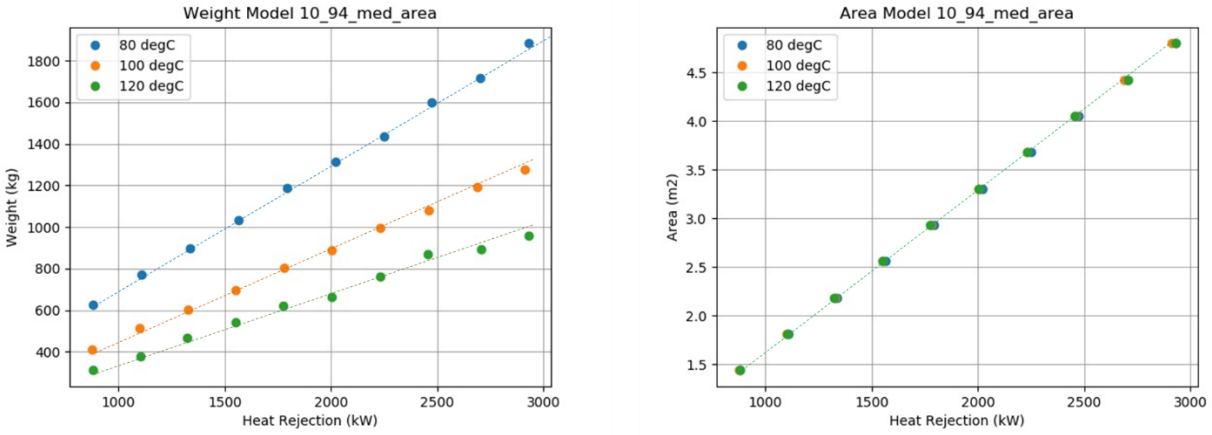

Figure 67 - Weight and Frontal Area (medium area range)

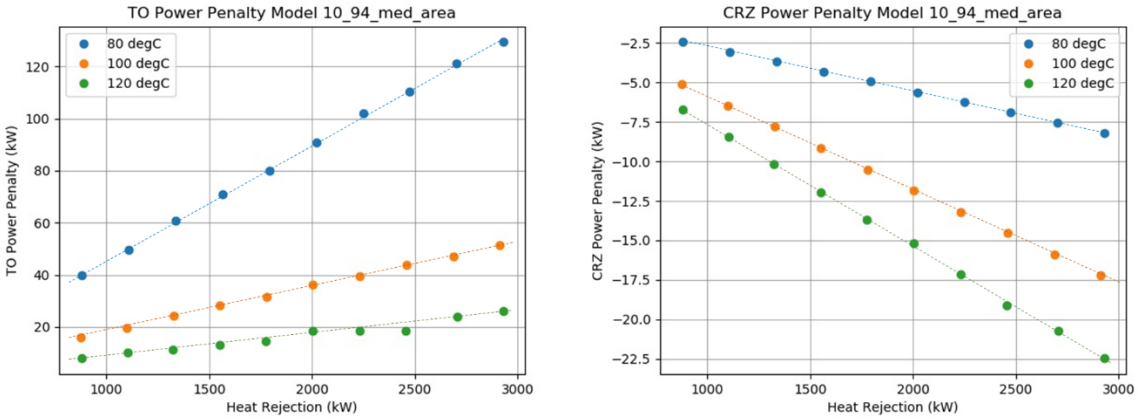

Figure 68 - Takeoff and Cruise Power Penalty (medium area range)

In this case, the overall run also results in a linear relationship between the thermal management parameters (Weight, radiator frontal area, TO power penalty and CRZ power penalty) and the desired heat dissipation. Another fact observed in the minimum area range case repeats for the medium area range case, which is the well-established relationship for each coolant temperature.

Table 8 shows a linear regression exercise made for the medium area range:

Table 8 - Parametric Equations (medium area range)

TMS / Liquid Temp	Weight (kg)	Area (m^2)	TO power penalty (kW)	CRZ power penalty (kW)
80 °C	0.61 Q + 92	0.0016 Q - 0.00043	0.044 Q + 1.349	-0.0028 Q + 0.022
100 °C	0.43 Q + 41	0.0017 Q + 0.00026	0.017 Q + 0.989	-0.00594 Q + 0.056
120 °C	0.32 Q + 33	0.0016 Q + 0.013	0.008 Q + 0.174	-0.0077 Q + 0.029

Note: Q is fuel cell heat dissipation in kW

Figure 69 and Figure 70 show the TMS results for the maximum area range.

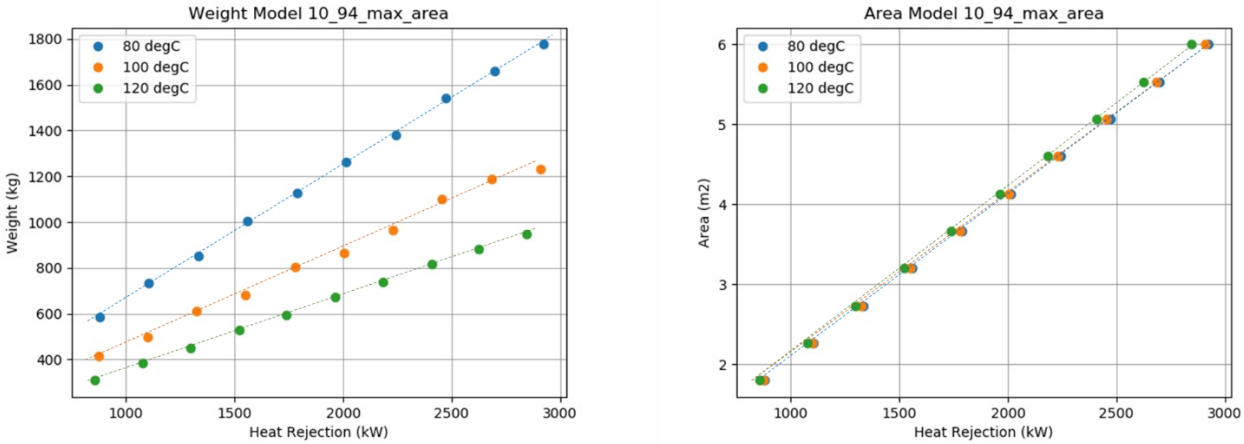

Figure 69 - Weight and Frontal Area (maximum area range)

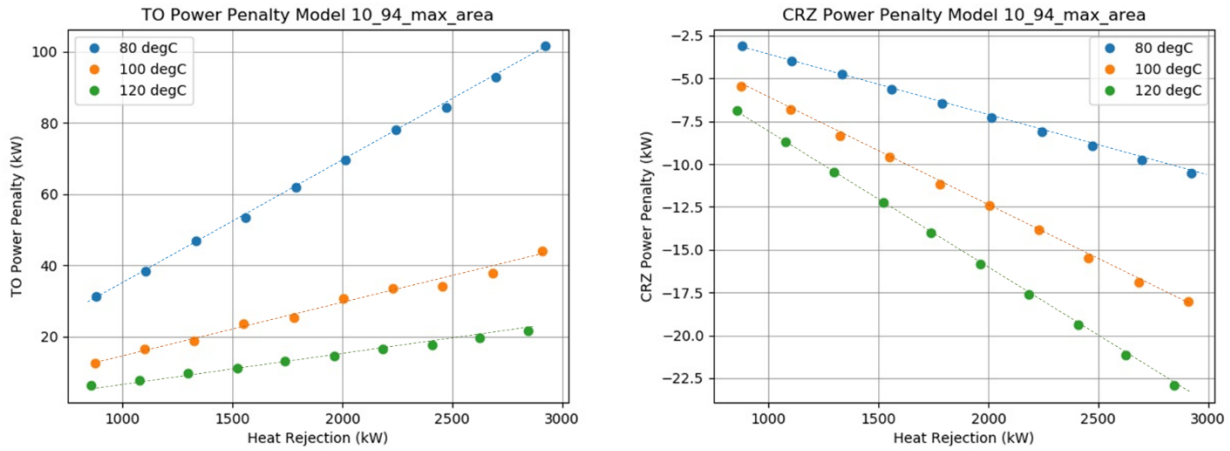

Figure 70 - Takeoff and Cruise Power Penalty (maximum area range)

In this last case, following the same behavior as the previous two, the overall run results in a linear relationship between the thermal management parameters (Weight, radiator frontal area, TO power penalty and CRZ power penalty) and the desired heat dissipation. Furthermore, the behavior observed in the minimum and medium areas range, which is the well-established relationship for each coolant temperature, is also present in the maximum area range.

Table 9 shows a linear regression exercise made for the maximum area range:

Table 9 - Parametric Equations (maximum area range)

TMS / Liquid Temp	Weight (kg)	Area (m^2)	TO power penalty (kW)	CRZ power penalty (kW)
80 °C	0.58 Q + 84	0.0021 Q - 0.00023	0.034 Q + 0.898	-0.00363 Q + 0.053
100 °C	0.42 Q + 48	0.0021 Q - 0.0005	0.015 Q + 0.151	-0.00625 Q + 0.0095
120 °C	0.32 Q + 36	0.0021 Q - 0.0035	0.008 Q - 0.395	-0.00807 Q + 0.0101

Note: Q is fuel cell heat dissipation in kW

5.4 Results Review

All cases show linear correlation between critical TMS parameters (Weight, Area, TO power penalty and CRZ power penalty) and the intended dissipation power, which confirms that a parameterized model can be built.

It can be noticed, by reviewing the area parametric model, that the results selected by the optimized routine were found at the maximum area within each correspondent range. Since the area has a relationship to the radiator pressure drop, as already explored in section 5.1, it shows that the routine is searching for biggest possible areas to reduce pressure drop and drag, consequently.

The TO power penalty present positive values (which means that it causes drag) while the CRZ Power penalty present negative values (which means it causes thrust). In takeoff, the balance between the exit cooling air flow momentum and the inlet air flow momentum is negative, in other words, the air decelerates, due to the radiator pressure loss, and the fact that the acceleration caused by the heat dissipated by radiator is not enough to overcome it. In the CRZ condition, however, the same balance is positive, i.e., the air flow accelerated by the radiator heat overcomes the pressure loss. Such an inversion occurs basically because, at takeoff, the thermal management system operates at its most stressed condition, highest heat exchange demand and lowest

temperature difference between liquid and the ambient, which requires the biggest air flow for the heat dissipation and consequently inducing the highest radiator pressure loss. In the CRZ condition, operating at lower power and lower ambient temperature, the required air flow is much less and, since it is actively controlled by the variable area exhaust nozzle, it results in less pressure loss. That result is in line with conclusions from Meredith (1935) which anticipates that with a proper radiator design and adoption of a variable area nozzle, the thermal management system can actually create thrust in cruise.

It is worth emphasizing that the plots showed very well separated lines for the different liquid operating temperatures. Moreover, as explored in section 5.1, the higher the operating liquid temperature is, the lower the thermal management system load is, and this fact appears clearly in the equations, showing the lower weight, TO power penalty and CRZ power penalty.

5.5 Modeling Use and Recommendation

An aircraft designer can use the linear models in Table 7, Table 8 and Table 9 to estimate the weight, the TO and Cruise power penalties and the required frontal Area.

The sequence is: from a required propeller shaft power (which must be provided by the Fuel Cell), calculate the desired heat dissipation with equation 4.34. The designer must be aware of the operating liquid temperature at which its fuel cell can operate (among the options offered, 80°C, 100 °C and 120 °C) and use the correspondent equation to calculate the critical parameters to assist the aircraft design.

A more practical way to estimate the TMS parameters is the adoption of KPI (Key Performance Indicator) which is a singular number that correlates two parameters. The KPIs values can be created from the ratio: parameter of interest over exchanged heat. That approach can be done because of the linearity of the models. It is extremely practical but may incur in an error, which is acceptable depending on the purposes of the analysis.

KPIs for Weight, Frontal Area, TO penalty and CRZ penalty is created based on the average of the ratio found in the extremes of the range covered in section 5.4 models. It can be

anticipated that this procedure, for this analysis, creates an error or the order of +/-5%, since the equations from section 5.4 do not have a null bias.

Figure 71 shows the KPI for radiator frontal Area, which is presented here as the dissipated heat divided by the required area (inverse of the rate term of the equations).

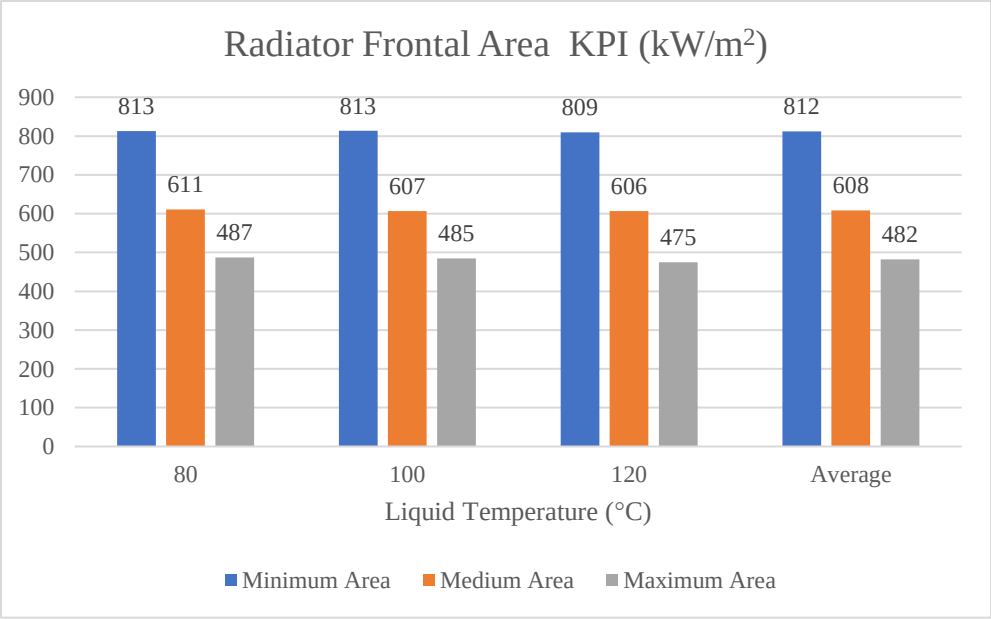

Figure 71 - Area KPI

One can notice that area KPI for the different temperatures are very close. That fact is just a confirmation of observations made on section 5.4, that optimizer solution is always running to the maximum tested area ranges to minimize the drag. Thus, an Average KPI is suggested covering all temperature options.

Figure 72 shows the KPI for the thermal management system weight, which is presented as the dissipated heat divided by weight, typically known as specific power:

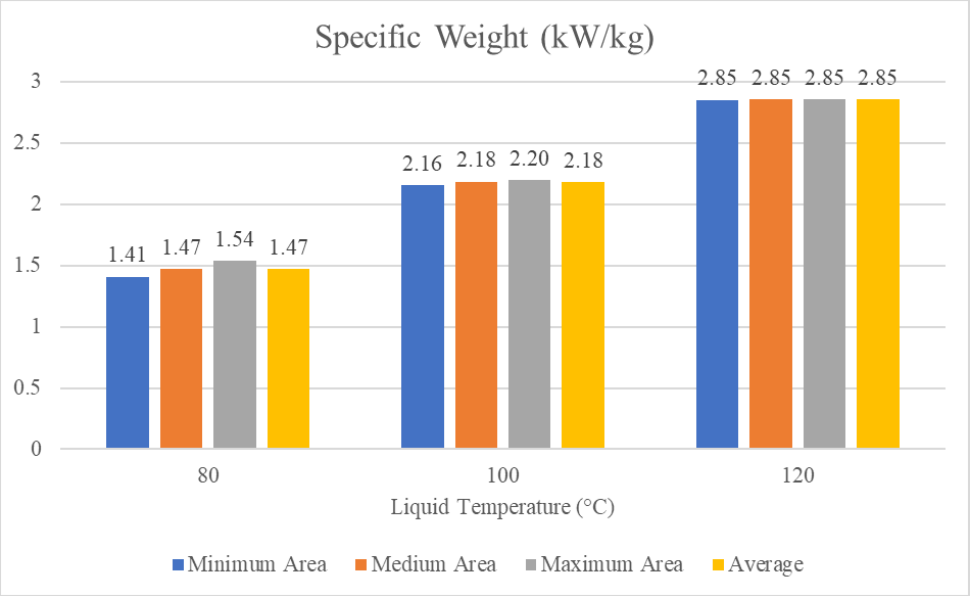

Figure 72 - Weight KPI

One can notice that weight KPIs for the different temperatures are very different and are in line with observations made on section 5.1, that the higher the liquid/air temperature difference the lower is the heat management system demand. Very close weights are found for the three different areas ranges, thus an average specific power KPI is suggested encompassing the 3 different areas. At this point it is important to explain why three different area ranges results in the same weight. A certain frontal area radiator is lighter than a larger one if all parameters are kept equal. However, if kept the air flow constant, a radiator with a certain frontal area, to absorb the same heat as a larger one, requires a combination of more depth and more liquid flow. Operating with more depth or operating with higher liquid flow increases its weight, compensating somehow the weight reduction due to the smaller area. A smaller frontal area radiator, kept constant depth and liquid flow (which would present less weight), requires more air flow and increases the drag, in a magnitude that does not compensate the weight reduction, them being discarded by the routine.

Figure 73 shows the KPI for the thermal management system TO power penalty. In this case though, since the unity of the rate term of linear equations is kW/kW, this KPI will be presented in %.

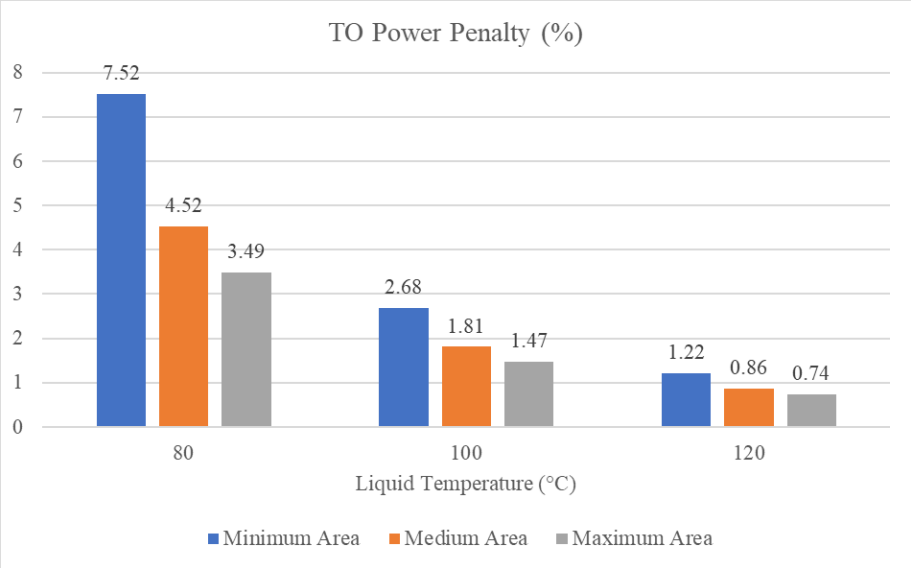

Figure 73 - TO Power Penalty KPI

The TO power penalty KPI for the different temperatures are very different and also in line with observations made on section 5.1, that the higher the liquid/air temperature difference the lower the heat management system demand. The three different area ranges also show a trend that the larger the area the smaller is the TO power penalty.

Figure 74 shows the KPI for the thermal management system CRZ power effect. As demonstrated, the CRZ power penalty are negative values because thermal management system, indeed, cause thrust and not drag in these conditions. Instead of plotting a negative penalty, this work will present the CRZ effect in terms of a positive power addition. Figure 74 shows the KPI for the thermal management system CRZ power addition, presented in % as well.

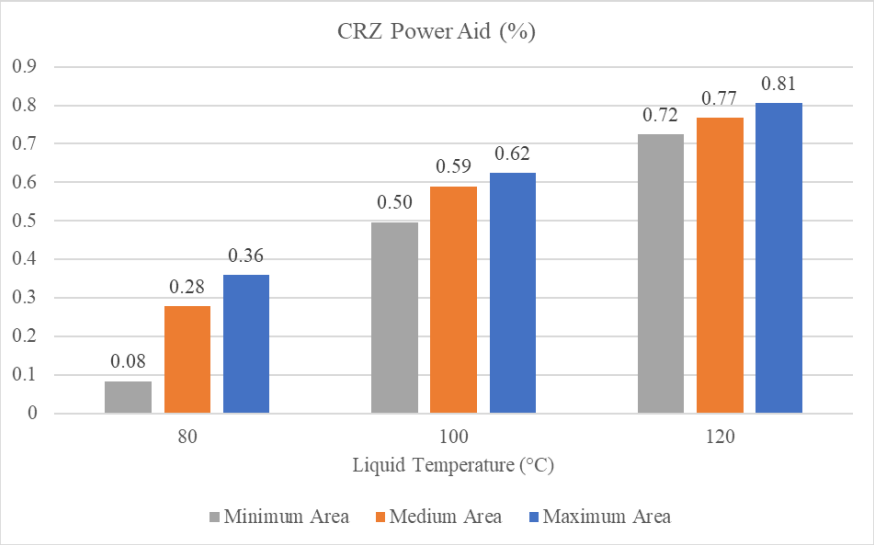

Figure 74 - CRZ Power Aid KPI

The same exercise has been done to another radiator, from the ones described in Appendix C (10_93), which was indicated in the beginning of section 5 as another radiator option to be evaluated. Figure 75, Figure 76 and Figure 77 shows the difference between the radiator 10_94 and 10_93 for the medium frontal area range.

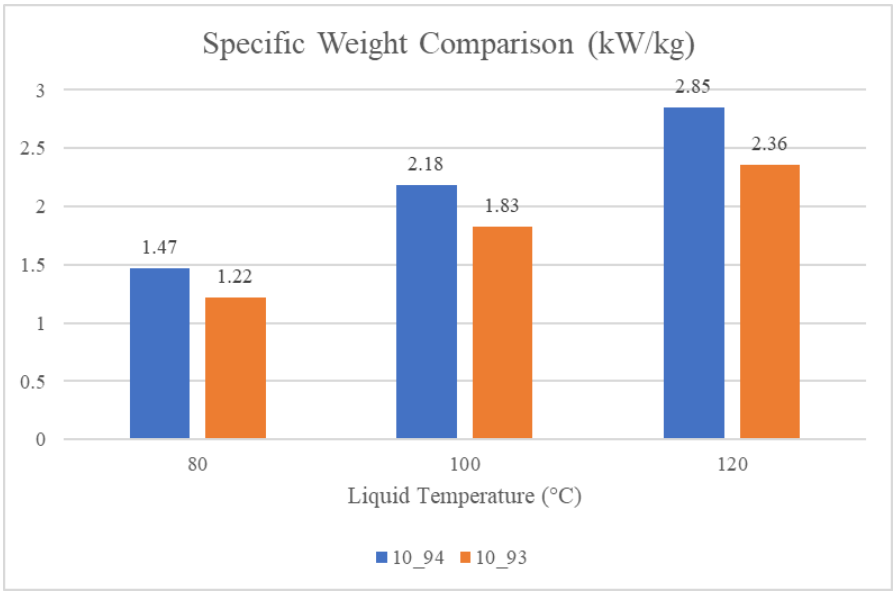

Figure 75 - Specific Weight Comparison (10_94 versus 10_93)

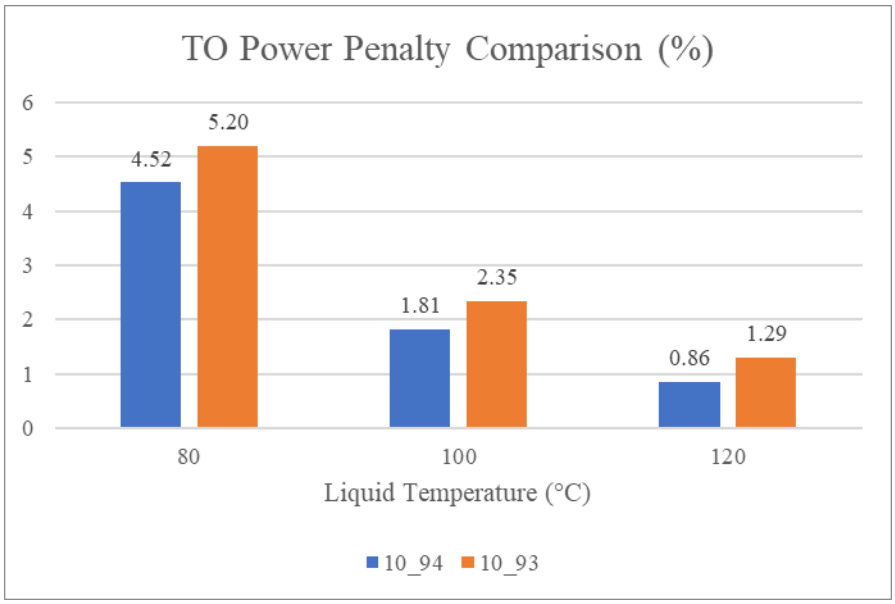

Figure 76 - TO Penalty Comparison (10_94 versus 10_93)

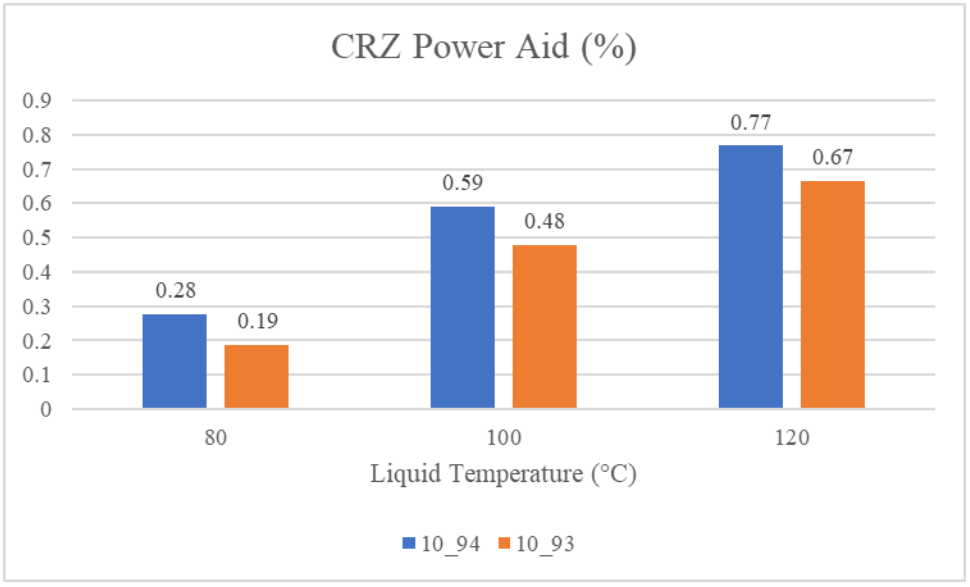

Figure 77 - CRZ Aid Comparison (10_94 versus 10_93)

It is clear that the radiator designated as 10_94 presents the better results, and it remains, therefore, recommended for conceptual design analysis instead of 10_93.

5.6 Model Premises, Limits and Comments

The parametric model was produced with a typical radiator, whose geometric and performance data are found on Kays and London (1984). Better performance radiators, like the ones manufactured by Mezzotech (n.d.), may produce better results, with pressure loss up to 40% less than typical radiators. However, care should be taken before taking such positive aspect into consideration, because other aspects need to be considered as this section will further explain.

This work concentrated effort on the internal air flow only, however, an air flow based thermal management system requires a smooth and well-integrated to the aircraft cowling structure. The cowling alone creates at least friction drag, which has not been accounted. Other sources of drag, such as spillage drag and air flow separations, might be present as well, depending on the aerodynamic integration. These drag sources can be minimized with careful design as Meredith (1935) states. but the total wet area to cover the radiator will always remain as an important source of friction drag.

It can be noticed also that the frontal radiator areas are relatively large. The required frontal area for a 2000 kW Fuel Cell, for instance, which reaches 6.0 m^2, represents 50% of the area covered by the propeller of that aircraft, approximately 12 m^2. That is a significant physical installation challenge. Solutions like shown in Figure 78 can be implemented, that is, installing the radiator in inclined position relatively to the air stream. But this kind of arrangement might impose some loss in the radiator effectiveness or even increase the air flow pressure loss, which has not been captured in the present work. However, such arrangement is just a first attempt to integrate the radiator.

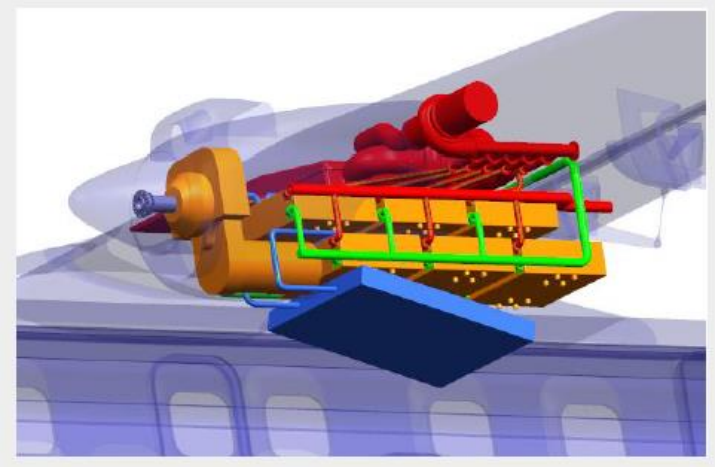

Figure 78 - Inclined Radiator Installation Example, Source:(Bjorn Fehrm ,2022)

More arrangements alternatives may be thought by designers to install such big radiators in the airplane (like in Figure 79) and minimize the losses.

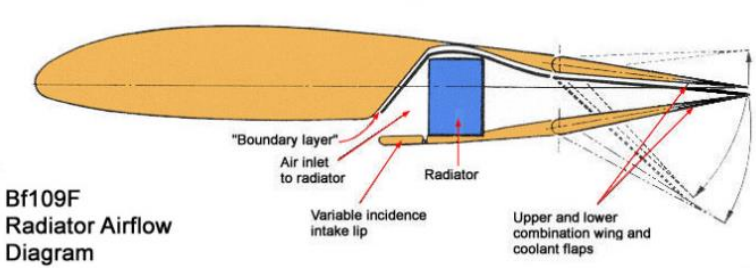

Figure 79 - BF109 (Inside Wing Integrated Radiator, Inlet and Cowling Installation), Source: (Piancastelli et al, 2015)

The inlet adopted in this work is also a simplification and a real inlet in a real design might be different, eventually creating more losses. However, the design of the inlet, joined to the design of the radiator and the radiator cowling, all integrated to the airplane, create an universe of opportunities and challenges for airplane designers, with advantages and disadvantages, and all requiring too many details to be defined. It is, therefore, considered premature, at concept design phase, to start looking at more complex solutions.

While a conventional radiator has been adopted to produce the parametric modeling, which may be considered a conservative approach, since there are possible improvements coming from state-of-the-art radiators and heat exchange enhancement techniques, more work on the aerodynamic integration of the radiator, inlet and cowlings is required to achieve the final performance values. Therefore, the currently model is proposed to be used as a conceptual design tool, for initial investigation of Fuel Cell powered aircraft ROM capabilities, having awareness that deeper analysis might be necessary depending on the context and criticality of the results.

6 Conclusion

The present work produced a framework of calculations that can be used to create a thermal management system parametric model. With such framework, a parametric thermal management system model has indeed been created to be used for Fuel Cell powered aircraft conceptual design activity, with documented limitations.

The model provides regression equations correlating the thermal management system parameters (weight, required radiator frontal area, takeoff power penalty and cruise power penalty) to the fuel cell required heat dissipation. This work proves that the correlations between thermal management system parameters and fuel cell dissipated heat is linear. A simple data manipulation can also show that the model, depending on designer expectation or tolerance for error, can be translated to a single value known as KPI.

The work confirms: thermal management systems are heavy, presenting weight KPIs on the order of 1.5 kW/kg for lowest fuel cell operating temperatures and 2.8 kW/kg for high operating temperatures fuel cells. As a notion of how heavy this is, the current aeronautical Gas Turbines present weight KPI on the order of 4 kW/kg, while a Fuel Cell solution needs not only the Thermal Management System, but also the Fuel Cell Stack, a Turbo-compressor and an electric motor.

This work also finds consistent prediction for the drag in takeoff condition, that is, an almost constant percentage of power loss is obtained throughout the range of heat dissipation of concern. The cruise drag ended up resulting in negative drag, i.e., it can be stated that the thermal management system creates thrust in cruise condition, in line with Meredith (1935).

The model development brings another indirect practical result, the radiator frontal area imposes an integration challenge to the aircraft. Since the thermal management system causes a significant drag, and larger frontal areas reduce drag, the optimization routines used for the parametric model creation tend to select the biggest area possible. The frontal areas that the model predicts are very large (reaching values as big as 50% of the propeller area), thus, integration to aircraft is a real anticipated challenge. Working with smaller frontal areas, even slightly smaller like 4.8 m^2 or 3.6 m^2), makes the drag to increase significantly, reaching more than 7% of power penalty at takeoff condition, so it tends not to be an option. This large frontal area fact alone creates

some degree of uncertainty over the model itself, because integrating so large radiators in the fuel cell, restricted to the airplane geometry limits, may impose non ideal inlet design and large cowling as well. Therefore, conceptual designer must be aware of such context and judge when deeper analysis must be done before accomplishing a feasibility or tradeoff study.

This work suggests, for future research, the exploitation of various alternatives for radiators integration to the aircraft, in which the inlet and cowling contours, as well as the radiators positioning are studied. It is suggested that the pressure losses from inlet and eventual external drag studies make use of Computational Fluid Dynamics and the Radiator Effectiveness when exposed to different incidence angles make use of real experiments.

It is also of much interest to study the radiator improvement opportunities by making this assessment with state-of-the-art radiators (like the ones which use microtubes technology) and consider radiators effectiveness improvement by use of water spray. Integrating micro-tubes radiators maps to the procedure developed in this work may become a straightforward work, but the mapping of improvement of these radiators effectiveness with water spray will require experiments.

7 References

ADZAKPA, K. P.; RAMOUSSE, J.; DUBÉ, Y.; et al. **Transient air cooling thermal modeling of a PEM fuel cell.** Journal of Power Sources, v. 179, n. 1, 2008.

American Water Heaters Expansion Tanks. (n.d.). Available in: <https://www.americanwaterheater.com/media/22209/NPESS00111.pdf> (accessed May 30, 2024).

ATR 42/72 TCDS. (n.d.). Available in: <https://www.easa.europa.eu/en/downloads/7358/en/> (accessed April 14, 2024).

BARGAL, M. H. S.; ABDELKAREEM, M. A. A.; TAO, Q.; et al. **Liquid cooling techniques in proton exchange membrane fuel cell stacks: A detailed survey**. Alexandria Engineering Journal, 2020.

BEECHCRAFT 1900D TCDS. (n.d.). Available in: <https://www.aviationhistorycanada.ca/type_certs/Beechcraft_1900D_(TC).pdf> (accessed May 30, 2024).

BJORN FEHRM. **Bjorn's Corner: Sustainable Air Transport. Part 20. Dimensioning the Fuel Cell system**: Available in: <https://leehamnews.com/2022/05/20/bjorns-corner-sustainable-air-transport-part-20-dimensioning-the-fuel-cell-system/>. (accessed March 10, 2024).

BUCK, A. L. **New equations for computing vapour pressure and enhancement factor**. Journal of Applied Meteorology, v. 20, n. 12, 1981.

CASTRO, A. L. A. DE; LACAVA, P. T.; MOURÃO, C. H. B. **Feasibility of Using Fuel Cell in a Small Aircraft**. AIAA Aviation and Aeronautics Forum and Exposition, AIAA AVIATION Forum 2021, 2021.

CHAPMAN, JEFFRYES W; SCHNULO, S. L.; NITZSCHE, M. P. **Development of a thermal management system for electrified aircraft**. AIAA Scitech 2020 Forum.. v. 1 PartF, 2020.

CHASE, M. W.; Jr **NIST-JANAF Thermochemical Tables**, Fourth Edition, J. Phys. Chem. Ref. Data, Monograph 9, 1998, 1-1951.

CHUGH, S.; CHAUDHARI, C.; SONKAR, K.; et al. **Experimental and modelling studies of low temperature PEMFC performance**. International Journal of Hydrogen Energy, v. 45, n. 15, 2020.

CLARKE, J.-P.; COUSIN, J. M.; GLINER, L.; et al**. Systems and Methods for Multi-module of Hydrogen Powered Hybrid Electric Powertrain. , 2022**. United States of America: Universal Hydrogen CO.

DATTA, A. **PEM Fuel Cell Model for Conceptual Design of Hydrogen eVTOL Aircraft**, 2021, NASA/CR—20210000284,

DICKS, A. L.; RAND, D. A. J. **Fuel Cell Systems Explained**. 3rd ed., , J. Wiley & Sons, 2018.

EMB-120 TCDS (n.d.). Available in : < https://www.easa.europa.eu/en/downloads/127185/en/> (accessed April 14, 2024).

ENGINEERING TOOLBOX (2004)., **Air - Specific Heat vs. Temperature at Constant Pressure**.,. Available in: <https://www.engineeringtoolbox.com/air-specific-heat-capacity-d_705.html > (accessed June 16, 2024).

_____ (2005) **Hot Water Expansion Tanks - Sizing**. Available in: <https://www.engineeringtoolbox.com/expansion-tanks-d_885.html>. (accessed September 9, 2023)

_____ (2008)., **Hydrogen - Thermophysical Properties**. Available in: https://www.engineeringtoolbox.com/hydrogen-d_1419.html>. (accessed August 14, 2023)

_____ (2010)., **Water - Heat of Vaporization vs. Temperature**. Available in: <https://www.engineeringtoolbox.com/water-properties-d_1573.html>. (accessed April 21, 2023).

FRANGOUL, A (2021). **Ryanair CEO Worried about sustainable aviation fuel and food prices**. Available in: <https://www.cnbc.com/2021/10/21/ryanair-ceo-worried-about-sustainable-aviation-fuel-and-food-prices-.html>. (accessed April 21, 2023).

GEMMECOTTI PUMPS. (n.d.). Available in: <https://www.gemmecotti.com/chemical-pumps/downloads-catalogues/> (accessed May 30, 2024).

GUDMUNDSSON, S. **General Aviation Aircraft Design: Applied Methods and Procedures**. 1st ed., Butterworth-Heinemann, 2014.

HOLMAN, J.P. Heat Transfer. 10th Edition, McGraw-Hill, New York, 2009

HOOGENDOORN, J. **Fuel Cell and Battery Hybrid System Optimization**, Student Theses, TU Delft Aerospace Engineering, 2018..

HOWE, D. **Aircraft Conceptual Design Synthesis**. 1st ed. Professional Engineering Publishing Limited, 2000.

HUANG, M.; LI, X. **Transient heat transfer model of proton exchange membrane fuel cell stack with internal humidification**. Beijing Hangkong Hangtian Daxue Xuebao/Journal of Beijing University of Aeronautics and Astronautics, v. 35, n. 4, 2009.

IEA (2021). **CO2 Emissions in 2021 Global emissions rebound sharply to highest ever level**. Available in: <https://iea.blob.core.windows.net/assets/c3086240-732b-4f6a-89d7-db01be018f5e/GlobalEnergyReviewCO2Emissionsin2021.pdf>. (accessed Augusts 14, 2023).

_____ (2022), **Global CO2 emissions from transport by sub-sector in the Net Zero Scenario**, 2000-2030. Available in: <https://www.iea.org/data-and-statistics/charts/global-co2-emissions-from-transport-by-sub-sector-in-the-net-zero-scenario-2000-2030>. (accessed August 14, 2023).

INCROPERA F. P., DEWITT D. P., BERGMAN T. L., LAVINE A. S. **Fundamentals of Heat and Mass Transfer**, 7th Edition, J. Wiley & Sons, 2011.

KATZOFF, S., **High-Altitude Cooling, V—Cowling and Ducting**, NACA Wartime Rept. L-775, 1945.

KAYS, W. M.; LONDON, A. L. **Compact Heat Exchangers**. 3rd ed., Medtech, 1984.

KELLERMANN, H.; LÜDEMANN, M.; POHL, M.; HORNUNG, M**. Design and optimization of ram air-based thermal management systems for hybrid-electric aircraft**. Aerospace, v. 8, n. 1, 2021.

LAURENCELLE, F.; CHAHINE, R.; HAMELIN, J.; et al. **Characterization of a Ballard MK5-E Proton Exchange Membrane Fuel Cell Stack**. Fuel Cells, v. 1, n. 1, 2001.

MEREDITH F.W., **Note on the cooling of aircraft engines with special references to ethylene glycol radiators enclosed in ducts**, British ARC, Reports and memoranda n°1683, London, England, Aug. 1935

MEZZOTECH. (n.d.). Available in: <https://mezzotech.com/radiators.html/>. (accessed September 16th 2023).

MILEY, S. J. **Review of liquid-cooled aircraft engine installation aerodynamics**. Journal of Aircraft, v. 25, n. 3, 1988.

MYERS, K. F.; DORAN, P. T.; COOK, J., KOTCHER, J. E., **Consensus revisited: Quantifying scientific agreement on climate change and climate expertise among Earth scientists 10 years later**. *Environmental Research Letters*, 16 (2021). https://doi.org/10.1088/1748-9326/ac2774.

NG, W.; DATTA, A. **Hydrogen fuel cells and batteries for electric-vertical takeoff and landing aircraft**. Journal of Aircraft, v. 56, n. 5, 2019.

O'HAYRE, R.; CHA, S.-W.; COLELLA, W.; PRINZ, F. B. **Fuel Cell Fundamentals**, 3rd ed., J. Wiley & Sons, 2016.

PALLADINO, V.; JORDAN, A.; BARTOLI, N.; et al. **Preliminary studies of a regional aircraft with hydrogen-based hybrid propulsion**. AIAA Aviation and Aeronautics Forum and Exposition, AIAA AVIATION Forum 2021.

PENG, Y.; MAHYARI, H. M.; MOSHFEGH, A.; et al. **A transient heat and mass transfer CFD simulation for proton exchange membrane fuel cells (PEMFC) with a dead-ended anode channel**. International Communications in Heat and Mass Transfer, v. 115, 2020.

PIANCASTELLI, L.; FRIZZIERO, L.; DONNICI, G. **The Meredith ramjet: An efficient way to recover the heat wasted in piston engine cooling**. ARPN Journal of Engineering and Applied Sciences, v. 10, n. 12, 2015.

PT6A TCDS. (n.d.). Available in: <https://www.easa.europa.eu/en/document-library/type-certificates/engine-cs-e/easaime008-pratt-and-whitney-canada-pt6a-67-series/> (accessed April 14, 2024).

PW100 TCDS. (n.d.). Available in: <https://www.easa.europa.eu/en/downloads/7725/en/>(accessed April 14, 2024).

RAUSCHER, M.; PHILLIPS, W. H. **Propulsive Effects of Radiator and Exhaust Ducting**. Journal of the Aeronautical Sciences, v. 8, n. 4, 1941.

RAYMER D. P. **Aircraft Design: A Conceptual Approach**, 2nd ed, AIAA (American Institute or Aeronautics and Astronautics), 1999.

RIBEIRO, R. F. G.; TRAPP, L. G.; LACAVA, P. T. **Economical Aspects of Aircraft Propulsion Electrification**. AIAA Propulsion and Energy Forum, 2021, 2021.

ROSKAM, J., Lan, C. T. E., **Airplane Aerodynamics and Performance, 1st ed.,** DAR corporation, 1997.

RUBIO, A.; AGILA, W. **Dynamic model of proton exchange membrane fuel cells: A critical review and a novel mode**l. 8th International Conference on Renewable Energy Research and Applications, ICRERA 2019., 2019.

SHOMATE, C. H. **A method for evaluating and correlating thermodynamic data**. Journal of Physical Chemistry, 1954.

SOZER, E.; MALDONADO, D.; BHAMIDIPATI, K.; SCHNULO, S. L. **Computational evaluation of an oml-based heat exchanger concept for heather**. AIAA Propulsion and Energy 2020 Forum, 2020.

THULUKKANAM, K. **Heat Exchanger Design Handbook**, SECOND EDITION. CRC Press, 2013.

U.S. DEPARTMENT OF ENERGY. **SAF Grand Challenge Roadmap**. 2022. Available in: <https://www.energy.gov/eere/bioenergy/articles/sustainable-aviation-fuel-grand-challenge-roadmap-flight-plan-sustainable> (accessed June 18, 2024)

WALSH, P. P. **Gas Turbine Performance**. 2nd ed., Blackwell Publishing, 2004.

WEN-JEI, Y.; CLARK, D. W. **Spray cooling of air-cooled compact heat exchangers. International** Journal of Heat and Mass Transfer, v. 18, n. 2, 1975.

YOSHIDA, T.; KOJIMA, K. **Toyota MIRAI fuel cell vehicle and progress toward a future hydrogen society**. Electrochemical Society Interface, v. 24, n. 2, 2015.

APPENDIX A – Fuel Cell Performance Tables

This section describes the fuel cell performance and heat tables.

Table 10 - Fuel Cell Polarization Curve, adapted from Datta (2021)

	v (Volt) at reference pressure			
Current Density (A/cm^2)	1 atm	1.5 atm	2 atm	2.5 atm
0	0.848	0.831	0.849	0.864
0.1	0.805	0.805	0.824	0.840
0.2	0.774	0.784	0.803	0.820
0.3	0.750	0.765	0.785	0.802
0.4	0.729	0.748	0.768	0.786
0.5	0.710	0.732	0.753	0.771
0.6	0.693	0.716	0.739	0.757
0.7	0.677	0.702	0.725	0.744
0.8	0.661	0.687	0.712	0.731
0.9	0.646	0.673	0.699	0.719
1	0.630	0.658	0.686	0.707
1.1	0.615	0.643	0.673	0.695
1.2	0.599	0.628	0.660	0.683
1.3	0.581	0.610	0.647	0.671
1.4	0.560	0.591	0.633	0.659
1.5	0.530	0.565	0.618	0.646
1.6	-	0.519	0.602	0.632
1.7	-	-	0.583	0.618
1.8	-	-	0.557	0.602
1.9	-	-	0.512	0.583
2	-	-	-	0.559
2.1	-	-	-	0.513

Table 11 - Fuel Cell Normalized Power Chart, adapted from Datta (2021)

	FC_Power_Norm (W/cm2) at reference pressures			
Current Density (A/cm^2)	1 atm	1.5 atm	2 atm	2.5 atm
0	0	0	0	0
0.1	0.080	0.081	0.082	0.084
0.2	0.155	0.157	0.161	0.164
0.3	0.225	0.229	0.235	0.241
0.4	0.292	0.299	0.307	0.314
0.5	0.355	0.366	0.377	0.386
0.6	0.416	0.430	0.443	0.454
0.7	0.474	0.491	0.508	0.521

0.8	0.529	0.550	0.569	0.585
0.9	0.581	0.606	0.629	0.647
1	0.630	0.658	0.686	0.707
1.1	0.676	0.708	0.740	0.764
1.2	0.718	0.753	0.792	0.820
1.3	0.755	0.794	0.841	0.872
1.4	0.784	0.827	0.886	0.922
1.5	0.796	0.847	0.927	0.969
1.6	-	0.830	0.963	1.012
1.7	-	-	0.990	1.051
1.8	-	-	1.003	1.084
1.9	-	-	-	1.108
2	-	-	-	1.117
2.1	-	-	-	1.078

Table 12 - Fuel Cell Stack Power Chart Data at Different Pressures

1 atm		1.5 atm		2 atm		2.5 atm	
W_{H_2}(kg/s)	FC_Stack_Power (kW)	W_{H_2}(kg/s)	FC_Stack_Power (kW)	W_{H_2}(kg/s)	FC_Stack_Power (kW)	W_{H_2}(kg/s)	FC_Stack_Power (kW)
0.0006	0	0.0012	0	0.0012	0	0.0012	0
0.0016	72	0.0022	72	0.0022	74	0.0021	76
0.0025	139	0.0032	141	0.0031	145	0.0031	148
0.0035	202	0.0041	207	0.0041	212	0.0041	217
0.0044	262	0.0051	269	0.0051	277	0.0050	283
0.0054	320	0.0061	329	0.0060	339	0.0060	347
0.0063	374	0.0070	387	0.0070	399	0.0070	409
0.0073	426	0.0080	442	0.0080	457	0.0079	469
0.0082	476	0.0090	495	0.0089	513	0.0089	527
0.0092	523	0.0099	545	0.0099	566	0.0098	582
0.0101	567	0.0109	593	0.0108	617	0.0108	636
0.0111	609	0.0118	637	0.0118	666	0.0117	688
0.0120	647	0.0128	678	0.0127	713	0.0127	738
0.0130	680	0.0138	714	0.0137	757	0.0137	785
0.0139	705	0.0147	744	0.0147	798	0.0146	830
0.0149	716	0.0157	762	0.0156	834	0.0156	872
-	-	0.0168	747	0.0166	867	0.0165	911
-	-	-	-	0.0176	891	0.0175	946
-	-	-	-	0.0185	903	0.0185	976
-	-	-	-	-	-	0.0194	998
-	-	-	-	-	-	0.0204	1005

Table 13 - Fuel Cell Required Cooling Heat Chart Data at Different Pressures

1 atm		1.5 atm		2 atm		2.5 atm	
FC_Stack_Power (kW)	Heat (kW)	FC_Stack_Power (kW)	Heat (kW)	FC_Stack_Power (kW)	Heat (kW)	FC_Stack_Power (kW)	Heat (kW)
0	54	0	112	0	107	0	103
72	99	72	158	74	152	76	146
139	148	141	208	145	199	148	191
202	201	207	259	212	249	217	239
262	255	269	313	277	300	283	289
320	313	329	370	339	354	347	341
374	373	387	428	399	410	409	395
426	435	442	489	457	468	469	451
476	499	495	552	513	528	527	508
523	566	545	618	566	590	582	568
567	636	593	686	617	654	636	630
609	709	637	758	666	721	688	693
647	785	678	833	713	790	738	759
680	867	714	914	757	861	785	827
705	956	744	1001	798	937	830	897
716	1061	762	1102	834	1016	872	971
-	-	747	1242	867	1100	911	1047
-	-	-	-	891	1193	946	1128
-	-	-	-	903	1300	976	1215
-	-	-	-	-	-	998	1310
-	-	-	-	-	-	1005	1421

APPENDIX B – Reference Aircraft Data

This section documents the calculations that require existing aircraft reference data. It includes the rational to obtain the pressure boost provided by the propeller, the rational to define the heat dissipations ranges for the TMS parameterized model and the rational to define a corner point temperature for the thermal management system design condition.

For propeller reference data, the characteristics from a list of airplanes certified and under operation today, which are described in Table 14, will be used: (BEECHCRAFT 1900D TCDS, n.d.), (EMB-120 TCDS, n.d.) and (ATR 42/72 TCDS, n.d.). These planes are representative from the regional turboprop segment, which is focus of this work.

Recapping efficiency equations 4.62 and 4.63, assuming 61 m/s as takeoff speed (which is a typical value), and two characteristics of typical turboprop aircraft (propeller diameter and propeller rotational speed) the propeller efficiency at takeoff condition can be calculated and shown in Table 14.

Table 14 - Propeller Efficiency Results

Aircraft	Propeller Diameter (m)	Propeller Speed Rotation (rpm)	J at 61 m/s	Prop Efficiency
Beechcraft B200, B200C	2.5	2000	0.73	0.63
Beechcraft B300, B300C	2.67	1700	0.81	0.66
EMB120	3.35	1300	0.84	0.67
ATR42	3.93	1200	0.78	0.65
ATR 72	3.93	1200	0.78	0.65

With equations 4.65, the propeller efficiency described in Table 14, the takeoff engine power from the these airplanes, (PT6A TCDS, n.d.) and (PW100 TCDS, n.d.), the pressure boost can be calculated and it is shown in Table 15.

Table 15 - Propeller Pressure Boost Results

Aircraft	Engine Power (kW) at takeoff	Propeller Diameter (m)	Propeller Efficiency	Propeller pressure Boost (Pa)
Beechcraft B200, B200C	634	2.5	0.63	1334
Beechcraft B300, B300C	850	2.67	0.66	1642.6
EMB120	1342	3.2	0.67	1832.8
ATR42	1846	3.93	0.65	1621.6
ATR 72	2051	3.93	0.65	1801.7

An average value of 1314 Pa is obtained from Table 15 which corresponds to, in average, 1.63% of the ambient pressure at Sea Level (which is the chosen design condition) and that will be the pressure boost selected for this work.

The calculation for Heat Dissipation range for thermal management system sizing will use as input the engine power required by the list of airplanes considered as references in this work. Table 16 describes the reference airplanes, the adopted engine power, the Fuel Cell Efficiency (as a result from section 4.), and the calculated required Heat Dissipation:

Table 16 - Heat Dissipation

Aircraft	Engine Power (kW) at takeoff	Heat to Power Ratio	Required Heat Dissipation (kW)
Beechcraft B200, B200C	634	1.42	900
Beechcraft B300, B300C	850	1.42	1207
EMB120	1342	1.42	1906
ATR42	1846	1.42	2621
ATR 72	2051	1.42	2912

Considering Table 16 (Required Heat Dissipation column), 900kW of heat dissipation up to 2900 kW is satisfactory range of coverage for the model construction.

By reviewing the information from the Type Certification Data Sheets from the engines that equip these aircraft (PT6, and PW100), their corner point temperature varies from 25°C up to 45°C. Choosing a value within this range, as a corner point for the fuel cell TMS, is actually a project

decision. Designing for an elevated temperature may ensure performance at higher temperatures but carries a penalty for the rest of the envelope, because it involves a higher TMS weight.

This work will assume 30°C as a maximum rated power, which provides a satisfactory coverage of biggest markets as United States and Europe and does not impose a too severe design condition for the thermal management system which would penalizes the whole operation envelope with its weight.

APPENDIX C – Radiators Data

All performance data (j and f curves varying with Reynolds) and geometric topology of the Radiator used in this work are found in Kays and London (1984). The Radiator described in figure 10.94 of such reference will be designated as 10_94 in this work and it has been chosen due to its low friction coefficients, which is critical to reduce thermal management system drag. Radiator 10_93 will be used for comparison.

Figure 80 and Figure 81 show the radiators friction and Colburn factors, while Table 17 documents the radiators core geometry features.

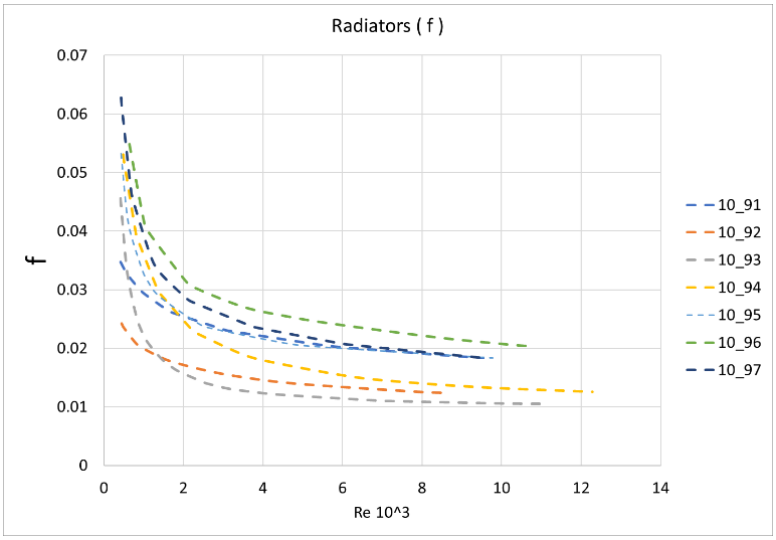

Figure 80 - Radiators f coefficients, adapted from Kays and London (1984)

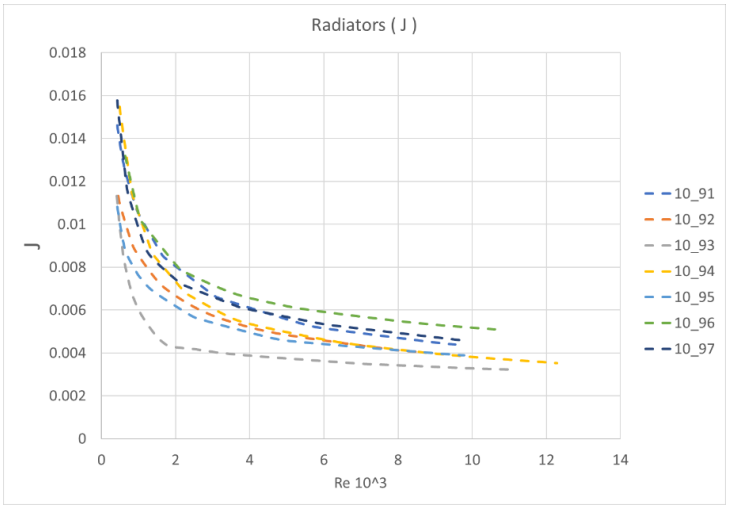

Figure 81 - Radiators j coefficients, adapted from Kays and London (1984)

Table 17 - Radiators Core Geometry Information, Source (Kays and London, 1984)

Features \ Radiator Reference	10.91	10.92	10.93	10.94	10.95	10.96	10.97
Radiator Generic Code	8.0-3/8T	7.75-5/8T	9.68-0.87	9.1-0.737-8	9.68-0.87-R	9.29-0.737-SR	11.32-0.737-SA
Tube type	circular	circular	flat	flat	flat	flat	flat
Compactness (ft2/ft3) σ_{air}	169	179	229	224	229	228	270
Compactness (ft2/ft3) σ_{liq}	16.95	9.7	46.2	40.5	46.2	40.5	40.5
Hydraulic Radius (rh) (ft)	0.00285	0.00298	0.00295	0.00345	0.00295	0.00338	0.00288
Fin area / Total area (air side)	0.95	0.913	0.795	0.813	0.795	0.814	0.845
Free Flow Area / Frontal (air side)	0.481	0.534	0.697	0.788	0.697	0.788	0.78
Fin thickness (in)	0.013	0.013	0.004	0.004	0.004	0.004	0.004
Liquid Ducts Spacing Transverse to air Flow Direction (in)	0.598	0.824	0.316	0.45	0.316	0.45	0.45
Liquid Ducts Spacing ta Air Flow Direction (in)	0.494	1.074	0.19	0.053	0.19	0.053	0.053
Liquid Flow Area / Total Liquid Flow Side Area	0.127907	0.128752	0.183919	0.132014	0.183919	0.132014	0.132014
Fin Length (in)	0.299	0.412	0.158	0.225	0.158	0.225	0.225
Liquid Duct Hydraulic Radius (rh) (ft)	0.00775	0.013667	0.003728	0.002999	0.003728	0.002999	0.002999
Liquid Duct Thickness (in)	0.01	0.01	0.01	0.01	0.01	0.01	0.01
Liquid Duct Depth (in)	0.382	0.656	0.87	0.737	0.87	0.737	0.737
Liquid Duct Width (in)	0.382	0.656	0.12	0.1	0.12	0.1	0.1

APPENDIX D – Air and Hydrogen Properties Tables

Table 18 - Air Properties, Source: (Engineering Toolbox, 2004)

Temperature		Cv	Cp	γ
[K]	[°C]	[kJ/kg K]	[kJ/kg K]	[-]
200	-73.2	0.7163	1.007	1.406
220	-53.2	0.7163	1.006	1.404
240	-33.2	0.7164	1.006	1.404
260	-13.2	0.7168	1.006	1.403
273.2	0	0.7171	1.006	1.403
280	6.9	0.7173	1.006	1.402
288.7	15.6	0.7175	1.006	1.402
300	26.9	0.718	1.006	1.402
320	46.9	0.7192	1.007	1.4
340	66.9	0.7206	1.009	1.4
360	86.9	0.7223	1.01	1.398
380	107	0.7243	1.012	1.397
400	127	0.7266	1.014	1.396
500	227	0.7424	1.03	1.387
600	327	0.7641	1.051	1.375

Table 19 - Hydrogen Properties, Source: (Engineering Toolbox, 2008)

Molecular Weight	2.016
Specific Gravity, air = 1	0.07
Density of liquid at atmospheric pressure (lb/ft3, kg/m3)	4.43, 71.0
Specific Heat - c_p - (*Btu/lb°F or cal/g°C, J/kgK*)	3.42, 14310
Specific Heat Ratio - c_p/c_v	1.405
Boiling Point - saturation pressure 14.7 psia and 760 mm Hg - (*°F, °K*)	-423, 20.4
Latent Heat of Evaporation at boiling point (*Btu/lb, J/kg*)	192, 447000


EESC • USP